Heat Engine Driven by Shape Memory Alloys: Prototyping and Design

Ean H. Schiller

Thesis submitted to the Faculty of
Virginia Polytechnic Institute and State University
in partial fulfillment of the requirements for a degree of

Master of Science
in
Mechanical Engineering

Dr. Charles Reinholtz, Chairman
Dr. Harry Robertshaw
Dr. Donald J. Leo

September 19, 2002
Blacksburg, VA

Keywords: shape memory alloy, SMA, Nitinol, heat engine

Heat Engine Driven by Shape Memory Alloys: Prototyping and Design

Ean H. Schiller

(ABSTRACT)

This work presents a novel approach to arranging shape memory alloy (SMA) wires into a functional heat engine. Significant contributions include the design itself, a preliminary analytical model and the realization of a research prototype; thereby, laying a foundation from which to base refinements and seek practical applications.

Shape memory alloys are metallic materials that, if deformed when cold, can forcefully recover their original, "memorized" shapes, when heated. The proposed engine consists of a set of SMA wires stretched between two crankshafts, synchronized to rotate in the same direction. Cranks on the first crankshaft are slightly longer than cranks on the second. During operation, the engine is positioned between two distinct thermal reservoirs such that half of its wires are heated while the other half are cooled. Wires on the hot side attempt to contract, driving the engine in the direction that relieves the heat-induced stress. Wires on the cold side soften and stretch as the engine rotates. Because the force generated during heated recovery exceeds that required for cooled deformation, the engine is capable of generating shaft power.

Limited experimental measurements of shaft speed were performed. An analytical model of the engine predicts that the maximum output power for the prototype, under test conditions, should be 0.75 W. Thermal efficiency, though not measured or calculated in this work, is expected to be low. Potential applications may include the conversion of waste heat into shaft power.

Acknowledgements

I am grateful to the following individuals for their gracious support of this work:

Dr. Charles Reinholtz

Dr. Donald J. Leo

Dr. Harry Robertshaw

Jerry Schiller

Noah Schiller

William Whittier

Table of Contents

List of Figures

Chapter 1: Introduction and Overview

1.1 Introduction

Revealed and explored within, is a novel scheme for arranging shape memory alloy (SMA) wires into a functional heat engine. This work chronicles the design, evolution and subsequent realization of a research prototype; thereby, laying a foundation from which to base refinements and seek practical applications.

Significant contributions of this effort include:

- the introduction and development of an engine design that uses straight wire in place of coiled springs
- an analytical model to simulate performance of the proposed engine
- a demonstrated working prototype

Chapter 1 introduces the concept, discusses motivations for the work and details conventions used throughout this document. Chapters 2 and 3 provide background material on shape memory alloys and SMA engines. Chapter 4 includes specifics and analysis of the proposed design. Chapter 5 addresses construction and Chapter 6 presents experimental results. Chapter 7 finishes with a summary and speculation about uses for the technology.

1.2 Overview

Shape memory alloys are materials with the capacity to sustain large deformations when cold, but return to their original, "memorized" shapes, when heated. As wire, deformation usually involves elongation, where shape recovery is the contraction back to a pre-stretched length. The effect, due to changes in the material's crystal structure, is unrelated to thermal expansion and contraction [1].

Consider a weight suspended by an SMA wire. Applying heat contracts the wire and lifts the weight. When the heat is removed, the wire stretches and the weight descends. Because it can lift more weight during heating than is required to stretch it when cold, the material has potential to do work. SMA engines exploit this potential as they convert heat energy into shaft power.

The prototype consists of a set of SMA wires stretched between two synchronized crankshafts. When heat is applied, the engine rotates. Any heat source, of sufficient temperature, may be used. Unfortunately, the low thermal efficiency of this type of device relegates its use to applications where thermal energy is abundant and inexpensive. For those applications, this machine's simplicity and flexible power requirements could make it an attractive alternative to existing sources of shaft power.

1.3 Motivation

Why harvest thermal energy? Because it's there! As stated, this machine is only valuable in cases where thermal energy is abundant and cheap; however, there are many such cases. Evidence of thermal energy is the shimmering look of a parking lot in the sun, or the steam escaping from a utility vent. Both cases represent untapped or otherwise wasted resources. Volcanoes are obvious thermal sources, so are hot springs and some undersea vents. Many industrial facilities generate waste heat. Then there are forms of energy that are more portable, but easy to convert to heat, firewood for example. Cold areas would work too: lakes, caverns, tunnels, or a recessed basement. Any temperature difference is a potential source of thermal energy. It is nearly infinite and often free. Why not use it? Even if the mechanical work output is a small percentage of the potential, a small percentage of infinite is still worthwhile.

Of course, there are expenses associated with equipment and complications with channeling heat into the engine. Then there are issues of energy density and storage; running the prototype requires a larger temperature difference than is commonly available between outside air and the average basement. To harness diffuse solar energy, it would probably be necessary to store and concentrate the heat before it could drive an engine.

Obviously, the technology is not ready to revolutionize the power generating industry, but there is potential, and beginning to exploring that potential is the motivation for this work.

1.4 Convention

This thesis includes seven chapters each with multiple subsections, as well as appendices and references. To advance directly to a specific section, use the document map. Links are designated with blue underlined text. Clicking a link will open the referenced object or advance to a specific point in the document. Use the back button to return from the linked location to a previous position.

Metric units are used exclusively, except where referring to purchased parts specified in English units by the manufacturer. Due to software limitations, sub- and superscripted variables in the text have different symbols when referenced in graphics and computer code. Table A1-1 is a comprehensive listing of all referenced variables and their symbols. References are denoted by a number in brackets. All sources are cited in the Reference List. Each reference is also linked to its citation. Patent references link to images of the patent filing.

(PDF Version - the only supported links are those associated with the video clips of Chapter 6)

Chapter 2: Shape Memory Alloys

2.1 Scope

The goal of this work is to build an SMA heat engine for further study. Accordingly, this chapter does not propose any new theories regarding the underlying influences of material performance. Nor is it a comprehensive review of the metallurgy, crystallography, material mechanics, and related governing principles. Instead, the following sections provide a brief overview of macroscopic behavior typical of shape memory alloys.

Furthermore, while material can be produced in a variety of forms including ribbon, tubing, sheets and bars, wire is most common and available. For this reason, discussion, though applicable to all forms, focuses on SMA wire.

2.2 Definition

Shape memory alloys are metallic materials that, if deformed when below a critical temperature, can forcefully recover their original shape when heated. Apparent plastic deformation and subsequent full recovery is the shape memory effect (SME).

2.3 History

In 1932, Chang and Read discovered shape memory transformations in samples of AuCd [2]. They published the first account of the shape memory effect in 1951 [3]. In 1962, Buehler and co-workers, at the Naval Ordnance Laboratory (now the Naval Surface Warfare Center), developed an alloy of nickel and titanium (NiTi) with a more pronounced shape memory effect than had been possible with AuCd [4]. The new material was named Nitinol, derived from Nickel Titanium Naval Ordnance Laboratory [2][5][6]. Buehler's development spawned a surge in research and led to the discovery of many other alloy systems with shape memory capability. Nitinol remains the most commercially significant because of its good cyclic stability, biocompatibility, corrosion resistance and capacity to recover large strains (8%) [2][6].

Commercial applications are far-reaching. Examples include: toys, actuators, control valves, circuit-board edge connectors, hydraulic couplings, blood clot filters, guide wire for steering catheters, orthodontic arch wires, eyeglass frames and even wrinkle-proof travel shirts [2][6][7][8][9].

Noting that the force required to deform the cool material is significantly less than that generated during shape recovery, many researchers sought to extract work from shape memory phenomenon. The first patent relating to extracting work was issued to Buehler himself in 1968; thus beginning the pursuit of a practical shape memory alloy heat engine [US3403238].

2.4 Novel Behavior

2.4.1 Shape Memory Effect

The basic phenomenon is characterized by a deformed specimen changing shape when heated. Cooling has no effect on its shape. Consequently, for cyclic operation, an external force is required to re-deform the material. Because shape change only occurs during heating, the process is called one-way shape memory.

In two-way shape memory, a properly processed sample can exhibit one shape when cold, change to a second shape when heated and return to its original shape when cooled again, all without mechanical intervention. Shape change occurs in two directions, during both heating and cooling, although no appreciable force is developed during the transition from a high to a low-temperature shape [2].

All-around effect is a third variation in which a specimen's high and low temperature shapes are inversions of one another. For example, a segment of SMA ribbon could have a concave curvature when cool and change to a convex curvature when hot [6]. All-around shape memory is rarely discussed in the context of SMA wire.

Whether a given sample exhibits one-way, two-way, or all-around shape memory is determined by its thermomechanical processing. This procedure, including forging and heat treatment, also embeds the "memorized" shapes. Two-way and all-around effects require more processing to setup and are less reliable than one-way memory [6]. Moreover, materials "trained" for two-way operation attain smaller shape changes than one-way materials [2][10].

Due to their simplicity, reliability and large displacement potentials, SMA's with one-way memory are used for the prototype.

2.4.2 Superelasticity

A second characteristic, closely related to shape memory, is superelasticity. When SMA material is above some critical temperature, it will assume and maintain its high-temperature shape. If sufficiently stressed, the material will soften and deform easily; however, as soon as the load is removed, the material spontaneously returns to its original, high-temperature, shape. Superelastic wire has a springy feel.

2.5 Crystal Structure

The unique capabilities and characteristics of the SMA are due to its crystal structure. Shape memory alloys consist of two distinct crystallographic phases: austenite and martensite. Austenite is the high temperature parent phase. It has a homogenous cubic crystal structure and relatively high modulus of elasticity [3][10][11][12]. Cooling austenite transforms it into martensite. Unstressed martensite has a twinned monoclinic structure and lower modulus of elasticity [3][6][12]. Although some sources mention an additional annealing phase and intermediary "R" phase, they concede that austenite and martensite are the principle constituents [2b][6][7].

Crystal structure refers to how the atoms are arranged. Cubic crystals have atoms located at each corner of an imaginary cube, while monoclinic crystals resemble 3-dimensional parallelograms [13]. Figure 2.1 is a simple illustration of these structures.

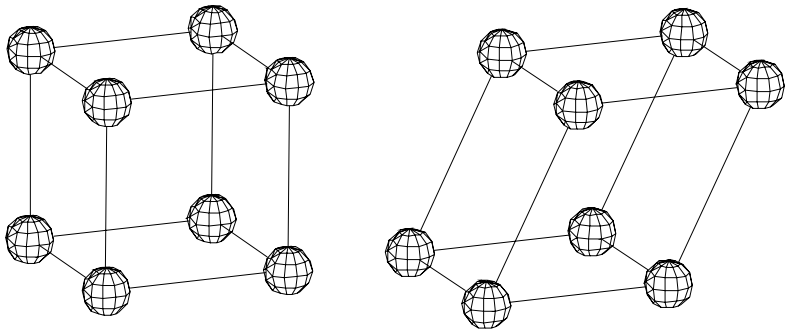

Figure 2.1: Reduced-sphere representation of a cubic crystal (left) and monoclinic crystal (right).

Twins are regions of material whose crystal lattices are symmetrically oriented about a particular grain boundary, the twin boundary. They form in small, randomly distributed, domains of alternately sheared platelets, called variants [2][3][7].

Twinning, the process of forming twins, neutralizes the strain energy associated with changes in crystal structure, thereby minimizing the macroscopic strain in the specimen [2][12]. Consequently, an SMA wire can undergo the phase transformation from cubic austenite to monoclinic martensite without changing

length. Since twins accommodate the strain energy, this transformation is said to be "self-accommodating" [2][3].

If a small load is applied to twinned martensite, the material exhibits linear elastic behavior, with strain increasing linearly with stress. Increasing the load will cause the randomly oriented variants to align in a direction that minimizes the stress. This conversion from a twinned to an aligned structure is called detwinning, and allows a small rise in stress to effect a large macroscopic strain [6]. The result is bounded by the martensitic strain limit (ε_L), also called maximum recoverable strain, and is the point at which the material is completely detwinned [10]. When the load is removed, the material does not re-twin but instead holds the strain as if plastically deformed. Provided strain has not exceeded the martensitic strain limit, of approximately 8% for Nitinol, any shape change will be completely recovered as the material is heated and returned to austenite [10]. In the case where a stressed sample of austenite is permitted to cool, martensite will emerge directly into its detwinned formation. Figures 2.2 and 2.3 are 2D illustrations of how each phenomenon would occur.

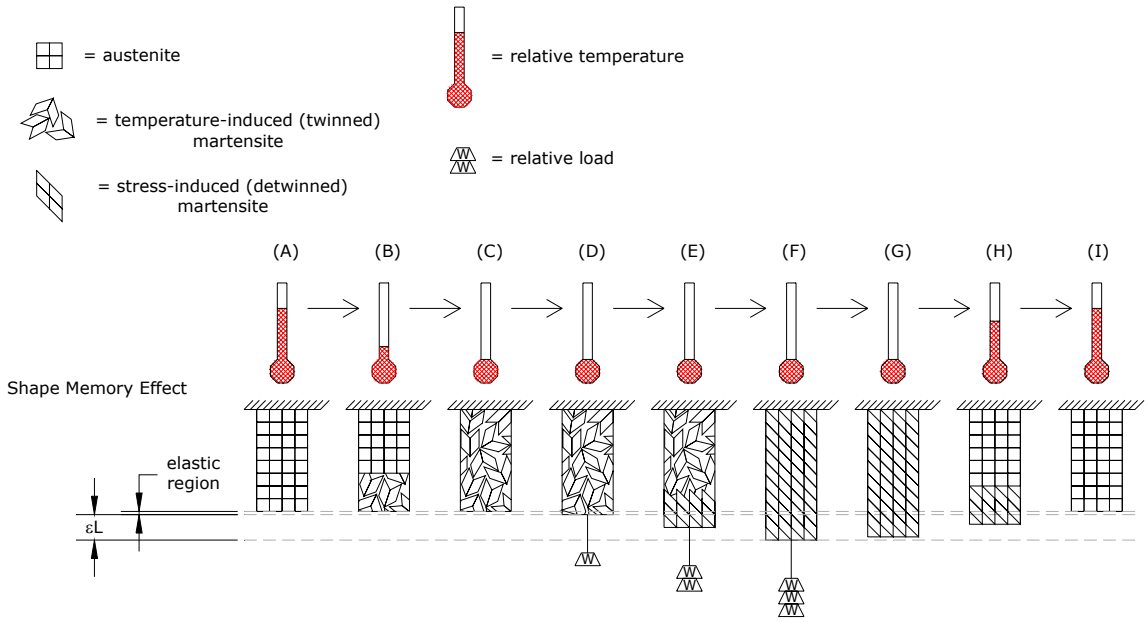

Figure 2.2: Illustration of shape memory effect with temperature-induced martensite formation.

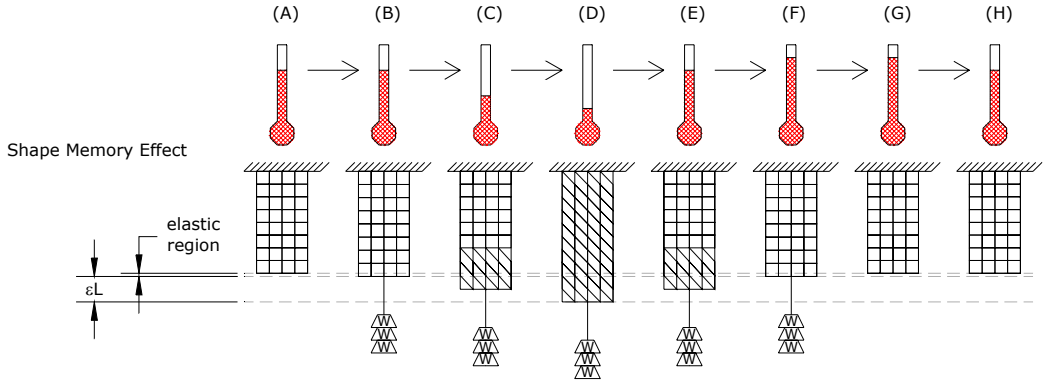

Figure 2.3: Illustration of shape memory effect with direct conversion from austenite to stress-induced martensite.

Additional shape change is marked by a second linear elastic region, and if continued, permanent plastic deformation. Permanent deformation involves breaking atomic bonds and requires much higher stresses than does detwinning, which merely distorts the crystal lattice [2b][3][13]. Note that because martensite can exhibit more than one linear elastic region, literature specification for modulus of elasticity refers to that of completely detwinned martensite. There is no such issue for austenite because the phase only has a single configuration. Figure 2.4 illustrates the change in the crystal structure for a series of loads, the largest of which, causes permanent plastic deformation

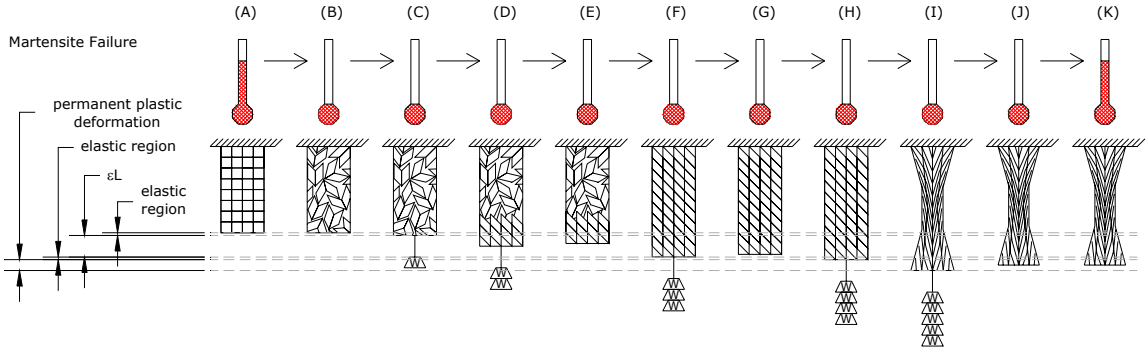

Figure 2.4: Illustration of changes in crystal structure leading to failure in the martensite phase.

It is possible for stress to convert austenite to martensite without a change in temperature, as occurs in superelastic behavior [12]. Applying a force to austenitic material will put it in a linear elastic region governed by austenite's modulus of elasticity. When enough stress is present, the material transforms directly into detwinned martensite, also known as stress-induced martensite. The conversion proceeds in exactly the same manner as when transforming between temperature-induced (twinned) martensite and its stress-induced counterpart. That is, the specimen softens and exhibits large strains in response to small increases in stress. The only obvious difference is that the conversion from austenite to stress-induced martensite takes place at higher temperatures and stresses than the twinned to detwinned transformation. However, unlike its low temperature analog, martensite induced at high temperatures is not stable and will spontaneously revert to undeformed austenite when the stress is removed [3][2c]. Figure 2.5 illustrates superelasticity.

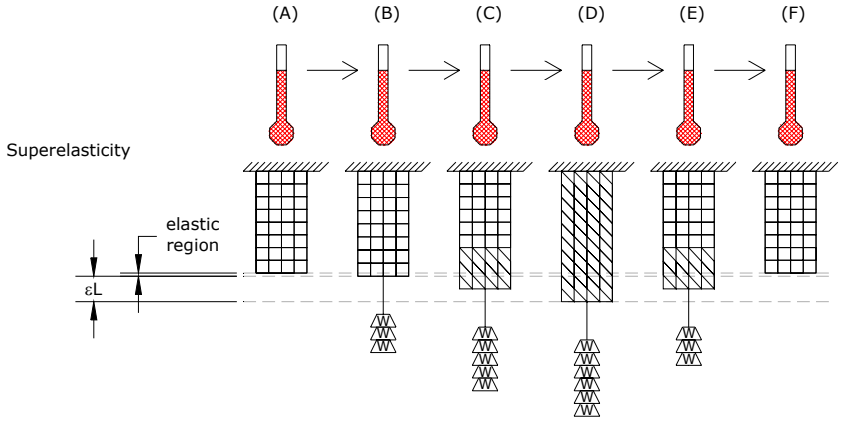

Figure 2.5: Illustration of the superelastic effect.

2.6 Transformation Temperatures and Hysteresis

Transformations between the two component phases can be driven by temperature, stress or a combination thereof. In the absence of applied stress, phase changes are characterized by the following four transformation temperatures: martensite start (M_s), martensite finish (M_f), austenite start (A_s) and austenite finish (A_f) [12]. Transformation temperatures are material properties that specify the respective ranges for the forward (austenite to martensite) and reverse (martensite to austenite) transformations [10]. Figure 2.6 illustrates a typical SMA phase change with respect to the four characteristic temperatures.

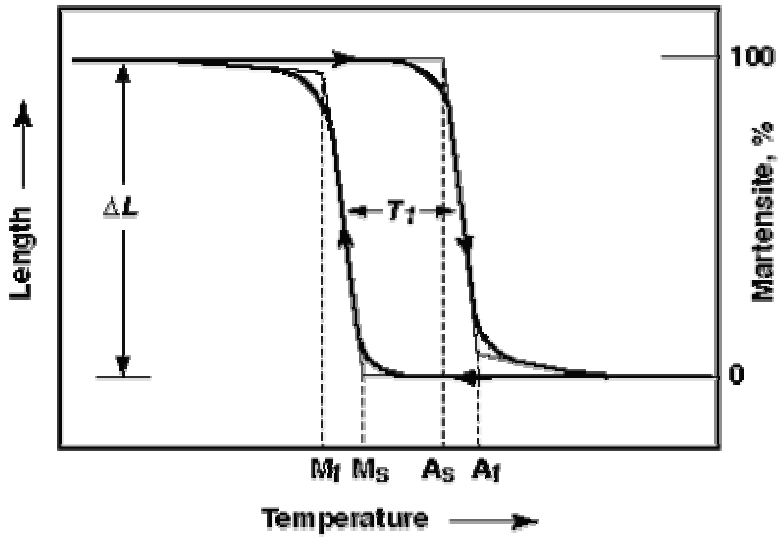

Figure 2.6: "Typical transformation versus temperature curve for a specimen under constant load (stress) as it is cooled and heated. T_1: transformation hysteresis; M_s: martensite start; M_f: martensite finish; A_s: austenite start; A_f: austenite finish" [2].

Phase transformations do not take place at a single temperature, but over a temperature range. While the total range between the start and finish of a transformation may be quite large, most of the phase change happens in a much narrower band. Also evident in Figure 2.6 is the fact that the forward and reverse processes follow different paths, a consequence of transformation hysteresis. Hysteresis is due to the friction generated between crystals as their structures change [6]. The effect is quantified as a hysteresis width, the difference between the martensite peak (M_p) and austenite peak (A_p) temperatures. M_p and A_p are defined as the respective temperatures at which the forward and reverse transformations are 50% complete [2][2b][2d].

The "high", "hot", "low" and "cold" descriptors of previous sections refer to transformation temperatures. Cold is less than M_f and hot is greater than A_f. To use the shape memory effect, heating is required to reach temperatures above A_f and cooling is necessary if the ambient temperature is greater than M_f. Likewise, superelastic performance requires the application's operating temperature to be above A_f.

Transformation temperatures change with stress level. All four characteristic temperatures shift rigidly toward higher values in linear proportion to stress (load), as shown in Figure 2.7 [3][10]. The slope of the stress-temperature curve is called the stress influence coefficient [14]. Although, in the figure, all four stress-temperature curves are shown with the same slope, this is not necessarily a general case [3].

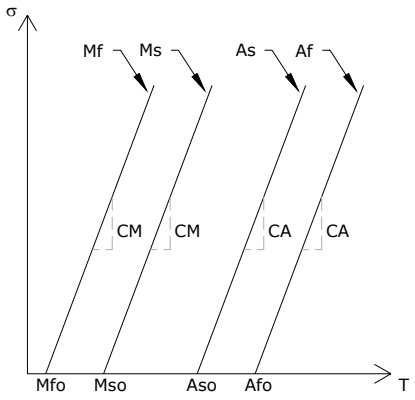

Figure 2.7: Transformation temperatures as functions of applied stress. M_{fo}, M_{so}, A_{so} and A_{fo} represent the "original", unstressed transformation temperatures. C_A and C_M are stress influence coefficients.

Reconsider superelasticity: an unstressed specimen consists entirely of austenite at room temperature. Originally, the temperature corresponding to the unstressed start of martensite formation, M_{so}, is well below the ambient temperature. When the specimen is stressed, M_s shifts upward until it reaches and exceeds room temperature. The specimen begins transforming into stress-induced martensite. If the stress is great enough, the M_f temperature also rises above the ambient and the specimen converts entirely to martensite. All conversions occur while the ambient temperature remains constant and above M_{so}. This scenario, illustrated in Figure 2.5, exemplifies the fact that original transformation temperatures (M_{fo}, M_{so}, A_{so}, A_{fo}) are only directly applicable to unstressed material.

Other useful temperatures for classifying SMA behavior include the M_d temperature, above which martensite cannot exist. Stressing a specimen when above M_d will reveal a linear elastic region followed by plastic deformation of the austenite phase, without any transition to martensite [2]. Figure 2.8 is an illustration of this case. Transition or activation temperatures are occasionally mentioned when discussing the point at which an actuator begins shape recovery [7]. Both terms are synonymous with the austenite start temperature [15]. The Active Austenite Finish (*Active* A_f) temperature is a common specification, and is measured with the bend-free recovery test [2d]. *Active* A_f is the temperature at which heated shape recovery is nearly complete [2e].

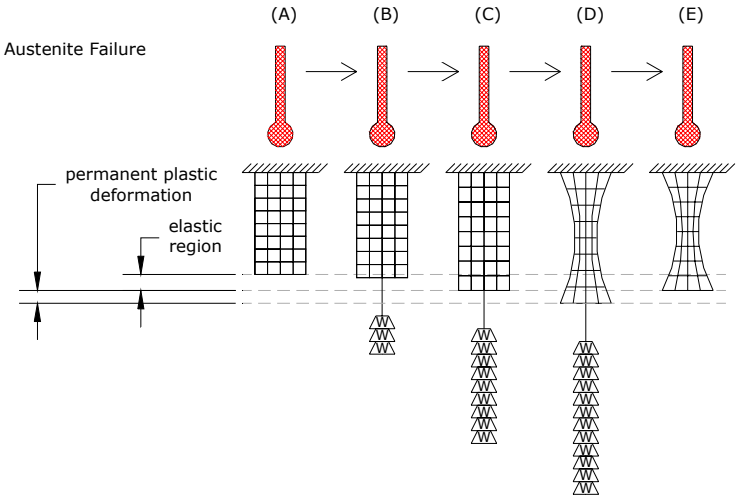

Figure 2.8: Loading austenite to failure, above the M_d temperature.

Finding the right transformation temperatures is usually the most critical step to using SMA materials effectively. Fortunately, these and other material properties, such as hysteresis width and overall shape memory capacity, are products of chemical composition [6]. Individual Nitinol alloys may operate anywhere between -50 and 110 °C depending on the precise ratio of nickel and titanium atoms used in manufacturing [2][6]. Table A2-1 provides example transformation temperature sets for Nitinol. Table A2-2 is a comparison of properties across the common alloy systems.

It is useful to note that although not often available in published form, there are techniques for measuring a specimen's transformation temperatures [2e]. Also, while most manufactures claim to be able to precisely set the activation temperature, such precision is not always economical or even commercially available in small quantities [2d].

2.7 Stress-Strain Relations

Although most of the relevant stress-strain relationships have been described in the context of previous sections, a few additional remarks are warranted. First, SMA stress-strain behavior is highly path dependent. Path, in this case, refers to the temperature, strain and loading history of the specimen. Consider Figure 2.9, typical stress-strain curves at a series of constant temperatures, and notice how the loading and unloading paths differ.

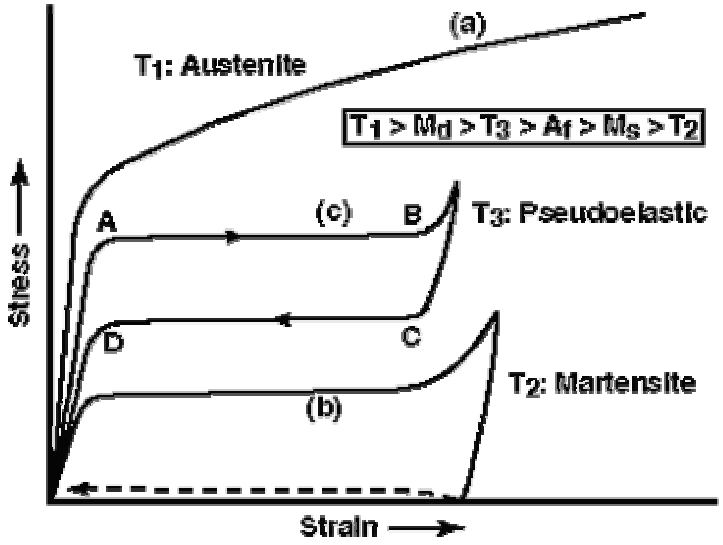

Figure 2.9: Typical stress-strain curves for constant temperatures [2].

In case (a) the temperature is above M_d, therefore the material acts as any conventional metal would when stressed to failure. There is an initial linear elastic region, followed by plastic deformation. This case is the subject of Figure 2.8.

Case (b) illustrates shape memory as it is most often applied. Stress causes a large, apparently plastic deformation, which is only fully recovered upon heating (represented by the dashed line near the bottom of the figure). Figure 2.2 is the corresponding illustration.

Superelasticity is case (c). Here, the temperature is above the austenite finish temperature. Applying stress, after an extended linear elastic region, again leads to large plastic deformations. When the stress is released, the material automatically recovers the strain, without any additional heat input. Figure 2.5 is the matching illustration.

2.8 Constitutive Model

Constitutive refers to that which makes a thing what it is. Constitutive models of SMA behavior seek to explain the critical aspects of the material in a unified and consistent manner. Many such models have been proposed and are still being researched, but the explanations, descriptions and analysis of this work are primarily based on the Brinson model. Interested readers should refer to reference [3]. This section covers relevant aspects of the model that have not already been mentioned.

Essentially, SMA material exists in three forms: austenite, temperature-induced martensite and stress-induced martensite. A specimen's overall behavior is the combination of behaviors of its constituent parts [16]. The degree of effect exerted by each part depends on its volume fraction, which is a function of the thermomechanical loading history of the sample. In the Brinson model, transformation progress is marked by the volume fraction of martensite. For example, a transformation from martensite to austenite that is 25% complete will have a martensite fraction of 75%. Similarly, a 25% complete transformation from austenite to martensite will have a martensite fraction of 25%.

Fractions of stress and temperature-induced martensite are phenomenologically represented by cosine functions. This means that being 25% through the temperature range does not make the transformation 25% complete; instead, due to the shape of the cosine function, the transformation would only be about 15% complete. The overall volume fraction of martensite is the sum of these stress and temperature-induced components. By keeping track of a specimen's composition, it is possible to predict, and numerically simulate its shape memory behavior.

The fact that the temperatures critical to phase transformation, change with stress, has already been discussed; however, there are also critical stress values associated with changes into stress-induced martensite from the other constituents. Denoted σ_s^{cr} and σ_f^{cr}, these are the stress values corresponding to the start and finish of stress-induced martensite formation. Although constant below M_s, these values increase in linear proportion to temperature according to the stress influence coefficient. Figure 2.10 shows how these quantities fit into the stress-temperature space.

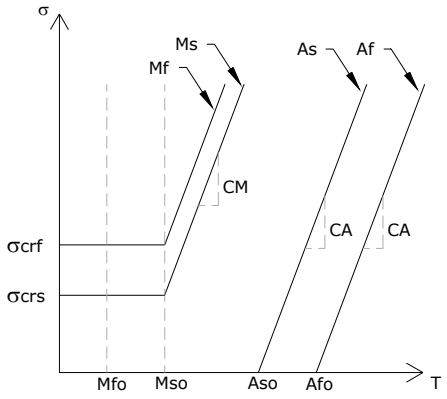

Figure 2.10: Stresses marking the start and finish of stress-induced martensite formation.

Constitutive models lay out the qualitative explanation and give the equations to make it useful. The Brinson equations are not repeated here; however, the following numerical example presents some qualitative implications. Critical stresses play a role in determining the fractions of martensite. Because stress-induced martensite is synonymous with strained martensite, knowing the relative fractions of each constituent allows one to predict strain.

Consider a material with the properties of Table 2.1, the same values used in the Brinson paper [3]. Note that although not discussed here, the thermoelastic tensor is a material property used by the constitutive equations and is included in Table 2.1.

Let the specimen start as 100% austenite from 60 °C and then cool to 5 °C, all at a constant stress. Figure 2.11 shows two, vertically aligned, series of plots. The leftmost group, labeled (a), is for a relatively low constant stress of 50 MPa. Similarly, the (b) plots to the right, are for the high stress of 250 MPa. Both groups show the material's path in stress-temperature space, corresponding fractions of martensite and the resulting strain. Stress-induced (fM_S), temperature-induced (fM_T) and total (fM) fractions of martensite are shown.

Table 2.1: Example material properties [3].

Transformation Temperatures	Modulus of Elasticity	Transformation Constants	Martensitic Strain Limit
$M_f = 9$ °C	$Y_A = 67 \times 10^9$ Pa	$C_M = 8 \times 10^6$ Pa/°C	$\varepsilon_L = 6.7\%$
$M_s = 18.4$ °C	$Y_M = 26.3 \times 10^9$ Pa	$C_A = 13.8 \times 10^6$ Pa/°C	
$A_s = 34.5$ °C		$\sigma_s^{cr} = 100 \times 10^6$ Pa	**Thermoelastic Tensor**
$A_f = 49$ °C		$\sigma_f^{cr} = 170 \times 10^6$ Pa	$\Theta = 0.55 \times 10^6$ Pa/°C

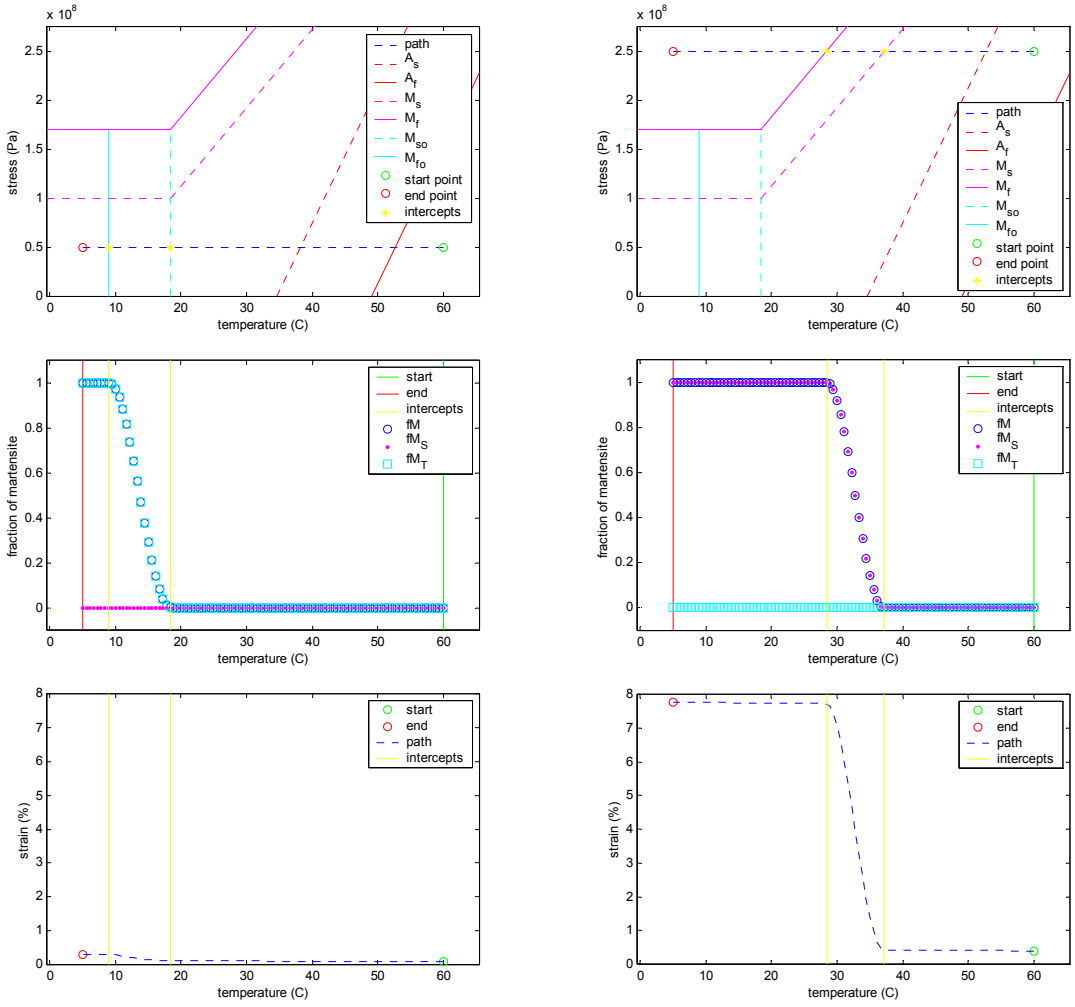

(a) σ = 50 MPa. (b) σ = 250 MPa.

Figure 2.11: Path in stress-temperature space, fractions of martensite and strain: (a) constant stress cooling for $\sigma < \sigma_s^{cr}$, (b) constant stress cooling for $\sigma > \sigma_f^{cr}$.

Notice that the first plots in each series, those showing the path in a stress-temperature domain, are simply the boundaries from Figure 2.10 overlaid with a blue path line. Path plots highlight the important

boundaries for a given direction. For example, when cooling from austenite, the A_s line is meaningless and not marked as an intercept on the path. Paths extend from the start point (green) to the end point (red). Intercepts are shown in yellow.

When stress is less than the starting critical stress, as is the case for Figure 2.11 (a), temperature-induced martensite begins to form when the temperature drops below M_{so}. Temperature-induced martensite does not have a direct effect on strain, as does stress-induced martensite; therefore, the increase in strain is attributable to elastic behavior. When the material transforms, its modulus of elasticity changes from that of stiffer austenite to that of softer martensite. At a constant load, this decrease in modulus causes an increase in strain, even with no stress-induced martensite present. Elastic strain is much less significant than that generated during the formation of stress-induced martensite.

Contrast the low-stress plots with their high-stress counterparts in Figure 2.11 (b). In this case, stress is above what is needed to form stress-induced martensite. Accordingly, martensite begins to form at a higher temperature, and when it does, it forms directly into stress-induced martensite. Strain increases in proportion to the stress-induced martensite. The final strain value exceeds ε_L because it includes linear elastic strain in addition to that from the phase transformation.

Figure 2.12 contains the same style of plots, but with (a) showing the case for cooling at a constant midlevel-stress, 150 MPa, and (b) showing an example of heating concurrent with decreasing stress. Of particular interest in (a) is how the fraction of martensite grows in two stages. First, stress-induced martensite forms when the path intersects the starting critical stress line, and as cooling continues, the temperature-induced variety fills in the remainder. Strain however, only rises with the formation of stress-induced martensite. Hysteresis, which causes heating behavior to differ from that of cooling, is evident in the contrasts between Figures 2.12 (a) and (b). Notice how the martensitic fractions at 5 °C in (b) do not immediately decline upon heating, as would occur if they reversed directions and followed the paths in (a). Instead, the martensite maintains its proportion until the stress-temperature path intersects the A_s line, as shown in (b).

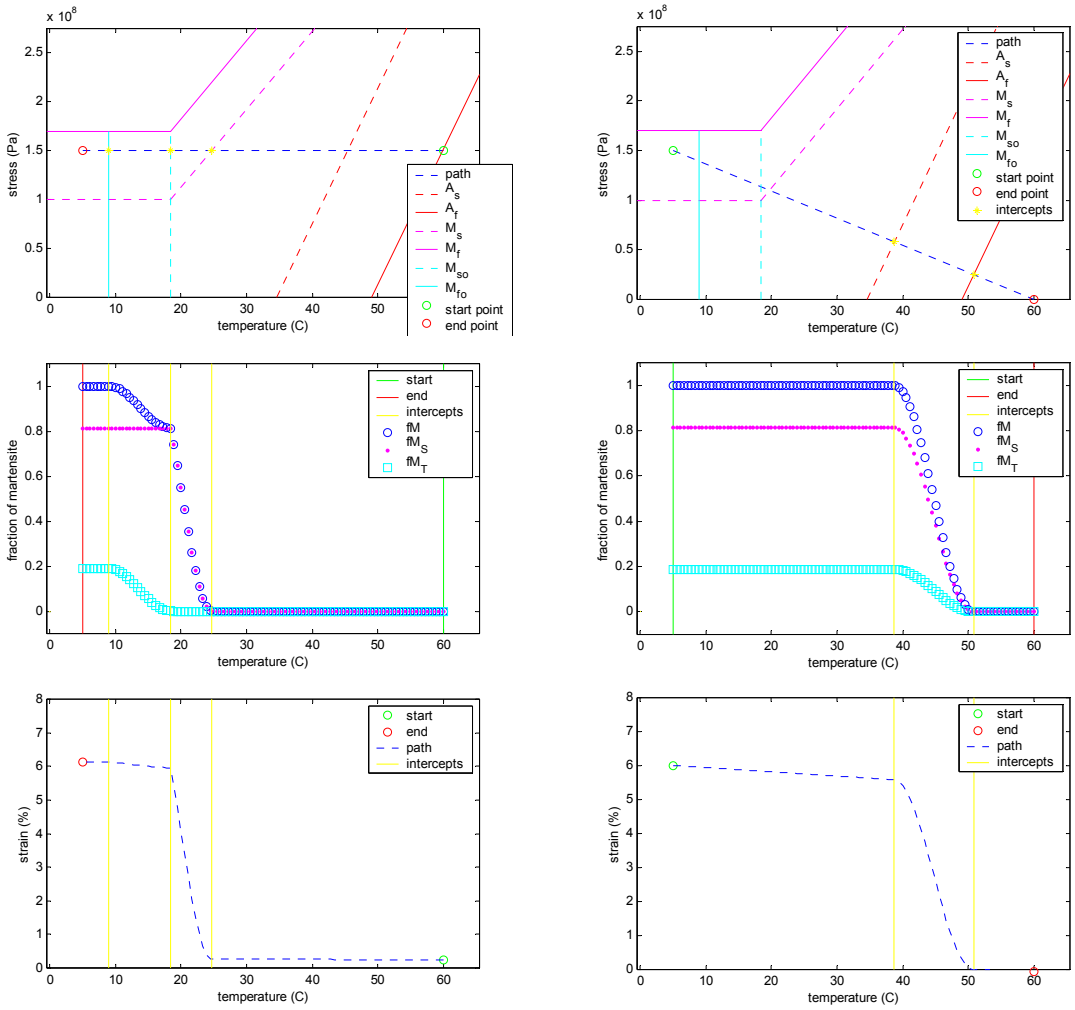

(a) σ = 150 MPa. (b) Decreasing stress.

Figure 2.12: Path in stress-temperature space, fractions of martensite and strain: (a) constant stress cooling for $\sigma_s^{cr} < \sigma < \sigma_f^{cr}$, (b) heating with decreasing stress.

Position in stress-temperature space determines a material's phase composition as well as strain. Figures 2.10 through 2.12 are slices from this space. Figure 2.13 shows the continuum for strain as a function of temperature at a series of constant stresses.

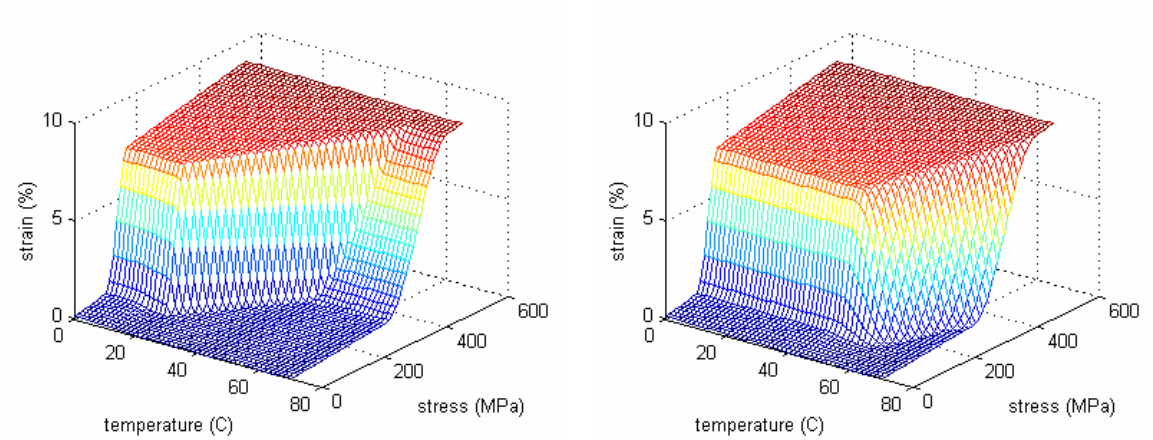

(a) Cooling. (b) Heating.

Figure 2.13: Stress-temperature-strain continuum for temperature range from 0 to 70 °C: (a) constant stress cooling, (b) constant stress heating.

One should note that although the plots shows a continuous surface they are only valid for paths that follow a constant stress between the same temperature limits as those in the plot. For example, consider varying stress from 0 to 600 MPa at a constant temperature of 40 °C. Which plot, heating or cooling, applies to increasing stress? At 40 °C and 200 MPa, each plot would give a different strain. Assume the previous temperature was 50 °C, so the cooling plot applies. When stress reaches 600 MPa and begins to decrease, these plots would indicate that strain drops with the stress. Actually, strain is maintained until shape recovery happens, at temperatures above A_s, as demonstrated in Figure 2.12 (b).

The same sorts of problems occur if one tries to apply the plot to a reduced temperature range. This is because, the "back wall" on the cooling plot, the range of strains corresponding to temperatures above M_s, is set at the maximum stress level attained during heating. Figure 2.14 shows the same plot as in Figure 2.13, but with the maximum temperature reduced from 70 °C to 55 °C. Notice how the stress levels for a given strain differ between the two figures. If an application worked between 0 and 55 °C, strains pulled from Figure 2.13 would be inaccurate.

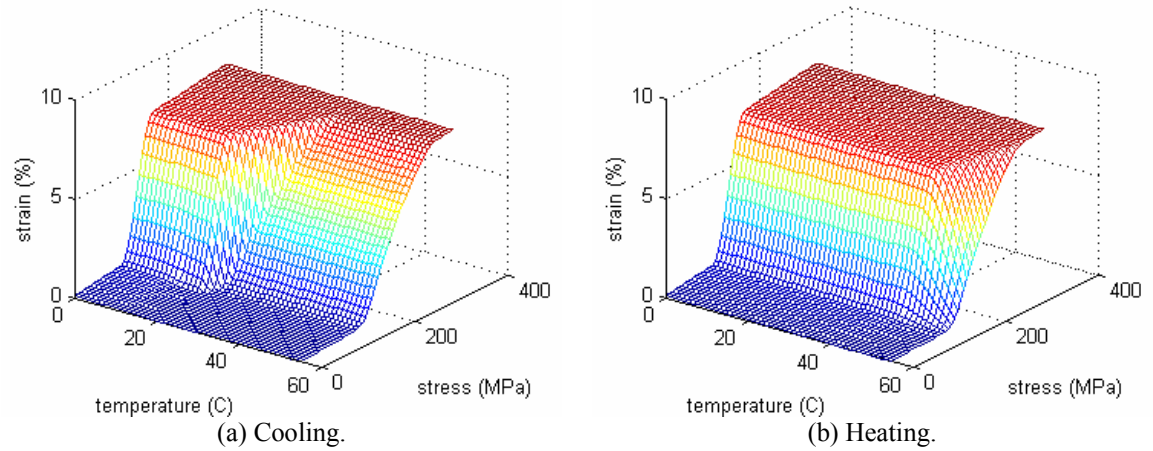

(a) Cooling. (b) Heating.

Figure 2.14: Stress-temperature-strain continuum for temperature range from 0 to 55 °C: (a) constant stress cooling, (b) constant stress heating.

These comparisons reiterate the strong path-dependency of SMA behavior. Unless an application only operates in two state dimensions, there is no easy way to pre-determine the condition of the material. For example, if temperature and stress are known, strain cannot simply be pulled from a plot or table. This characteristic complicates analysis of SMA applications.

Chapter 3: SMA Heat Engines - Prior Art

3.1 Overview

SMA heat engines convert thermal energy into mechanical energy using shape memory alloy material. The state of the art in SMA heat engines has been determined by a thorough patent search. The US Patent and Trademark Office permits individuals to perform low-volume patent searches on their Internet database (http://www.uspto.gov/). Through their facilities, one can perform a variety of searches based on keywords, patent classes and patent numbers. Table A-3.1 is a collection of US patents relating to shape memory alloy heat engines, issued between 1968 and January 2002. Arranged in descending order by patent number, this table details the evolution of the SMA engine since it was first introduced by Ridgway Banks in 1974. Some patents listed in Table A-3.1 do not directly relate to shape memory alloy heat engines, but are related to either SMA's or heat engines.

J. J. Zhu and colleagues suggest that engine concepts can be divided into four categories: offset crank engines, turbine engines, field engines and miscellaneous engines [17]. While reviewing patents, I found it convenient to separate the concepts into six categories based on their driving mechanism. The fifth column in Table A-3.1 gives these rough distinctions as the engine type: crank, pulley, field, swash plate, reciprocating and sequential. Descriptions of each type are included in the following sections.

Journal articles related to crank and pulley engines were reviewed to complement the patent results. The prototype is a crank engine; accordingly, the crank section is discussed in some detail.

3.2 Crank Engines

3.2.1 General

Crank engines convert the reciprocating linear motion of an SMA actuator into continuous rotary motion, by eccentrically connecting the actuator to the output shaft. The actuators are often trained to form extension springs. Some configurations require a flywheel to drive the crank through the mechanism's limit positions. Examples of patented crank engines are shown in Figures 3.1 (a), (b) and (c). An interesting component of the engine in Figure 3.1 (a) is its synchronizer (label 8). The synchronizer forces the cranks (label 2) to keep the same relative orientation while rotating in opposite directions. Twenty of the patents listed in Table A-3.1 can be classified as crank engines. Crank related papers include references [18][19][20].

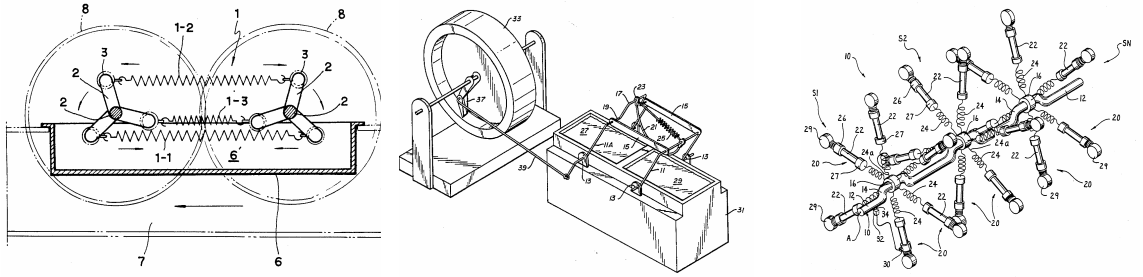

(a) US4683721. (b) US4691518. (c) US5279123.

Figure 3.1: Patented crank engines.

3.2.2 Counter-Synchronized Twin-Crank Engine

Zhu published a two-part paper in 2001 on a specific form of the crank engine. The first part derived general constitutive equations for SMA's and the second part used those equations to simulate the operation

of a twin-crank engine [17][20]. Simulation results were compared to experimental research conducted on the engine by Iwanaga in 1988 [21]. Figure 3.2 is a schematic diagram of a twin-crank heat engine. Although the engine of reference [21] used six SMA springs with cranks offset by 60°, instead of the four springs and 90° offsets shown, the concept is still the same. Figure 3.3 is an end-view with two of the four springs represented. The red and blue springs in this figure correspond most closely to springs *S1* and *S3* respectively, of Figure 3.2.

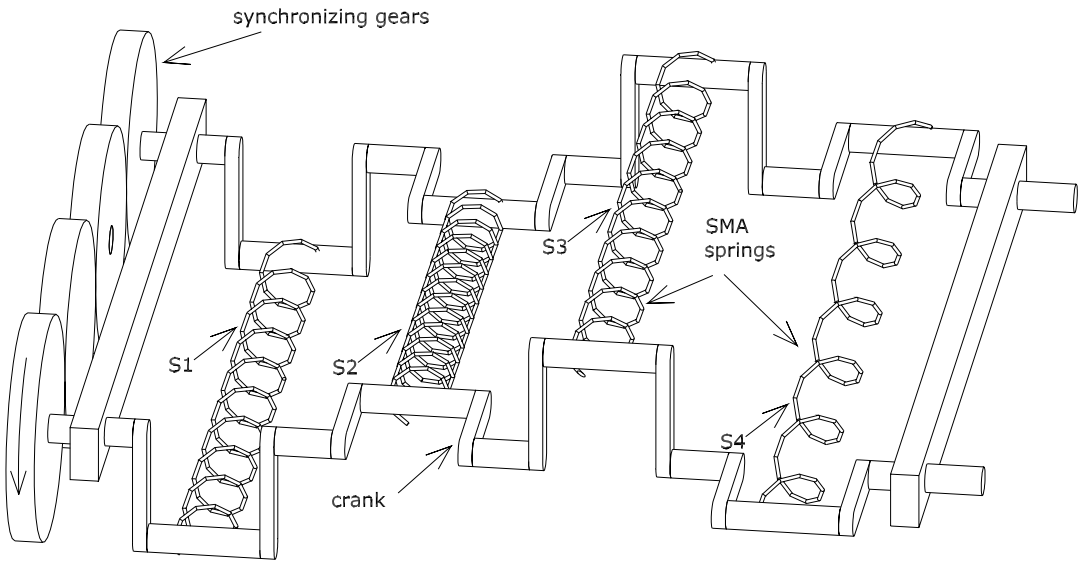

Figure 3.2: Diagram of a counter-synchronized twin-crank engine.

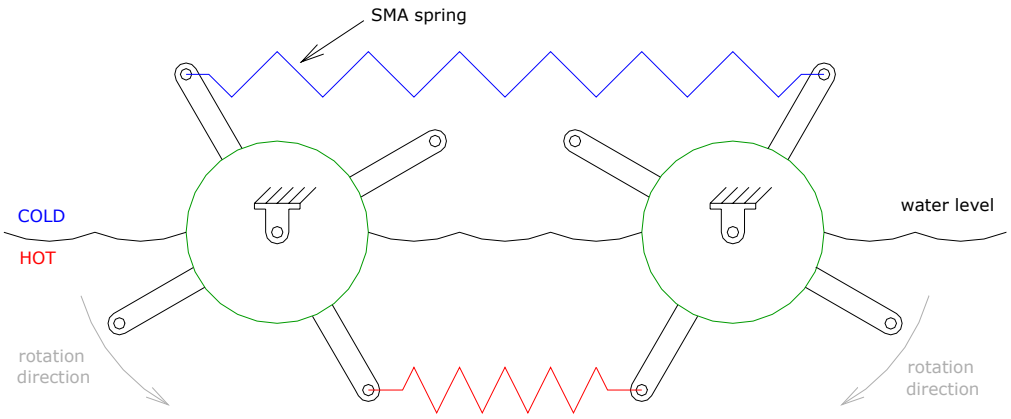

Figure 3.3: Simplified end-view of the twin-crank engine.

This engine consists of SMA coiled springs, labeled *S1*, *S2*, *S3* and *S4*, connected between identical parallel crankshafts. SMA springs contract when heated but are extendable when cool. In Figure 3.3, the hot side is above the A_f transformation temperature while the cold side is below M_f. The force with which a heated spring contracts is greater than that required to deform a cold spring. This force imbalance drives the engine. Each spring is uniformly constructed such that its fully contracted length is slightly less than the minimum distance between aligned cranks. A heat sink (room-temperature air) and heat source (hot-water bath) are located above and below the center plane of the engine, respectively. Four identical synchronizing gears force cranks on the first shaft, and corresponding cranks on the second shaft, to keep a symmetric,

and opposing, orientation. Since cranks rotate in opposite directions, this will be referred to as a counter-synchronized engine.

To illustrate operation, assume that *S1* starts in the high temperature area. Since the temperature is higher than A_f, *S1* tries to contract. At the same time, *S2* is poised to leave the high temperature section while *S4* is about to enter from the cold side. The contraction of *S1* forces *S2* out of the heat and into the cooler area. Although both *S1* and *S2* are in their high temperature states, the perpendicular distance between the spring and its axis of rotation is greater for *S1*. Torque is proportional to distance from the axis of rotation, thus the torque produced by *S1* is at a maximum while that produced by *S2* is nearly zero. Consequently, *S1* has a mechanical advantage and overpowers *S2*. As *S2* is forced out of the heat, *S4* is drawn in. When *S4* reaches its most assertive point, *S1* will be pushed out of the hot area and begin to cool. Cooling softens the spring and allows it to stretch, as the engine rotates with the contraction of *S4*. *S1* continues to stretch until it reenters the high temperature area, and starts the cycle anew.

This style of engine is either dimensionally restrictive or plagued by low efficiency. Consider the special case illustrated in Figure 3.4. In this orientation, two of the springs align with the axis of rotation; thus, they do not generate torque. As shown, the crank radius, *r*, also happens to equal the perpendicular distance, r_p, between the force and rotation axis.

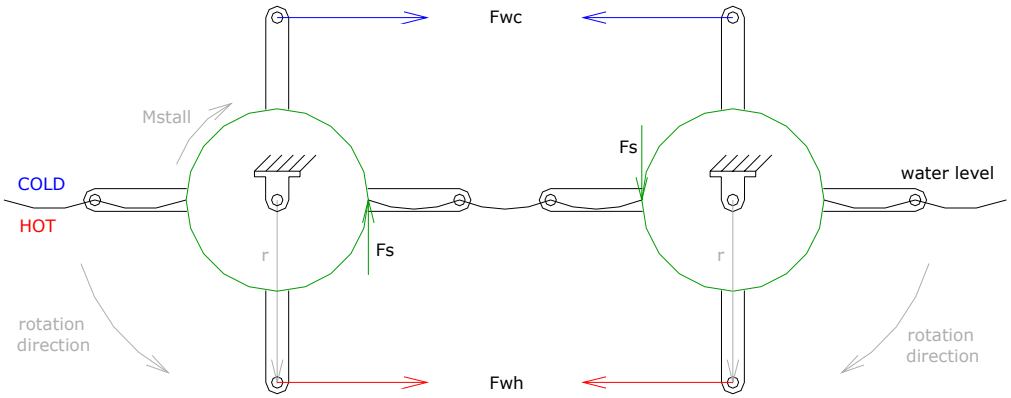

Figure 3.4: Schematic of static forces in a counter-synchronized crank engine.

Summing moments about the center of each crankshaft and solving for the torque required to prevent rotation, M_{stall}, yields

$$M_{stall} = 2r_p(F_{wh} - F_{wc}) \tag{3.1}$$

where, F_{wh} and F_{wc} are forces in the hot and cold springs, respectively. Since the synchronizer force, F_s, is common to both crankshafts, its effects cancels and do not appear in the equation. With two contributing wires, equation (3.1) is only valid for the four-wire engine when it is oriented as shown. However, for two wires, with 180° between adjacent cranks, this equation is the general expression for stalling torque in any orientation. Total stalling torque, for engines with multiple pairs of opposing wires, is the summation of stalling torques for each pair.

To increase torque, one could increase the crank radius or the force difference between hot and cold springs. For a given type of wire, operating between set temperature limits, the forces are fixed. Crank radius, for this design and a given strain, is determined by the distance between crankshafts.

Referring to Figure 3.2, springs are longest at the position of *S4* and shortest at the position of *S2*. The difference in length between these extremes is equal to four times the crank radius. SMA springs can accommodate large changes in length without overstraining the wire; however, if this design were to use straight SMA wire it would be poorly proportioned.

For example, consider straining a straight wire to a repeatable 4%. If the wire were 25 cm long, the total length change would be 1 cm, making each crank 0.25 cm in length. With such small cranks, it would be difficult to separate the heat source and sink while still being able to cycle the wires between the two temperature regions.

The motivation for using straight wire instead of coiled springs is an improvement in efficiency. Springs operate in torsion, the wire twists as the spring extends. At the conclusion of their study, Zhu and colleagues suggested that the potential efficiency of a torsion-based engine is much less that that of an engine driven by uni-axial tension [20]. This is because the shape memory effect is more efficient when contracting than when untwisting.

3.3 Pulley Engines

Pulley engines use continuous belts of SMA wire as the driving mechanism. A pulley engine can be unsynchronized or synchronized. Pulley related papers include references [11][18][19][22][23][35].

3.3.1 Unsynchronized

In unsynchronized engines, the pulleys are free to rotate independently of one another. The only link between different elements is rolling contact with the wire loops. For example, there is no gear train forcing the pulleys to keep the same speed or phase relationship. Engines of this type usually operate in bending, extracting work as a bent wire straightens when heated. Figure 3.5 shows two unsynchronized pulley engines.

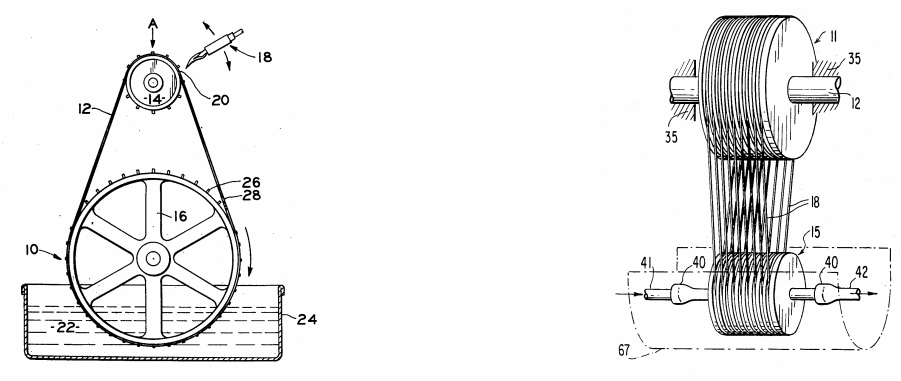

(a) US4010612. (b) US4275561.

Figure 3.5: Patented unsynchronized pulley engines.

3.3.2 Synchronized

Synchronized engines are constrained such that their pulleys rotate in a fixed relationship. Synchronization is commonly used to ensure that two shafts turn at the same speed or keep the same relative orientation. This is useful for holding the tension caused by heating a restrained wire. If the engine is set up properly, the taut wire will cause the entire engine to rotate in whatever direction reduces the tension. Figure 3.6 shows three examples of synchronized engines.

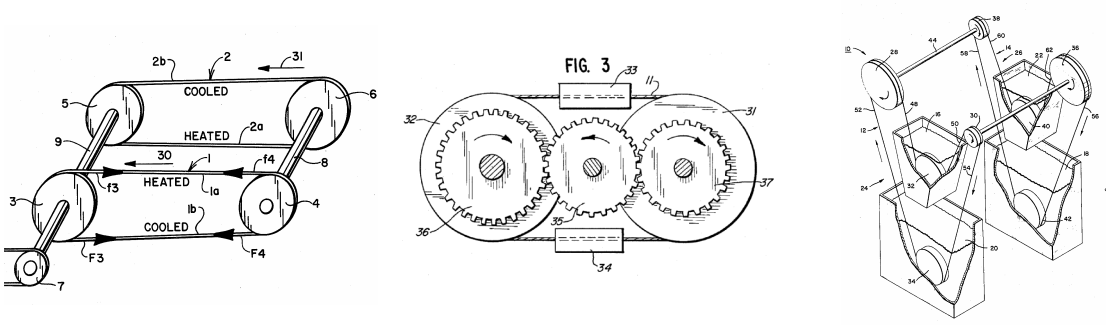

(a) US4150544. (b) US4246754. (c) US4305250.

Figure 3.6: Patented synchronized pulley engines.

Pulley engines are usually based on friction, instead of a positive connection. They are susceptible to losing power when the loops of SMA wire slip on the pulleys.

3.4 Field Engines

This category includes engines that work against a recovering force, such as a gravitational or magnetic field. In the engines of Figure 3.7, a series of attractive elements, such as weights, are attached along a loop of SMA wire. Heating a section of the loop will cause the wire to contract and increase the element density in that area. The denser section will be drawn toward the force field (gravity), creating a rotation.

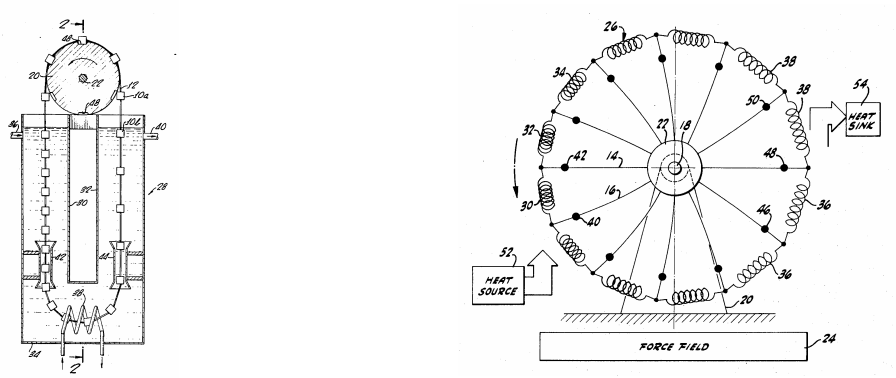

(a) US4027479. (b) US4281513.

Figure 3.7: Patented field engines.

3.5 Swash Plate Engines

Swash plates are similar to cranks except that their axis of rotation is roughly parallel to the direction of the applied force, instead of perpendicular as for cranks. The concept is well suited for SMA wires, in that small but powerful displacements are converted directly into bulk rotations. Figure 3.8 illustrates two machines that operate on the swash plate principle.

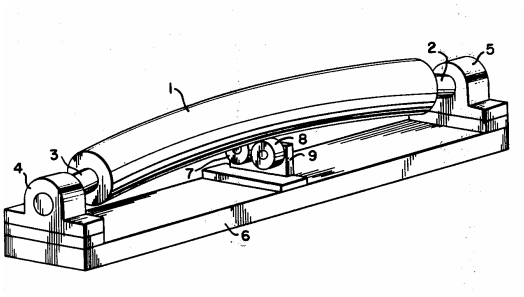

(a) US4175390.

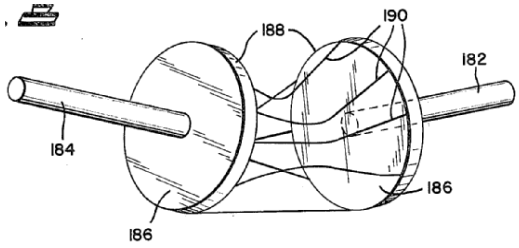

(b) US4305250.

Figure 3.8: Patented swash plate engines.

Figure 3.8 (a) shows a bowed elastic rod. Bending the shape compresses material on the inner surface and stretches material on the outer surface. When heat is applied to the inner surface, thermal expansion forces the machine to rotate, thus moving the hot expanding material to the stretched outer surface of the rod. Although the patent does not specifically relate, the concept could be applicable to SMA material.

3.6 Reciprocating Engines

Reciprocating engines operate linearly, in a back-and-forth fashion, as opposed to cyclically. SMA's are best suited for axial strain and recovery. The challenge with reciprocating engines is thermally cycling the wire without physically moving it between temperature regions. Many times, external pumps are used to circulate heating and cooling fluids over the wires, inevitably lowering overall efficiency. Figure 3.9 (a) shows a piston head actuated by hollow SMA coils. Figure 3.9 (b) illustrates a band of parallel wires that connect to a piston by way of a linkage plate.

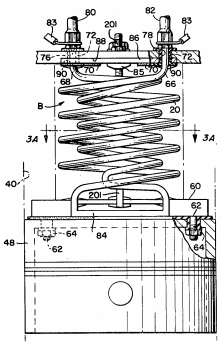

(a) US4434618.

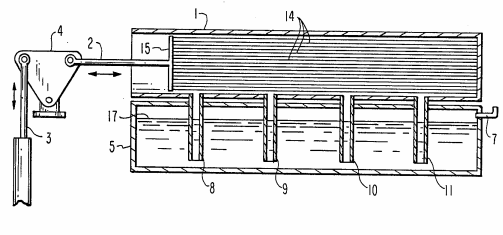

(b) US4759187.

Figure 3.9: Patented reciprocating engines.

3.7 Sequential Engines

Sequential engines move with small, powerful steps, which sum to substantial displacements. They work like an inchworm, extending the front part by a small step and then pulling the back part along. With the back part nearby, the front part can extend again. Figure 3.10 (a) is a hollow, tubular gear, made from SMA material that meshes with a conventional gear. When sequentially heated, the gear teeth attempt to straighten, push off the meshing gear and rotate. Figure 3.10 (b) actually shows an electrically actuated wax motor, but is a good example of the sequential, inchworm concept. In the figure, the bellows (label 76) expand and contract in succession to propel the entire assembly along its path.

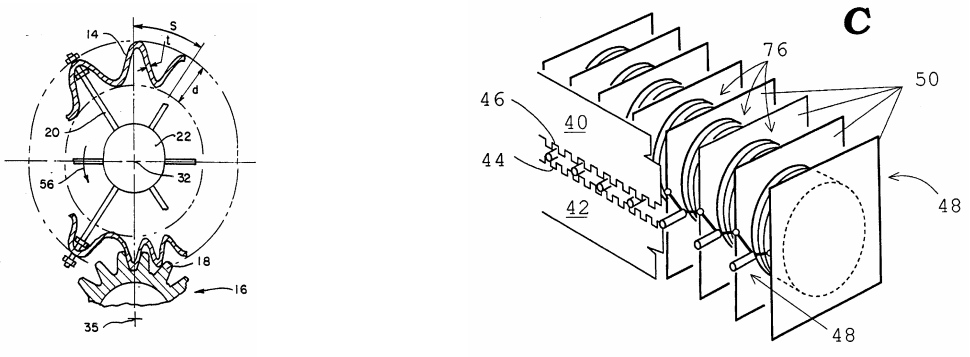

(a) US4938026. (b) US5901554.

Figure 3.10: Patented sequential engines.

3.8 Novel Contribution

After surveying the state of SMA heat engine technology, I believe the proposed design is a novel contribution. The closest related concept is the Iwanaga engine, similar to that shown in Figure 3.2. Both involve SMA material stretched between synchronized crankshafts. While the Iwanga engine is counter-synchronized, cranks in the proposed engine rotate in the same direction (same-synchronized). This advance eases dimensional constraints and makes using straight SMA wire a practical alternative to less efficient coil springs. A description and analysis follow to substantiate the supposition that the proposed design represents a marked improvement over previous crank engine concepts.

Chapter 4: Analysis and Design

4.1 Engine Description

4.1.1 Structure

The proposed SMA engine consists of two parallel crankshafts; each supporting multiple (six in the prototype) evenly spaced cranks. Every crank on the first shaft aligns with a like oriented but slightly shorter crank on the second shaft. A synchronizer connects the shafts and prevents them from rotating relative to one another, thus keeping the two sets of cranks in perfect phase. The prototype engine uses a timing belt and two identical pulleys for this purpose, although other means are possible. Lengths of SMA wire stretch between rollers, located at the end of each crank. Rollers reduce the friction that would be created if the wire slid over the cranks directly. The entire assembly sits between two thermal reservoirs, which heat one side of the engine while cooling the other. Hot water and room-temperature air are used for the prototype. Figure 4.1 is an illustration of the concept.

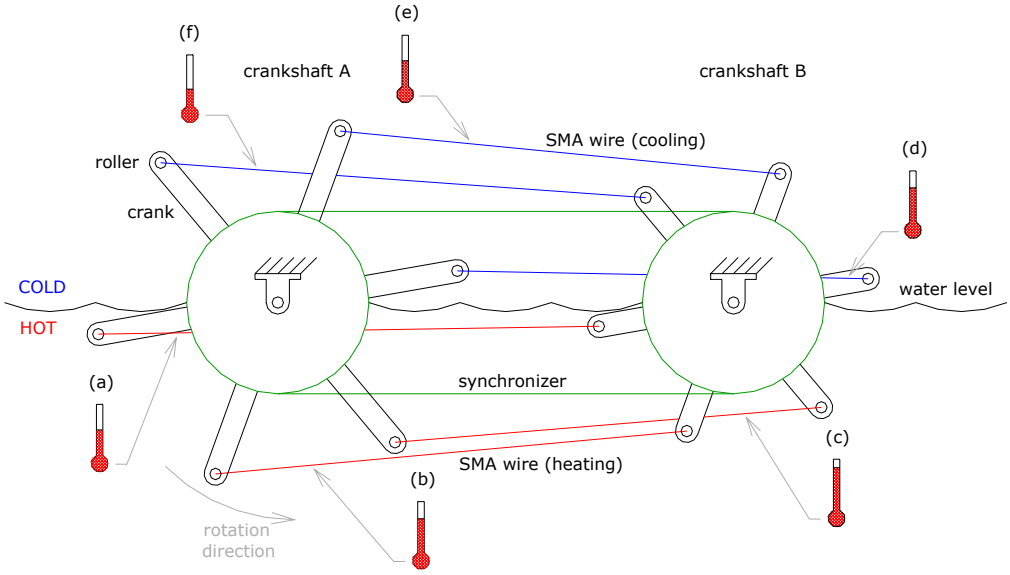

Figure 4.1: Schematic of the proposed, same-synchronized crank engine. Thermometer symbols indicate relative wire temperature.

Although the synchronizer forces both shafts to rotate in the same direction and at the same rate, the aligned cranks do not have the same length. Consequently, the distance between rollers changes with angular position, as shown for a single set of cranks in Figure 4.2. In the figure, crank A is the longer of the two. Note that the maximum wire length occurs when both cranks are horizontal and pointing toward the left. Likewise, the minimum distance between rollers is achieved with the cranks pointing to the right.

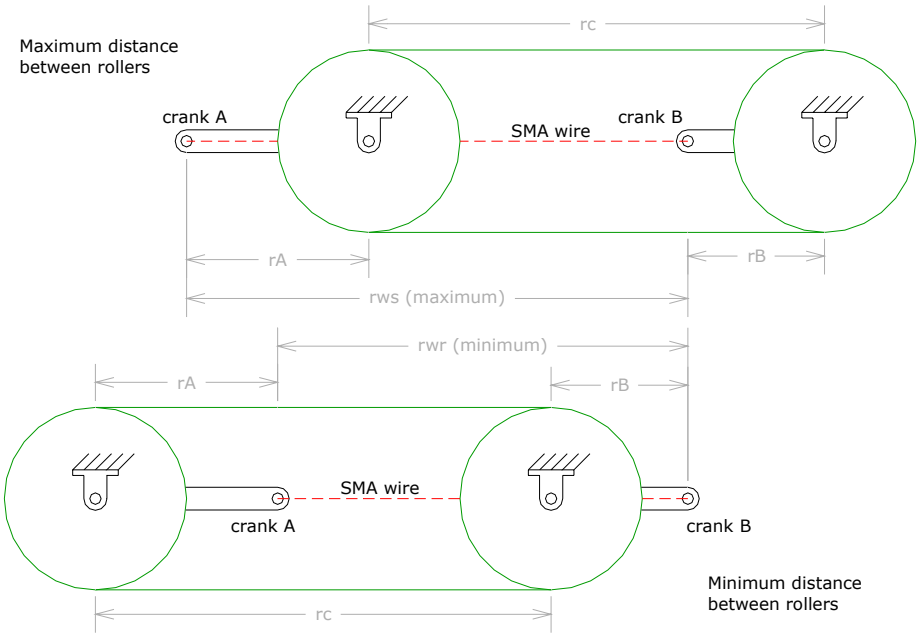

Figure 4.2: Limit positions for a pair of aligned cranks. Labels *rc*, *rws*, *rwr*, *rA* and *rB* represent center distance, wire length - stretched, wire length - retracted, length of crank *A*, and length of crank *B*, respectively.

Accordingly, wire should be installed such that its fully retracted length is just less than the minimum distance between rollers. This keeps the wire taut throughout its rotation. Engine dimensions such as center distance (the distance between crankshafts) and crank lengths, are set to ensure that the maximum distance between rollers does not exceed the wire's recoverable strain. Strains up to 8% may be recovered for a few cycles, but a 4% strain can be recovered reliably for thousands, or even millions, of cycles [1][2d]. The prototype engine strains the wire to 4.2%.

4.1.2 Operation

Heating a stretched SMA wire makes it contract. Consider a wire stretched between two crank rollers. When heated, the most natural way for the wire to contract would be to pull the rollers together by rotating both cranks towards one another. The synchronizer prevents such rotations; therefore, the only way for the wire to contract is for the entire machine to rotate in the direction that shortens the distance between rollers.

During operation, half of the engine's wires are submerged in the hot region while the other half are cooled in the cold reservoir. Wires on the hot side all try to contract, driving the engine in the direction that relieves tension. Wires on the cold side soften as they cool, allowing them to stretch as their rollers move farther apart. Because the force generated during heated recovery exceeds that required for cooled deformation, the recovery process is able to strain the cold wires while propelling the engine.

When a heated wire approaches its fully recovered length, the far right position in Figure 4.2, another heated wire pushes it through the minimum and into the cold region. This other hot wire is able to overpower the one sitting at the thermal boundary because of differences in torque. Torque is proportional to the perpendicular distance between the axis of rotation and the force's line of action. So, the farther a wire is from the engine's midline, the more torque it produces. Viewed from the side, as in Figure 4.2, a wire at either of its limit positions passes directly through the axis of rotation. A wire deep in the heated region will be farther from the midline, produce more torque and be able to overpower those at the boundary.

4.2 Analytical Overview

Subsequent sections address different aspects of engine analysis. Once all the subtopics are developed, they are compiled into a numerical model. The model further illustrates engine operation and shows the implications of changing major design features. While analysis is not the primary objective of this work, observations and modeling help to characterize the engine.

Topics developed in each section are as follows:

- Geometry - engine dimensions such as crank lengths, wire length, crankshaft center distance
- Statics - expressions relating torque to wire stresses, relationship between bearing loads and synchronizer pulley diameter
- Kinematics - relates crank position to wire length and perpendicular moment distance
- Heat transfer - gives wire temperature as a function of time and heating conditions
- SMA behavior - uses the constitutive model to finding stress-strain-temperature relations
- Compilation - combines the components to predict shaft speed and power output

Results from this analysis are compared to limited experimental data, listed in Chapter 6.

4.3 Specifications

Numerical analysis requires numbers. Reliable property data is difficult to find for SMA material. In most cases, the designer has to perform whatever experiments are necessary to find data for their application. Resources for an experimental study were not available, so property data was gathered from journal articles as well as hobbyist and vendor websites. Table A4-1 of Appendix 4 lists these sources and the property values extracted from them. Table 4.1 lists the values used for the computations in this chapter.

Table 4.1: Specifications and estimated material properties used to analyze the prototype engine.

Transformation Temperatures	**Modulus of Elasticity**	**Transformation Constants**	**Martensitic Strain Limit**
$M_f = 42$ °C	$Y_A = 82 \times 10^9$ Pa	$C_M = 14.2 \times 10^6$ Pa/°C	$\varepsilon_L = 8\%$
$M_s = 52$ °C	$Y_M = 28 \times 10^9$ Pa	$C_A = 14.2 \times 10^6$ Pa/°C	
$A_s = 68$ °C		$\sigma_s^{cr} = 62 \times 10^6$ Pa	**Thermoelastic Tensor**
$A_f = 78$ °C		$\sigma_f^{cr} = 160 \times 10^6$ Pa	$\Theta = 0.44 \times 10^6$ Pa/°C
Heat Transfer	**Heating**	**Forced Air Cooling**	**Still Air Cooling**
$\rho = 6450$ kg/m^3	$T_{h\infty} = 85$ °C	$T_{c\infty} = 26$ °C	$T_{c\infty} = 26$ °C
$c = 322$ J/kg/°K	$T_{hsur} = 85$ °C	$T_{csur} = 26$ °C	$T_{csur} = 26$ °C
$e = 0.5$	$h_h = 1500$ W/m^2/°K	$h_c = 150$ W/m^2/°K	$h_c = 100$ W/m^2/°K
Physical Specifications	**Strain**	**Synchronizer**	
$d = 3.81 \times 10^{-4}$ m	$\varepsilon_{max} = 0.042$	$r_s = 2.388$ in (6.064×10^{-2} m)	
$r_A = 7.62 \times 10^{-2}$ m	$\varepsilon_{min} = 0.002$		
$r_c = 0.6477$ m			
$n_c = 6$			
$n_w = 2$			

4.4 Geometry

4.4.1 Basic Dimensions

The engine must be proportioned correctly in order to exploit the wire's small stroke. Dimensions, core to performance, include center distance, crank and wire lengths and strain values. Which quantities are known and which are unknown, depends on the application.

Center distance sets the size and general output potential of an engine. Engines with long center distances can support more SMA wire and produce more power than shorter engines. Obviously, increasing the center distance makes a bigger engine that takes up more space.

Although the relative crank lengths are determined from strain specifications, the overall crank length affects bearing and synchronizer loads and can influence heat transfer characteristics. Longer cranks create larger moment arms. The extra moment must be countered in the synchronizer and supported by the bearings. Heating effectiveness is mentioned because longer cranks extend farther from the engine's midline, perhaps dipping deeper into a thermal reservoir and helping heat transfer.

Wire length is closely related to strain selection. There are three measures related to wire strain: maximum, minimum and range. Range is simply the difference between the maximum and minimum values. Maximum strain affects force generation and wire life: the larger the strain the higher the force and the shorter the life. Range determines the overall difference between the stretched and retracted lengths. Larger ranges accommodate larger differences in crank lengths and thus produce more torque. The minimum strain is that present in the wire at its shortest point. A value slightly greater than zero means the wire never fully recovers and exerts force for the entire heated portion of the cycle. Being continuously taut also reduces the chance of wires becoming entangled.

While any combination of these variables might be known, this derivation assumes that center distance, the length of crank A and the maximum and minimum strains are given. Referring to Figure 4.2, the fully stretched wire length, r_{ws}, is:

$$r_{ws} = r_A + r_c - r_B \tag{4.1}$$

where r_A is the radius of crank A, r_c is the center distance and r_B is the radius of crank B. Similarly, the fully retracted length, r_{wr}, is:

$$r_{wr} = r_B + r_c - r_A \tag{4.2}$$

Stretched and recovered lengths are related to the strain range (change in length divided by original length) according to

$$r_{ws} = (1 + \varepsilon) r_{wr} \tag{4.3}$$

where ε represents the strain range. Setting equation (4.1) equal to (4.3) produces

$$r_A + r_c - r_B = (1 + \varepsilon) r_{wr} \tag{4.4}$$

Substituting equation (4.2) into equation (4.4) for r_{wr} and solving for r_B yields

$$r_B = r_A - \frac{\varepsilon r_c}{2 + \varepsilon} \tag{4.5}$$

Engine torque is ultimately related to the difference in crank radii, Δr

$$\Delta r = r_A - r_B \tag{4.6}$$

Equation (4.5) substituted into equation (4.6) gives

$$\Delta r = \frac{\varepsilon r_c}{2 + \varepsilon} \tag{4.7}$$

showing that the difference in crank radii is only dependent on the strain range and the center distance.

Occasionally it is convenient to know the fully extended and contracted lengths as functions of strain and center distance. These results, found by solving equation (4.2) for r_B and substituting into equation (4.4), are

$$r_{wr} = \frac{2r_c}{2+\varepsilon} \tag{4.8}$$

Substituting (4.8) into equation (4.3) produces

$$r_{ws} = \frac{2r_c(1+\varepsilon)}{2+\varepsilon} \tag{4.9}$$

These relationships completely specify the dimensions relevant to engine operation.

4.4.2 Perpendicular Distances

The perpendicular distances between the wire and crankshafts A and B are denoted r_{pA} and r_{pB}. These quantities are used to find torque. Figure 4.3 illustrates, for a single crank assembly, two possible geometric configurations. θ_x and θ_y are the angles opposite of distances r_{pA} and r_{pB}, respectively. Dimensions and reference marks are shaded light gray.

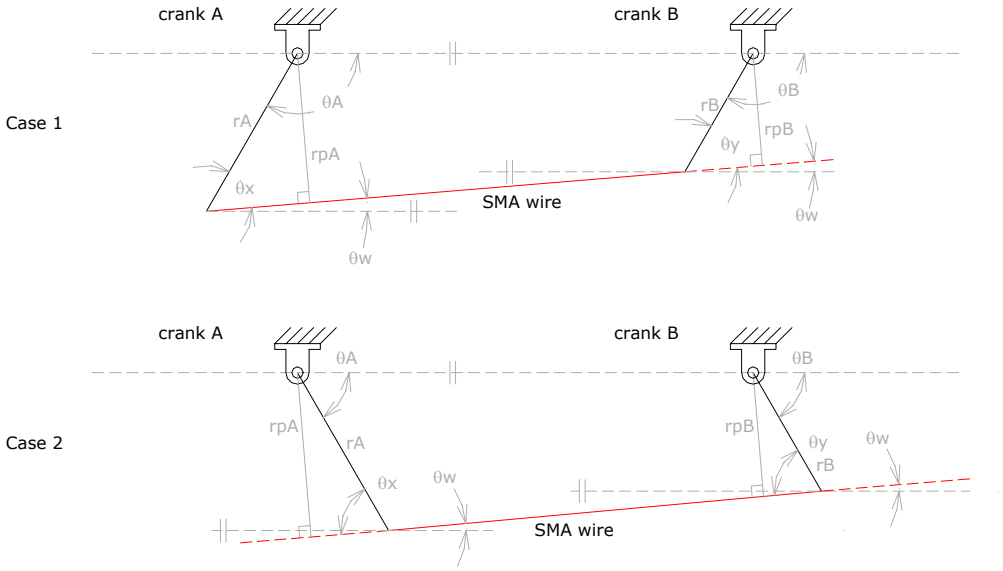

Figure 4.3: Geometry of perpendicular distance between SMA wire and the axis of rotation.

In case 1, the horizontal reference lines for θ_w are parallel to the midline passing through the crankshaft axles. Accordingly, for crank A, the summation of angles θ_A, θ_x and θ_w must equal 180°, making

$$\theta_x = 180 - \theta_A - \theta_w \tag{4.10}$$

Equation (4.11) is applicable to the right triangle formed by r_A, r_{pA} and the SMA wire,

$$\sin(\theta_x) = \frac{r_{pA}}{r_A} \tag{4.11}$$

Combining equations (4.10) and (4.11) yields the perpendicular distance r_{pA}

$$r_{pA} = r_A \sin(180 - \theta_A - \theta_w) \tag{4.12}$$

Repeat for r_{pB} to get

$$r_{pB} = r_B \sin(180 - \theta_B - \theta_w) \tag{4.13}$$

Crank angles θ_A and θ_B are equal, because of the synchronzier, making

$$r_{pB} = r_B \sin(180 - \theta_A - \theta_w) \tag{4.14}$$

Case 2 is handled the same way, resulting in equations (4.15) and (4.16)

$$r_{pA} = r_A \sin(\theta_A + \theta_w) \tag{4.15}$$

$$r_{pB} = r_B \sin(\theta_A + \theta_w) \tag{4.16}$$

Since the sine of an angle has the same value as the sine of 180° minus that angle, equations (4.12) and (4.15) produce the same result, as do equations (4.14) and (4.16). Therefore, either pair of equations can represent both cases. Distance is always taken as a positive quantity in this analysis; so, the sign of the equations is ignored.

4.5 Statics

At first glance, it can be difficult to "wrap your mind around" an engine concept. Discerning why or how an SMA engine moves is especially difficult because of the wire's limited range of motion. Statics relates to the balance of forces that keep an object in stationary equilibrium. Whatever forces prevent rotation are indicative of those produced by the engine. Starting with a single set of cranks, the results will be expanded to represent multiple-wire engines. Figure 4.4 shows the forces acting on an isolated pair of synchronized cranks.

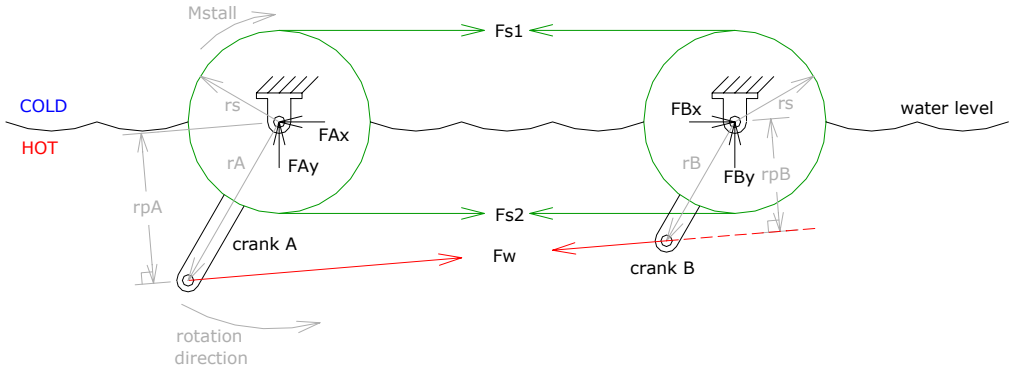

Figure 4.4: Forces between a single pair of synchronized cranks. Labels *rs*, *Fs1*, *Fs2*, *Fw*, *FAx*, *FAy*, *FBx* and *FBy* represent synchronizer radius, forces in each side of the synchronizer, force in the wire and the x and y-components of force at shaft A and at shaft B, respectively.

4.5.1 Torque

In static systems, the sum of the moments must equal zero; else the machine would rotate and not be static. So, consider the two crank assemblies separately and note the external torque, M_{stall}, acting on crankshaft A, as shown in Figure 4.4. The torque represents the load that will stall the engine; that load which perfectly balances the force in the wire and keeps the machine from rotating.

Begin by summing moments about the respective crank centers using a counterclockwise rotation for positive moments:

$$\sum M_A = -M_{stall} + F_w r_{pA} + F_{s2} r_s - F_{s1} r_s = 0 \tag{4.17a}$$

$$\sum M_B = -F_w r_{pB} - F_{s2} r_s + F_{s1} r_s = 0 \tag{4.17b}$$

where,

M_A = moment about the center of crank A
M_B = moment about the center of crank B
M_{stall} = stalling torque
F_w = force in SMA wire
F_{s1} = force in side 1 of the synchronizer
F_{s2} = force in side 2 of the synchronizer
r_{pA} = perpendicular distance for crank A
r_{pB} = perpendicular distance for crank B
r_s = radius of synchronizer pulleys.

Solving equation (4.17a) for M_{stall} and equation (4.17b) for the synchronizer terms gives

$$M_{stall} = F_w r_{pA} + r_s (F_{s2} - F_{s1}) \tag{4.18a}$$

$$r_s (F_{s2} - F_{s1}) = -F_w r_{pB} \tag{4.18b}$$

Since the synchronizer is common to both cranks, (4.18b) can be substituted into (4.18a) to yield

$$M_{stall} = F_w r_{pA} - F_w r_{pB} \tag{4.19}$$

which further simplifies to

$$M_{stall} = F_w (r_{pA} - r_{pB}) \tag{4.20}$$

Equation (4.20) is the torque required to keep a single-wire engine, static. This means that the engine generates equal torque in the opposite direction. Anytime the load is less than the torque given here, the engine will rotate in the direction shown in Figure 4.4.

Keep in mind that this is for one pair of cranks. A single wire can theoretically drive 180° of rotation. To complete a full revolution, an engine needs at least two wires to oppose one another. This way, the hot wire can provide the force to stretch the cold wire. Stretching the cold wire absorbs some of the engine's energy and in so doing, reduces torque output. The net stalling torque for an engine consisting of two sets of cranks, oriented 180° apart, is given in equation (4.21)

$$M_{stall}^{net} = (F_{wh} - F_{wc})(r_{pA} - r_{pB}) \tag{4.21}$$

where, F_{wh} and F_{wc} are the forces in the hot and cold wires, respectively. F_{wc} is negative because cold wires are located in the cooler region, above the midline of the engine. Consequently, any force in the cold wire resists the counterclockwise rotation induced by the heated wire. Counterclockwise is positive by convention, so any force that resists counterclockwise rotation is negative. Both hot-side and cold-side cranks yield identical moment distances, r_{pA} and r_{pB}, because of their perfectly out-of-phase orientation and the convention that distances are always positive.

When working with SMA material, it is more likely to know stress in the wire than the force. Force is simply stress multiplied by the cross-sectional area. Area is assumed constant throughout the cycle for heating and cooling. Also, more than one wire can be stretched between each set of aligned cranks. The prototype uses loops of wire strung between the rollers, effectively doubling the force generated with a single wire. Equation (4.22) accommodates both issues:

$$M_{stall}^{net} = n_w \left(\frac{\pi d^2}{4} \right) (\sigma_{wh} - \sigma_{wc})(r_{pA} - r_{pB}) \tag{4.22}$$

where, n_w is the number of wires between each set of aligned cranks, σ_{wh} and σ_{wc} are wire stresses, and d is the wire diameter. Equation (4.22) represents the net stalling torque for a single pair of opposing wires in the same-synchronized prototype. To find the stalling torque for engines with multiple pairs of cranks, apply equation (4.22) to each pair and sum the results.

Contrast equation (4.21) with the stalling torque for a counter-synchronized crank engine, introduced as equation (3.1) and repeated here

$$M_{stall} = 2r_p(F_{wh} - F_{wc}) \tag{3.1}$$

Both equations apply to a single set of opposing cranks. Since the forces are the same in both equations, the only possible difference is in the distance terms. For a given strain and unstretched wire length, the maximum perpendicular distance in equation (3.1) is the maximum change in wire length divided by 4. The maximum difference in perpendicular distances, r_{pA}-r_{pB}, in equation (4.21) is the maximum change in wire length divided by 2. Equation (3.1) has a factor of 2 built in, therefore both equations yield identical results and there is no difference in stalling torque between a same-synchronized and counter-synchronized engine. Same-synchronized engines, like the proposed design, have the advantage of being able to specify an extra geometric constraint, crank length. In counter-synchronized engines, the change in wire length determines the crank length. In same-synchronized engines the change in wire length and one of the crank lengths, determines the other crank length. The extra degree of freedom eliminates the dimensional problems associated with using straight wires in a crank engine, as mentioned in Chapter 3.

4.5.2 Forces

Aside from torque, statics can be applied to find bearing loads. Friction is proportional to load, so minimizing the bearing load improves performance. Again, consider Figure 4.3, which defines θ_w, and Figure 4.4, which shows forces on a crank assembly. Summing forces at each shaft, and solving for the components of bearing load, results in equation (4.23)

$$F_{Ax} = F_{s1} + F_{s2} + F_w \cos(\theta_w) \tag{4.23a}$$
$$F_{Ay} = weight_A - F_w \sin(\theta_w) \tag{4.23b}$$
$$F_{Bx} = F_{s1} + F_{s2} + F_w \cos(\theta_w) \tag{4.23c}$$
$$F_{By} = weight_B + F_w \sin(\theta_w) \tag{4.23d}$$

where $weight_A$ and $weight_B$ are the effects of gravity on each of the crankshaft assemblies. Positive in the x and y directions is acting to the right and to the top of the figure, respectively. Aside from installation tension, forces in the synchronizer depend on wire tension and dimensioning. To illustrated, equation (4.18b) is solved for the difference in synchronizer forces,

$$(F_{s1} - F_{s2}) = F_w \frac{r_{pB}}{r_s} \tag{4.24}$$

Equation (4.24) shows that the net tension in the synchronizer belt, for a given wire force, is proportional to the ratio between perpendicular distance and the radius of the synchronizer pulleys. Perpendicular distance is tied to crank length; therefore, large pulleys and/or short cranks will minimize belt tension.

Again, the derivation has been for a single wire. For two opposing wires, equation (4.25) gives the difference in synchronizer tension and equation (4.26) lists the components of bearing load

$$(F_{s1} - F_{s2}) = \frac{r_{pB}}{r_s}(F_{wh} - F_{wc}) \tag{4.25}$$

$$F_{Ax} = F_{s1} + F_{s2} + F_{wh}\cos(\theta_{wh}) + F_{wc}\cos(\theta_{wc}) \tag{4.26a}$$
$$F_{Ay} = weight_A - F_{wh}\sin(\theta_{wh}) + F_{wc}\sin(\theta_{wc}) \tag{4.26b}$$
$$F_{Bx} = F_{s1} + F_{s2} + F_{wh}\cos(\theta_{wh}) + F_{wc}\cos(\theta_{wc}) \tag{4.26c}$$
$$F_{By} = weight_B + F_{wh}\sin(\theta_{wh}) - F_{wc}\sin(\theta_{wc}) \tag{4.26d}$$

where, θ_{wh} and θ_{wc} are angles of the hot and cold wires, respectively. In a two wire engine the cranks are separated by 180°, so θ_{wh} and θ_{wc} have the same magnitude but opposite signs.

A belt synchronizer only carries load in one side at a time. Assuming the force in the hot wire is greater than that in the cold wire, side 1 of the synchronizer will be in tension with side 2 in compression. Belts do not carry compression, so if installation tension is ignored, F_{s2} is zero. In multiple-crank engines, there are situations when the tension of a wire on the cold side is higher than the tension, in the opposing wire, on the hot side. Since only one of the two terms will be nonzero at a time, and both terms are positive in equation (4.26), it is not important which side of the synchronizer is loaded. Either term can be assumed zero and the magnitude of the result used in (4.26).

Letting F_{s2} be zero and substituting the absolute value of F_{s1} into equation (4.26) gives,

$$F_{Ax} = \left|\frac{r_{pB}}{r_s}(F_{wh} - F_{wc})\right| + F_{wh}\cos(\theta_{wh}) + F_{wc}\cos(\theta_{wc}) \tag{4.27a}$$
$$F_{Ay} = weight_A - F_{wh}\sin(\theta_{wh}) + F_{wc}\sin(\theta_{wc}) \tag{4.27b}$$
$$F_{Ax} = \left|\frac{r_{pB}}{r_s}(F_{wh} - F_{wc})\right| + F_{wh}\cos(\theta_{wh}) + F_{wc}\cos(\theta_{wc}) \tag{4.27c}$$
$$F_{By} = weight_B + F_{wh}\sin(\theta_{wh}) - F_{wc}\sin(\theta_{wc}) \tag{4.27d}$$

Total load on each set of bearings is the resultant of x and y component forces,

$$F_{A,result} = \sqrt{F_{Ax}^2 + F_{Ay}^2} \tag{4.28a}$$

$$F_{B,result} = \sqrt{F_{Bx}^2 + F_{By}^2} \tag{4.28b}$$

The total bearing load is found by substituting equation (4.27) into equation (4.28). For multiple-crank engines, apply equation (4.28) to each pair of opposing cranks and sum the result. If there are two bearings supporting each crankshaft, each bearing will see half of the predicted load for that shaft assembly.

Statics calculations are simple enough if all of the variables are known; however, all wire forces and the perpendicular distances vary with the angular position of the cranks. Stress, and force, in SMA material depends on its temperature, strain and phase composition, as dictated by the constitutive model. Finding wire stress is addressed in a later section.

Furthermore, r_{pA} and r_{pB}, by definition, must be perpendicular to the line of action of the force. The line of action is simply a straight line between rollers; however, such a line changes with crank angle. Statics is not adequate for determining these angle-distance relationships; that is left to kinematics.

4.6 Kinematics

Kinematics is the study of rigid motion, generally without regard to the forces that cause the motion [24]. Mechanism design and analysis are specialties of the discipline.

4.6.1 Derivation

Each pair of aligned cranks can be thought of as a planar 4-bar linkage consisting of two cranks, the connecting wire and the engine frame as ground. Kinematic position analysis is a convenient means of finding the wire position and orientation as functions of crank angle. Knowing the wire location makes it possible to find the perpendicular distances r_{pA} and r_{pB}, between the wire and the crankshafts. Figure 4.5 illustrates the four-bar linkage concept.

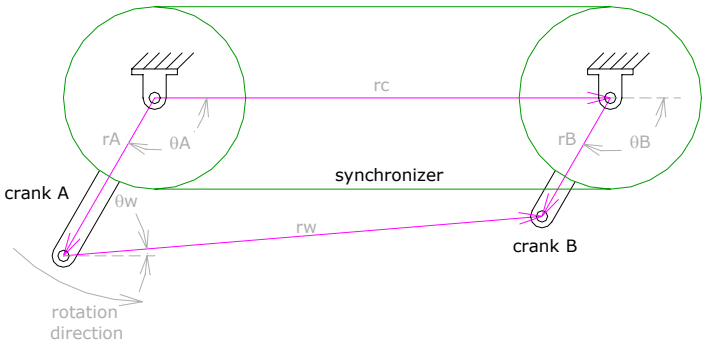

Figure 4.5: Kinematic 4-bar linkage representation for an isolated pair of cranks.

Vectors, shown in magenta, have lengths r_A, r_B, r_w and r_c representing cranks A and B, the SMA wire and the engine frame as ground, respectively. Vector directions θ_A, θ_B, θ_w and θ_g are measured from the horizontal, with positive angles extending in a counterclockwise direction. θ_g is not shown in the figure because it is zero for this case.

Using a technique known as loop closure, each vector is represented as a complex number. Signs are determined according to an arbitrarily chosen loop direction, counterclockwise in this case. If a vector points in the direction of the loop, it is positive; else, it is negative. The loop direction does not matter as long as the representation is consistent. The result is set equal to zero because the vector path starts and ends at the same point.

$$r_A e^{j\theta_A} + r_w e^{j\theta_w} - r_B e^{j\theta_B} - r_c e^{j\theta_g} = 0 \tag{4.29}$$

Using Euler's formula:

$$e^{j\theta} = \cos(\theta) + j\sin(\theta) \tag{4.30}$$

equation (4.29) can be broken into its real and imaginary parts:

$$\text{Real: } r_A \cos(\theta_A) + r_w \cos(\theta_w) - r_B \cos(\theta_B) - r_c \cos(\theta_g) = 0 \tag{4.31a}$$

$$\text{Imag: } r_A \sin(\theta_A) + r_w \sin(\theta_w) - r_B \sin(\theta_B) - r_c \sin(\theta_g) = 0 \tag{4.31b}$$

θ_g is zero and the synchronizer ensures that crank angles θ_A and θ_B are identical. Equation (4.32) reflects these simplifications.

$$\text{Real: } (r_A - r_B)\cos(\theta_A) + r_w \cos(\theta_w) - r_c = 0 \tag{4.32a}$$

$$\text{Imag: } (r_A - r_B)\sin(\theta_A) + r_w \sin(\theta_w) = 0 \tag{4.32b}$$

Physical dimensions of the engine are known. Variables θ_w, r_w and either θ_A or θ_B need to be determined. Since engine rotation is ultimately driven by wire length; r_w will be the independent quantity with θ_w and θ_A the unknowns. This forms a solvable problem of two equations and two unknowns.

Solving the equations of (4.32) is facilitated by squaring and then adding the equations. First, both equations are rearranged such that the terms containing the unknown length are by themselves on one side of the equation. Although all lengths are theoretically known, r_w terms are separated in this case because an expression for r_w will be solvable for θ_A.

The rearranged equations are

$$\text{Real: } r_w \cos(\theta_w) = -(r_A - r_B)\cos(\theta_A) + r_c \tag{4.33a}$$

$$\text{Imag: } r_w \sin(\theta_w) = -(r_A - r_B)\sin(\theta_A) \tag{4.33b}$$

Next, both sides of both equations are squared, as shown

$$\text{Real: } (r_w \cos(\theta_w))^2 = (-(r_A - r_B)\cos(\theta_A) + r_c)^2 \tag{4.34a}$$

$$\text{Imag: } (r_w \sin(\theta_w))^2 = (-(r_A - r_B)\sin(\theta_A))^2 \tag{4.34b}$$

By adding the equations together and applying the identity

$$\cos^2(\theta) + \sin^2(\theta) = 1 \tag{4.35}$$

r_w is separated from the sine and cosine terms as shown

$$\begin{aligned} (r_w \cos(\theta_w))^2 &= (-(r_A - r_B)\cos(\theta_A) + r_c)^2 \\ +\,(r_w \sin(\theta_w))^2 &= (-(r_A - r_B)\sin(\theta_A))^2 \\ \hline r_w^2 &= (-(r_A - r_B)\cos(\theta_A) + r_c)^2 + (-(r_A - r_B)\sin(\theta_A))^2 \end{aligned} \tag{4.36}$$

The simplified expression for wire length is

$$r_w = \sqrt{r_c^2 + (r_A - r_B)^2 - 2r_c(r_A - r_B)\cos(\theta_A)} \tag{4.37}$$

Solving equation (4.37) for θ_A gives

$$\theta_A = \pm\cos^{-1}\left(\frac{r_c^2 - r_w^2 + (r_A - r_B)^2}{2r_c(r_A - r_B)}\right) \tag{4.38}$$

The cyclic nature of the engine allows two crank angle possibilities for a given wire length. Positive angles are toward the cold side and negative angles extend the wire into the high temperature region.

Once θ_A is known, wire angle θ_w is found by rearranging equation (4.32b)

$$\theta_w = \sin^{-1}\left(\frac{(r_B - r_A)\sin(\theta_A)}{r_w}\right) \tag{4.39}$$

At this point, all kinematic quantities are known for a given wire length.

4.6.2 Illustrations

This subsection illustrates the relationships between some of the important geometric and kinematic quantities. The dimensions represented in the following plots are the same as those used in the prototype, except with two cranks shown instead of six.

Figure 4.6 (a) shows the relationship between wire length and crank angle. While the engine is ultimately driven by changes in wire length, the relations are more intuitive when plotted against crank angle. Figures 4.6 (b), (c) and (d) relate strain, wire angle, and perpendicular distances, respectively, to the crank angle.

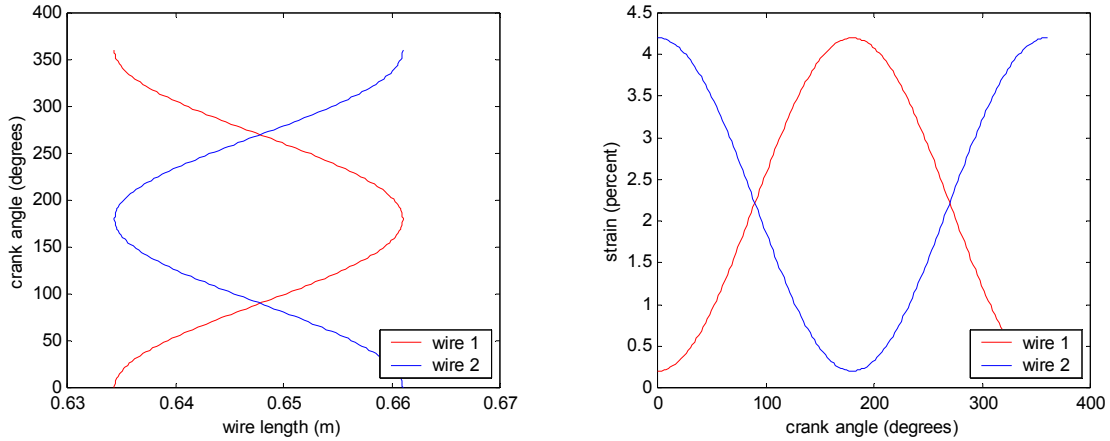

(a) Crank angle versus wire length.

(b) Strain versus crank angle.

(c) Wire angle versus crank angle.

(d) Perpendicular distance.

Figure 4.6: Plots relating geometric and kinematic quantities for a two-crank synchronized engine (r_A = 0.0762 m, r_c = 0.6477 m, ε_{min} = 0.2%, ε_{max} = 4.2%).

4.7 Heat Transfer

Shape memory behavior is largely a function of wire temperature. Being able to predict wire temperature as a function of time, under different thermal conditions, is convenient for design and critical for predicting engine speed. While there are some empirical correlations between experimental temperature data and heating conditions, most apply to wire being resistively heated with electric current [6][14]. Data for heating by hot water bath is not readily available; although, there are expressions for still and forced-air cooling. For consistency, this analysis pulls heating and cooling times from a general heat-transfer equation, but uses the air-cooling relationships as comparison when selecting one of the constants in the theoretical equation.

The wire is thin and the parallel cranks bring the entire length of wire into and out of the hot water at nearly the same time; therefore, the wire temperature is assumed uniform throughout. Heat transfer occurs primarily by convection, but with some heat radiated to or from the surroundings. The change in temperature with time, of a solid rod heated (or cooled) by convection and radiation, is equation (4.40) [25]

$$\frac{dT}{dt} = \frac{-\pi\, d\, h\left(T - T_\infty\right) - \pi\, d\, e\, SB\left(T^4 - T_{sur}^4\right)}{\rho\, c\left(\frac{\pi\, d^2}{4}\right)} \tag{4.40}$$

where,

dT = change in temperature, °K
dt = change in time, s
π = pi
d = wire diameter, m
h = convection coefficient, W/m^2/°K
T = starting temperature, °K
T_∞ = free stream temperature, °K
e = emissivity of the wire
SB = Stefan-Boltzmann constant, W/m^2/°K^4
T_{sur} = temperature of the surroundings, °K
ρ = mass density, kg/m^3
c = specific heat of the wire, J/kg/°K.

To apply this equation, solve for dT and use a small dt value. Each change in temperature is added to the previous starting temperature to get the starting temperature for the next time step. The values for convection coefficient, free stream temperature and the temperature of the surroundings determine whether the equation represents heating or cooling.

For comparison, the empirical expression for convective air cooling of Nickel-Titanium wire, with variables substituted to match those in (4.40), is shown in equation (4.41) [6]

$$t_c = J_c \ln\left(\frac{T - T_\infty}{T_c - T_\infty}\right) \tag{4.41}$$

where,

t_c = cooling time (time required to reach T_c), s
J_c = time constant for cooling
T_c = target temperature, °C

Time constants for still-air cooling (free convection) and "moderate" forced-air cooling (forced convection) are shown in equations 4.42 (a) and (b) respectively

$$J_c = 13.25 + 18.7063\left(d \times 10^3\right)^2 \tag{4.42a}$$

$$J_c = 4.88 + 6.116\left(d \times 10^3\right)^2 \tag{4.42b}$$

Figure 4.7 is a comparison of heating and cooling curves as functions of time. The blue and green curves represent empirical relationships and matching theoretical predictions. The other curves show what is actually used in simulation. Convection coefficient has a substantial impact on engine speed. Manipulating h values turned out to be a convenient way of forcing the numerical model, discussed shortly, to match experimental results, presented in Chapter 6. The chosen values are still within the limits of possibility as listed in reference [25].

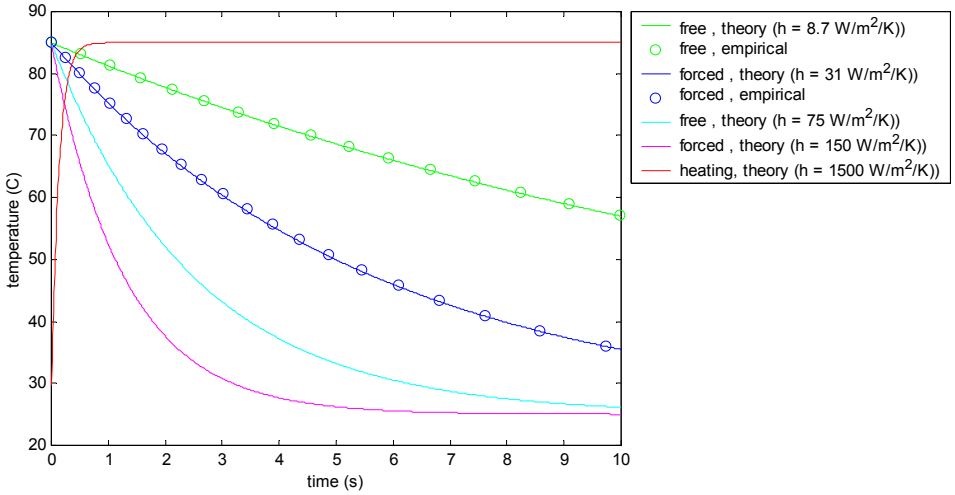

Figure 4.7: Comparison of heating and cooling predictions from theoretical and empirical expressions: $\varepsilon = 0.5$, $\rho = 6450$ kg/m^3, $c = 322$ J/kg/°K.

Note that these relationships are only approximations of the actual phenomenon. Heat transfer is an entire discipline of its own, thorough analysis of which, is beyond the scope of this work. These expressions only need to indicate trends and provide a rough link between time, wire temperature and ultimately, engine speed.

4.8 Shape Memory Alloy Behavior

Engine movement is driven by changes in wire length, strain. Strain is generally dependent on temperature, as introduced in Chapter 2. However, a given temperature does not translate directly into a given strain. Instead, strain is dependent on the temperature as well as the stress, phase composition and previous state of the material. To further complicate the SMA engine problem, all the wires are mechanically linked. Heated wires cannot contract until they generate enough force to stretch the cooler wires. To find strain in any wire, one needs to know the current and previous state of that wire as well as the current and previous states of every other wire in the engine.

Wire behavior is represented by the equations of the constitutive model. Those equations are not presented here. Computer code implementing the model is included in Appendix 4, and the complete description, explanation and derivation of the equations is available in the author's original work [3]. Only the qualitative points, relevant to this study, are discussed.

The constitutive equations consist of two parts. The first part concerns finding the phase composition of the material, that is, the total volume fraction of martensite and the percentage of its two constituents: stress-induced and temperature-induced martensite. Fraction of martensite is a function of the current and previous fractions of martensite as well as the current stress and temperature. The second part of the model is the stress expression. This equation relates stress to strain, temperature and fraction of martensite. Again, both the current and previous conditions are required. The formula can be rearranged to determine strain if stress is known.

Stress, strain and temperature are relevant to engine movement. Fraction of martensite is internal to the wire and only significant as a contributing factor in the stress-strain equation. Ideally, a simulation could handle simultaneous variation of all the important quantities. For a first attempt, this model only adjusts one variable at a time. Two different sections of the continuum are considered: stress as a function of temperature at constant strain and strain as a function of stress at constant temperature. Applying these relationships in succession, with small steps between increments, will approximate engine operation.

To isolate each relation, start from known initial conditions, for example: 100% temperature-induced martensite at 25 °C with no initial stress or strain. Increment one variable, temperature for example. Recalculate fraction of martensite using the new temperature and previous values for all other variables. Now calculate the variable of interest while keeping the third quantity constant; in this case recalculate stress for a constant strain. This new stress is plugged back into the fraction of martensite expression with the next increment in temperature. By starting from valid initial conditions and using small incremental changes, the constitutive behavior is broken into small, manageable pieces.

The two, now separate, relationships are shown in Figures 4.8 (a) and (b). Figure 4.8 (a) illustrates a phenomenon known as restrained recovery. When wire is heated, it tries to contract. If it is restrained from contracting, stress in the wire builds with temperature until it can overcome the restraining force. This corresponds to stress changing with temperature at a constant strain. The starting stress in Figure 4.8 (a) is 56 MPa, which is the load required to elastically strain martensitic material by 0.2%.

Figure 4.8 (b) represents the restraining force's point of view: stretching the wire. Increasing stress produces small, proportional increases in strain, up to the start of phase transformation. Applying additional load yields disproportionately large increases in strain. The stress threshold, for apparent plastic deformation, is higher at higher temperatures. This is the case of strain changing with stress at a constant temperature. Although, strain is the dependent quantity in Figure 4.8 (b), it is shown on the horizontal axis, as is convention for stress-strain plots. Also note, a smaller stress range is plotted for the 60 °C case in order to reduce overlap with the 85 °C curve.

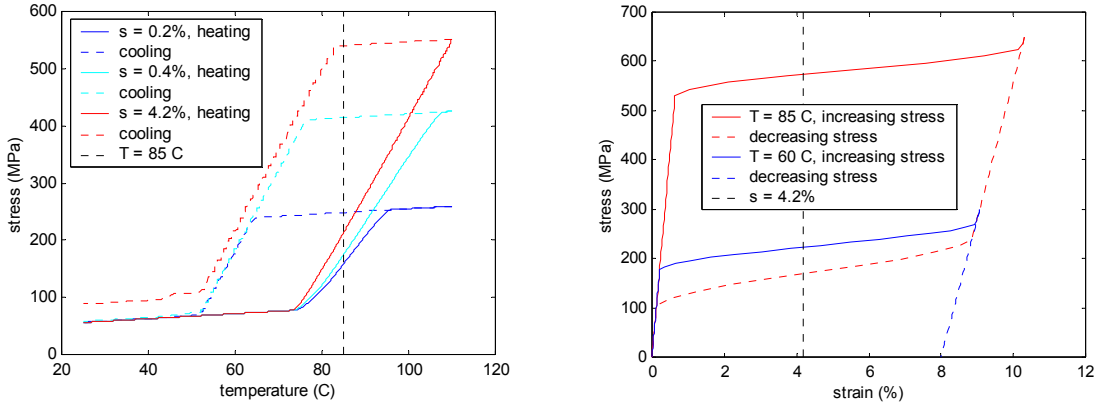

(a) Restrained recovery. (b) Stress versus strain.

Figure 4.8: Constitutive relations: (a) restrained recovery for a series of constant strains, each starting from the same initial stress (b) stress-strain curves at constant temperatures, both starting with zero initial strain.

The path dependency of SMA behavior is reiterated in these figures. In each case, the forward and reverse paths are different. Figure 4.8 (a) shows that, in restrained material, stress increases with temperature and with the amount of strain being retained, an observation confirmed in other works [26]. For small strains, the material is able to transform into austenite when heated, explaining the relatively horizontal path at high temperatures for 0.2 and 0.4% strains. With larger strains, increases in temperature, that drive the material toward austenite, induce larger increases in stress that force the material to remain as martensite. Consequently, the material never fully converts to Austenite and stress does not level off. When wire cools, it holds the stress until its temperature falls below the stress-shifted M_s temperature. Continued cooling, for low initial strains, will return the material to its starting point. For high initial strains, stress levels off at a value corresponding to the amount of strain in the specimen. For example, a material with 4% strain, and a maximum strain limit of 8%, will return to a stress that is approximately halfway between S_s^{cr} and S_f^{cr}.

A full cycle of restrained recovery does not usually occur. Instead, the wire's state changes in small steps, moving alternately along the paths of Figures 4.8 (a) and (b). That is, temperature changes at a constant strain, changing the stress (Figure 4.8 (a)). Next, the new temperature is considered constant while strain varies according to the new stress (Figure 4.8 (b)). The new strain becomes the constant strain for the next increase in temperature (Figure 4.8 (a)). Repeating this loop, for small increments in temperature, fully defines the wire status as a function of temperature. This process is the link between time and engine position.

4.9 Analytical Compilation

Results from previous sections can now be combined into a model to simulate engine motion.

4.9.1 Method

Analysis starts from initial conditions. Starting strain is directly related to the angular position of the cranks, as discussed in the kinematics section. Stress is that resulting from stretching each wire, at ambient temperature, just enough to fit between its respective rollers. To help get the simulation going, wires on the cold side of the engine start from the temperature of the hot water, while wires on the hot side start from the temperature of the cold air. These temperatures are closer to steady state values, and help the simulation to converge quickly.

Due to the nature of SMA material, and thus the constitutive model and its equations, every quantity relies on previous values of that quantity and the other related quantities. This interconnectedness makes it difficult to isolate and solve for any single variable and end up with a meaningful result. Instead, an iterative approach is applied as follows. From heat transfer, temperature is known as a function of time, the independent variable. Time advances by a small step, changing the temperature in each wire by a small amount. Whether the wire temperature increases or decreases, depends on its position, whether it is exposed to cool air or hot water.

The temperature change increases stress in the heated wires and reduces stress in the cooling wires. With new stresses, temperature is considered constant while finding strain. Force in a wire is the stress multiplied by its cross-sectional area. If the sum of forces in the hot wires is greater than the combined effect of external torque load and the sum of forces in the cold wires, the engine will rotate. Rotation changes the strain in every wire; the hot wires get shorter and the cold wires get longer. By changing strain, rotation relieves stress in the hot wires while increasing stress in the cold wires. Therefore, the engine rotates only enough to balances the force imbalance caused by the temperature change. This is a pseudo-static approach. Engine dynamics are never considered.

New stresses, strains, and positions for each wire, become the starting values for the next iteration. Time steps forward and the wire temperatures change again. For small time-steps, the simulation should approach the engine's continuous behavior.

This is the general approach. Specifics of finding stress and strain values depend on whether the wire is on the hot side of the engine or the cold side. Heated wires constantly try to contract against restraining forces imposed by the cold wires. From temperature, the stress in a hot wire is pulled from a plot similar to that in Figure 4.8 (a), except that heating is the only concern, so the cooling path is ignored. When the engine rotates, the computer code creates a new path with the new, lower strain and from that path, picks a stress value that corresponding to the current temperature. The vertical dashed line in Figure 4.8 (a) shows the source temperature for the prototype. So, at 85 °C, the intersection of the vertical line with the path for the particular strain, corresponds to the wire stress. As the strain drops the stress drops. A heating cycle starts with wire strained to 4.2% and ends when the wire reaches 0.2% strain. Notice that if the heat source temperature were higher, the intersections would occur at higher stress values. Higher stresses cause higher forces, which generate more torque.

Cooling values come from plots like Figure 4.8 (b), except since strain always increases on the cold side, only the forward paths are used. Each curve on the plot corresponds to a different temperature. When temperature changes, the new temperature sets the stress-strain path for each cold wire. Then, when the

engine rotates, the stress that corresponds to the new strain becomes the new stress. The vertical line in Figure 4.8 (b) is at the engine's maximum strain value. For a given strain, as the temperature drops the stress drops. Cooling starts at 0.2% strain and ends with 4.2% strain.

Appendix 4 contains the MATLAB code of the simulation.

4.9.2 Output

Figure 4.9 shows simulation results for the prototype engine, under zero-load conditions. Plots (a), (b), (c) and (d) show respectively, curves of wire temperature, stress, strain and crank angle, all against time. Crank angle is measured in degrees, so at 360° the angle resets to 0°. The vertical dotted line at 2.5 s is a convenient reference point for comparing the different measures at a common time.

(a) Temperature.

(b) Stress.

(c) Strain.

(d) Crank angle.

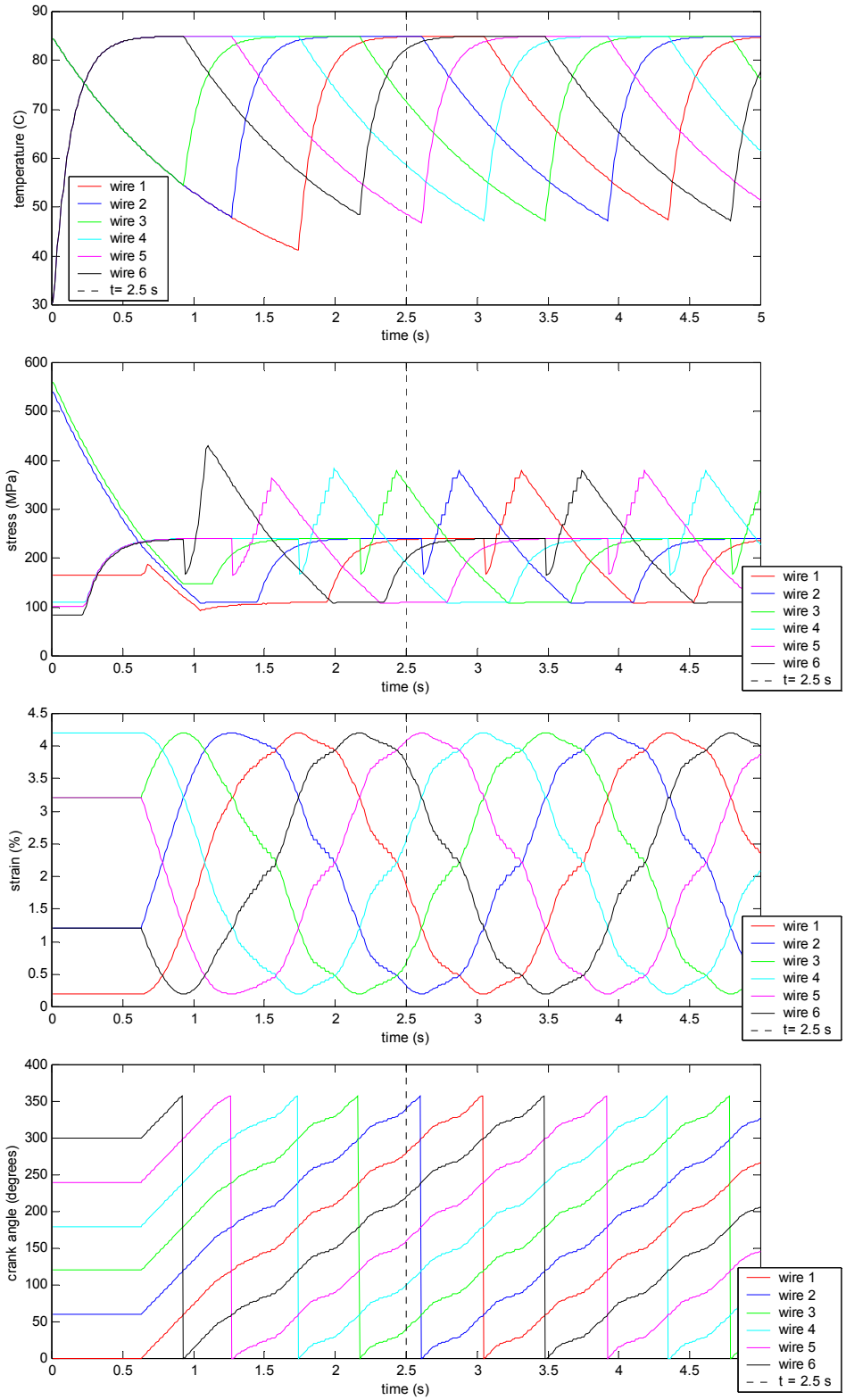

Figure 4.9: Simulation results under zero-load, forced convection conditions.

Crank angles of 180° and over correspond to the heated zone. At the start of simulation, wires 1, 2 and 3 are located on the cold side of the engine with wires 4, 5 and 6 in the hot water bath. Since the temperatures of the cold-side wires start from the water temperature, the engine is stationary for a little over 0.5 s, while the cold-side wires cool and the hot-side wires heat.

When the sum of forces in the hot wires exceeds that in the cold wires, the engine rotates. If the wire temperature of a "cold" wire is still high, rotation will induce large stresses in that wire, which decay as the wire cools.

Figure 4.9 generally represents engine behavior, but there are some problems with this method of simulation. For example, consider the boundary between the hot and cold sides, when strain is at 4.2%. The stress, from curves used to determine hot side values (Figure 4.8 (a)), differs slightly from the stress pulled from cold side curves (Figure 4.8 (b)). This causes the downward spikes, shown in Figure 4.9 (b), corresponding to when the wires first leave the hot water bath. Stress should not decline until the wire has had more time to cool. Startup is also misleading. In reality, cold wires do not start from a high temperature and thus, instead of sitting stationary for 0.5 s, the engine moves abruptly when first placed in the hot water.

4.10 Implications

As briefly mentioned in the section on heat transfer, the simulation uses convection coefficients that make the zero-load shaft speed match experimental results. Since the model matches the experiment in a base configuration, it should be possible to adjust parameters and see trends in the output.

4.10.1 Shaft Speed

Steady-state shaft speed comes from graphs like Figure 4.9 (d). Once startup fluctuations have leveled out, the speed is determined from the time it takes to complete one revolution. For example, the time between instances when a particular wire reaches a crank angle of 0°, is the cycle time. Sixty divided by the cycle time is shaft speed in revolutions per minute. This is an average value. The engine rotates faster during some portions of the cycle than during others.

4.10.2 Power Output

Power output is torque multiplied by shaft velocity,

$$P = M_{load}\,\omega \tag{4.43}$$

where, P is power, M_{load} is the imposed torque and ω is shaft velocity. Rotation direction is not a concern so speed, the magnitude of velocity, can be used. With adjustments for units, equation (4.44) gives shaft power in Watts, for a load torque in N-m and a speed, N, in rpm:

$$P = \frac{2\pi\, M_{load}\, N}{60} \tag{4.44}$$

4.10.3 Trends

Graphs in this section illustrate changes to the base configuration and their predicted effects. The base configuration is that of the prototype under forced convection, as given in Table 4.1. Figures 4.10 (a) and (b) show average shaft speed and power output as functions of load for different numbers of cranks, n_c, and numbers of wires per crank, n_w. For any configuration, there is a maximum load, above which, the engine will not rotate. The curves of Figure 4.10 end within 0.1 N-m of these loads.

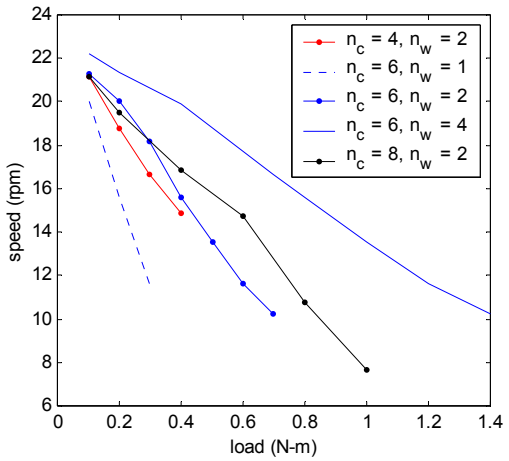

(a) Speed versus load.

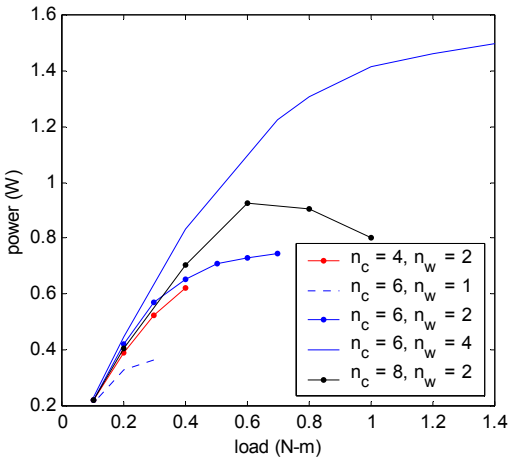

(b) Power versus load.

Figure 4.10: Shaft speed and power output as functions of torque load, under forced convection.

The solid blue line, with superimposed dots, represents the base configuration. Shaft speed is inversely proportional and linear with respect to load. Power output increases with the number of cranks or wires per crank. Aside from creating more power, additional equally spaced cranks smooth out spikes in the stress profile (Figure 4.9 (b)). A more uniform profile should result is smoother operation.

Figures 4.11 (a) through (d) show effects of varying reservoir temperature, at a fixed load. Results indicate that the engine will not run if the hot-side temperature is less than 81°C or the cold side is above 56 °C.

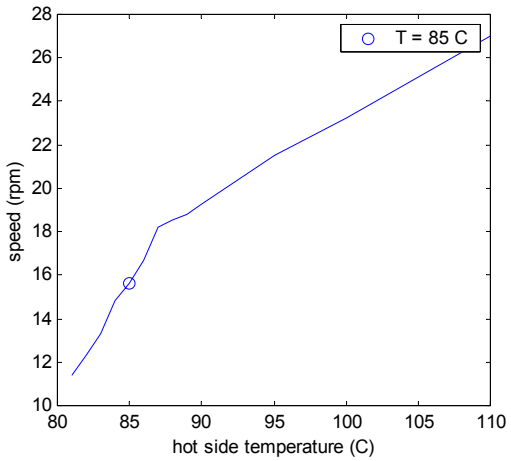

(a) Speed versus hot reservoir temperature.

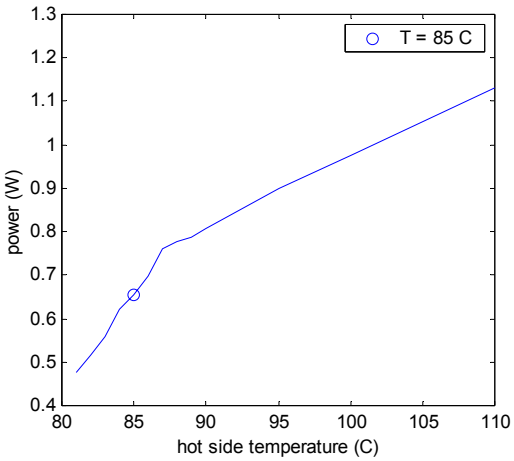

(b) Power versus hot reservoir temperature.

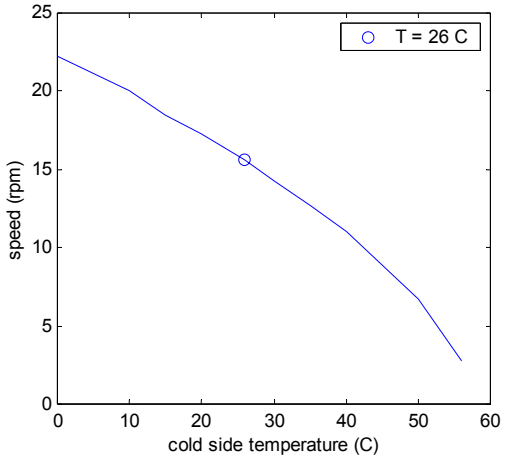

(c) Speed versus cold reservoir temperature.

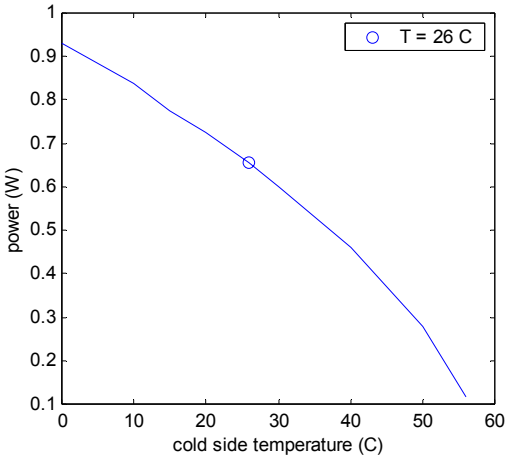

(d) Power versus cold reservoir temperature.

Figure 4.11: Shaft speed and power output as functions reservoir temperature for a fixed load of 0.4 N-m, under forced convection.

Table 4.2 lists other design variations and their results. The highlighted row is the predicted maximum power output for the prototype engine, as built.

Table 4.2: Shaft speed and power output for different operating parameters.

Configuration (base case is with all values as shown in Table 4.1)	Cycle Time (s/rev)	Shaft Speed (rpm)	Power Output (W)
base case, forced convection, no load,	2.65	22.6	-
base case, free convection, no-load	4.96	12.1	-
base case, forced convection, load = 0.7 N-m	5.88	10.2	0.748
Power and speed versus wire diameter			
forced convection, load = 0.4 N-m, d = 7.62 x 10^{-4} m	5.61		0.448
forced convection, load = 0.4 N-m, (base case: d = 3.81 x 10^{-4} m)	3.84	15.6	0.654
forced convection, load = 0.4 N-m, d = 1.91 x 10^{-4} m	no rotation	-	-
forced convection, load = 1.4 N-m, d = 7.62 x 10^{-4} m	7.14	8.40	1.23
Power and speed versus center distance			
forced convection, load = 0.4 N-m, rc = 0.972 m (150% of base case)	3.18	18.9	0.790
forced convection, load = 0.4 N-m, (base case: rc = 0.648 m)	3.84	15.6	0.654
forced convection, load = 0.4 N-m, rc = 0.324 m (50% of base case)	no rotation	-	-
Maximum load versus number of cranks (max torque to within 0.1 N-m)			
forced convection, load = 1.6 N-m, nc = 12	12.12	4.95	0.829
forced convection, load = 1.3 N-m, nc = 10	9.80	6.12	0.833
forced convection, load = 1.0 N-m, nc = 8	7.84	7.65	0.801
forced convection, load = 0.7 N-m, (base case: nc = 6)	5.88	10.2	0.748
forced convection, load = 0.4 N-m, nc = 4	4.04	14.9	0.622
Maximum load versus number of wires per crank (max torque to within 0.1 N-m)			
forced convection, load = 0.3 N-m, nw = 1	5.16	11.6	0.365
forced convection, load = 0.7 N-m, (base case: nw = 2)	5.88	10.2	0.748
forced convection, load = 1.4 N-m, nw = 4	5.88	10.2	1.50

The relations of Figure 4.11 as well as most of the configurations in Table 4.2 are for a fixed load of 0.4 N-m. Trends for one load may not match trends at another load. Consider the three wire diameter trials in Table 4.2. Power output dropped with the switch to larger wire, from that used in the prototype. Because larger wire takes longer to heat and cool, engine speed fell. Larger wires also have larger cross-sectional areas and can produce more force. At high loads, the higher force generating potential is more significant to power production than it is at 0.4 N-m. For example, at 1.4 N-m, the larger wire is predicted to produce nearly one and a quarter Watts, where the prototype configuration should not be able to rotate.

The following trends are indicated by model output:

- Average shaft speed decreases with applied load.
- Power output generally increases with the length of wire used in the engine.
- Power output is proportional to the temperature of the hot reservoir, $T_{h\infty}$.
- Power output is inversely proportional to the temperature of the cold reservoir, $T_{c\infty}$.
- Power output is proportional to the convection coefficients for heating and/or cooling.

4.11 Regarding Efficiency

Thermal efficiency is the ratio of heat energy put into an engine to work put out by the engine, over a complete cycle. Several papers have discussed calculating efficiency in SMA material [11][20][22][27][28]. Suggestions for the maximum theoretical efficiency, for an SMA engine, vary from less than 1 percent to 25 percent. Publications about engines that were actually constructed, either do not mention their efficiencies, or claim values less than a couple of percent.

In their study of the counter-synchronized engine, introduced in Chapter 3, Zhu and colleagues stated that the efficiency of a torsion-based heat engine could be 2-3% maximum. However, they also suggested that

the efficiency of an axial-based engine should be much higher [20]. The proposed engine operates by axial extension and contraction alone, so it has potential for higher efficiencies.

Since very little experimental data has been collected for comparison, efficiency calculations are not included.

Chapter 5: Design Evolution and Construction

5.1 Practical Design

This chapter discusses practical considerations and the evolution of a working prototype. From an analysis standpoint, problems like finding SMA wire with the right transition temperature, or determining a way to synchronize two shafts, are moot. However, the scale of SMA behavior, with its small stroke motivating a comparably larger engine, makes machine design quite relevant. Any slip or misalignment can disrupt the small force imbalances that create rotation. During the course of this project, at least half a dozen major prototypes were assembled, each being modified and revised several times. All but one of them failed. Because the trials were based on the same basic principles and analytical support, the failures can be attributed to implementation. The following sections highlight significant elements of engine design and chronicle the reasoning leading to their adoption.

5.2 Engine Components

5.2.1 Wire

Wire is the critical component of the machine. It is the force-generating element, a solid-state version of the internal combustion engine's piston and cylinder. Selecting and obtaining the right wire is the first step in building a viable engine.

Chapter 2 discusses the inner workings and outer behavior of shape memory alloys. Using the material should be a simple matter of matching its properties, such as transformation temperatures, to the specifics of the application. The problem is that neither the material nor its property data are readily available.

Every SMA manufacturer, identified during the course of this project [29], claims to be able to fine-tune the transformation temperatures of their wire. They tout a capacity to supply material in a wide range of sizes and form factors, from wire to ribbon to tubing. However, if an individual wishes to purchase small quantities of wire, off the shelf, there is only one obvious supplier. The others manufacture to custom specifications and in large quantities, so that using their products for prototyping is prohibitively expensive.

Dynalloy, Inc. sells Flexinol™ brand wire direct and through distributors. The material is advertised for electrical actuation and has an A_s temperature of either 70 °C or 90 °C. Multiple wire diameters are available, ranging from 0.0254 mm (0.001 in) to 0.381 mm (0.015 in). Although some material data is provided on their internet site, Dynalloy does not publish the other transformation temperatures, stress constants or critical stresses for their wire. Critical stresses are not uniformly referenced in constitutive models, so without a widely accepted manner for characterizing SMA material, it is unlikely to find a complete set of property values. Numbers are not crucial to construction, but they are useful for analysis, especially if the engine is to meet specific performance requirements.

The prototype engine uses 70° C wire with a diameter of 0.381 mm. Larger diameters produce more force when they contract, but take longer to transfer the heat. An engine using large diameter wire could generate more torque but would run slower than the same engine using thinner wire. For the prototype, it was not clear that torque could overcome friction. Hence, the largest available wire was selected, giving precedence to force generation over cycle time.

Lower transformation temperatures allow an engine to operate from a cooler heat source, provided they are still above the temperature of the heat sink. Since the wire is specified by A_s, the high temperature side of the engine receives most of the design attention. An essential requirement for the A_s temperature is that it be below that of the heat source, for two reasons. First, the A_s temperature marks the beginning of strain recovery, with completion occurring 10 - 20 degrees higher, at A_f. If the temperature of the heat source does not exceed A_f, full strain recovery will not occur and the engine will only be able to generate torque for part of each revolution. In addition, stress shifts transformation temperatures toward higher values. If a heat

source could only sustain 70 °C, stressing the wire would raise its transformation temperatures, halt strain recovery and prevent the wire from exerting any force. Ideally, the A_s temperature could be chosen to be below that of a convenient heat source; however, due to limited selection, the prototype engine uses wire with the lowest available A_s temperature and the heat source is determined accordingly.

Wire arrives from the factory as drawn; meaning it was pre-strained during manufacture. Before use, it should be cycled a few times to ensure it has fully recovered the residual strain and is performing reliably. Electric current is a convenient means of evenly heating a piece of wire. A heat gun also works. Wire is easy to stretch by hand, but it is important not to overstrain it. It is good practice to use a ruler or other means, to monitor the amount of strain in the sample. For example, to stretch a 1m length of wire by 4%, fixing the wire at one end and placing a reference ruler beside the other makes it easy to get 4 cm of length change.

Once the wire is selected, purchased and prepared, it needs to be connected to something. Joining SMA wire is difficult for the same reasons that make it well suited to powering an engine - its movement and corrosion resistance. If wire is twisted together or tied in a knot when cold, it will untwist and untie the knot when heated. Similarly, the slippery chemical composition of NiTi inhibits traditional metal to metal bonds. Although techniques for welding, soldering and gluing SMA materials have been successfully demonstrated, they require special care and additional processing [2f]. Soldering for example, requires a proprietary flux, which is licensed much like software. Mechanical connections are also common and used exclusively in the prototype. Several are shown in Figure 5.1.

The prototype uses loops of wire formed by connecting the ends of a single strand. Because a taut loop consists of two parallel strands, looping is an easy way of adding more wire to the engine, and thus increasing its torque, without the complexity of adding cranks or extra wire joints.

One method of forming a piece of wire into a loop involves routing the two ends through a coil-type spring pin. A coil-type spring pin is a small, tightly wound roll of spring steel. With wire passing through the hollow pin from both ends, a wedging device, such as a needle or seamstress' pin, can be jammed into the end of the spring pin to clamp the wires in place. This joint has a small profile and clean appearance, but can slip if the spring pin and wedging device are not the right size. The right size is determined by trial and error. Figure 5.1 (a) shows this joint.

Another way of creating an attachment point on a strand of wire is to form a loop and clamp it in place with a small bolt. Figure 5.1 (b) shows the bolted loop and Figure 5.1 (c) shows the loop hooked to a small crank roller. The bolt connection can form the small loops shown as well as large continuous loops like those formed with the spring pin method.

In a multiple-crank engine, each wire must perform identically if power output is to be consistent throughout the rotation. Therefore, all wire lengths and tensions need to be the same. Ideally, each loop would be sized properly from installation, with no adjustment necessary. Unfortunately, with only the crude joining techniques described here, a system for tuning the length and tension of each loop, after installation, is critically important.

The first approach involves a simple clamp. To adjust wire length, loosen the clamping plate, pull the slack out of the wire and retighten the plate to lock the wire in place. Shown in Figure 5.1 (d), this device is useful for single wires, less so for loops and does not allow small, measured adjustments.

Cable ties are cheap, lightweight, readily available and include a ratcheting mechanism that is perfect for taking up the slack in a loop of wire. A cable tie can be strung through bolted end loops to connect wire into a single large loop, as shown in Figure 5.1 (e). Standard cable ties could not handle the high temperatures needed to run the prototype engine. Heat stabilized varieties are available and may be well suited for future engines.

Figure 5.1 (f) shows the loop connection and tensioning system employed in the working prototype. Bolted end loops hook over wing nuts, which are threaded onto a central bolt. By adjusting the distance between the wing nuts, it is possible to make fine adjustments to wire tension.


(a) Spring-pin clamp.

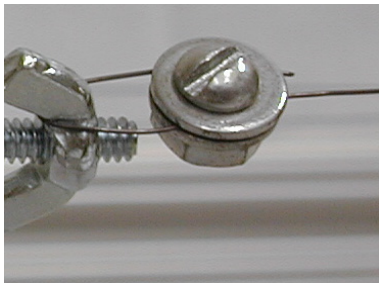
(b) Bolted loop.

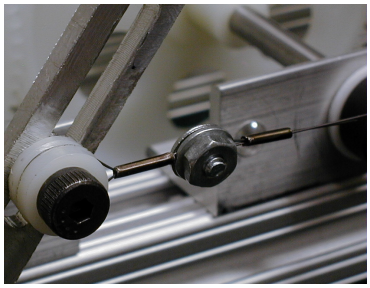
(c) Bolted loop.

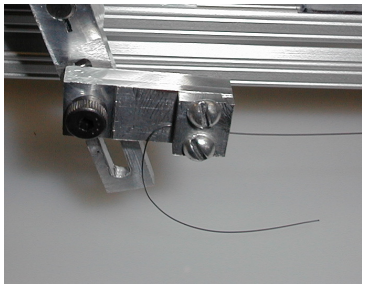
(d) Clamping plate.


(e) Cable ties.

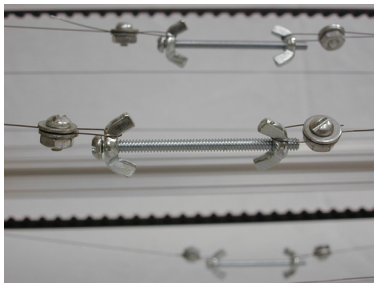
(f) Wing-nut tensioning system.

Figure 5.1: Methods for joining SMA wire.

5.2.2 Cranks

Wires are supported by the cranks. Cranks on the first crankshaft are longer than cranks on the second crankshaft. The ratio of crank lengths is determined by the strain range and the center distance between crankshafts.

Early in the prototyping process, a few adjustable length cranks were built. An example is shown in Figure 5.2 (a). While the concept allowed for adjustment, cranks of this type were difficult to machine and not stackable - they could not be connected in series to form larger crankshafts.

The next generation was assembled from multiple identically constructed, aluminum bars. Each bar had parallel clamping fixtures at both ends for gripping steel connecting rods. A crank consisted of two bars, a connecting rod and a grooved nylon roller for guiding the wire. Crankshafts were composed of four cranks connected in series and offset by 90°. The assembly, and reason for its dismissal, is shown in Figure 5.2 (b). Note that the two bars, making up the last crank, are not aligned. Clamps holding the connecting rods were not strong enough to support the forces generated during strain recovery. Adjacent bars rotated relative to one another and the crankshaft deformed. The deformation relieved tension in the wire and with it, all the force required to motivate shaft rotation.

In the working prototype, there are six cranks per crankshaft, instead of four. The increase was prompted by analytical results suggesting that the power output would be greater and the rotation smoother with more cranks. In addition, the four crank models seemed to have trouble rotating through the 90° arcs separating adjacent cranks. Of course, this observation is less significant in light of the rigidity problems plaguing the four-crank designs.

For the final prototype, opposing cranks, those offset by 180°, were machined from the same unbroken piece of metal. One-piece construction reinforced and compacted the crankshaft assembly. Cutting cranks

from rectangular stock creates a square cross-section at the location where the wires attach to the cranks. Dragging taut wire over a sharp corner creates a lot of friction, so the square edges of each crank are encased in a cylindrical nylon slider. The circular profile is better than a square one, but rolling would have been preferred. Figures 5.2, (c) through (f), highlight attributes of the prototype crank design.

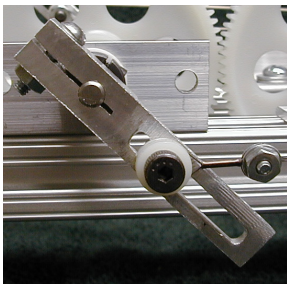
(a) Adjustable radius crank.

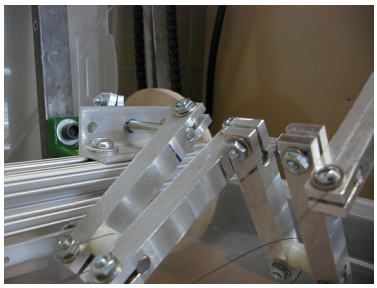
(b) Misaligned bar cranks.

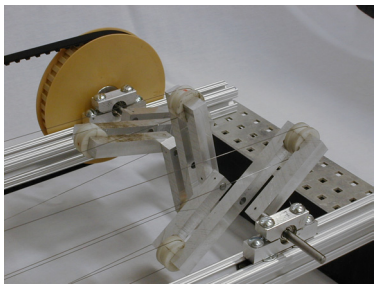
(c) Working crank design.

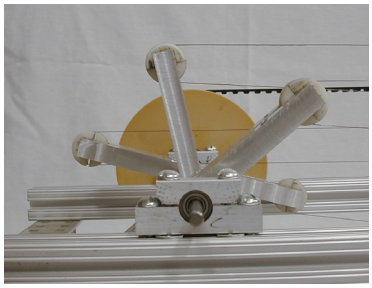
(d) Side-view showing sliders.

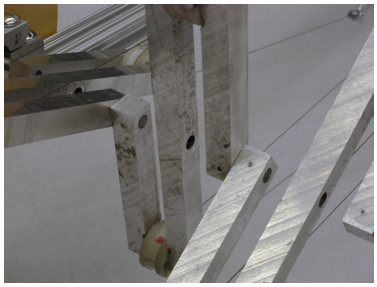
(e) Pinned joints.

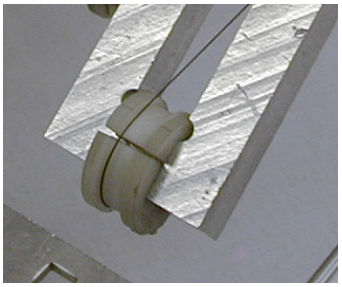
(f) Close-up of Slider.

Figure 5.2: Crank designs.

5.2.3 Synchronizer

The synchronizer prevents the cranks from releasing wire tension. Heated wire tries to contract during strain recovery. If not for the synchronizer, both crankshafts would rotate a few degrees toward one another, release the wire stress and allow the engine to sit idle. Synchronization prevents this mechanical "short-circuit" and forces the entire engine to move in response to heat-induced stress.

Convenient synchronizers can be installed, tensioned and engaged independently. Early attempts were not convenient. For example, the first synchronizer design used roller chain and steel sprockets. Removing slack from the drive necessitated high installation tensions; however, once the chain was installed it could not be adjusted to align the shafts. Keeping the shafts perfectly aligned, while tensioning the chain was not feasible. So, the shafts never quite lined up and the design was scrapped. Figure 5.3 (a) is a photograph of the machine.

The next incarnation used three meshing spur gears to drive the shafts in the same direction. Figure 5.3 (b) shows the layout. Gears do not require installation tension, reducing bearing load and associated friction. The center gear could be engaged and disengaged making it easy to align the cranks and then, lock in the synchronizer. The problem was in scale. With an outside diameter of slightly over 7 cm, the center distance was only about 14 cm. For a strain range of 4%, the length difference between crank radii had to be less than 0.3 cm. Scaling up the design would require more and/or larger gears. Larger gears are rare and for a similar center distance, the prototype would require nine, 7 cm gears, to connect the shafts. Synchronization with spur gears was not practical.

Sticking with the gear train concept, I tried the miter-gear based right-angle drive shown in Figures 5.3 (c) and (d). The design allowed large center distances, low installation tension and quick and easy synchronizer engagement. A solid rod connected two sets of miter gears to link the crankshafts. Here again, the problem

was with cost and scale. Miter gears are only stocked in small sizes - finding a 10 cm diameter miter gear is nearly impossible. Smaller gears see larger loads for a given shaft torque, adding friction to the drive. To cut costs, injection molded gears were used instead of machined metal versions. So, loads were high, friction was high, and clamping the plastic gears to the shafts proved to be a problem. Even with their hubs slotted and clamped with shaft collars, the gears slipped under load to release the wire tension.

Linkage-based synchronizers have the allure of being simple, adjustable and low friction, with only two pin joints per linkage. Figure 5.3 (e) is an example of the concept in which two slotted aluminum linkages connect between equal length pairs of cranks. The cranks are mounted to the ends of the shafts to be synchronized. Because a single linkage will lock when its cranks line up, a second linkage was installed roughly 90° out of phase with the first. Consequently, whenever one linkage reaches a toggle position the other should be at its most assertive point and able to keep the shafts rotating smoothly. Unfortunately, the system will not work unless both linkages have exactly the same length. Furthermore, by virtue of their 90 degrees of separation, the linkages make the machine unbalanced. The balance problem was anticipated and dismissed as being irrelevant at slow speeds, while the link length problem was underestimated. As it turned out, the links bound, despite efforts to match their lengths. The balance issue was also significant in that some wires had to propel extra weight while others did very little. In the end, the linkages were also abandoned.

The final working prototype is synchronized with a timing belt as shown in Figure 5.3 (f). Timing belts are similar in function to chain drives but are lighter and require less installation tension for an unsupported span. Considerations relating to timing belt specification are detailed in the technical section of the SDP/SI catalog [30]. An L-series belt was selected for its torque handling capacity, low cost and selection of stock loop lengths. Large diameter, just over 12-cm, timing pulleys reduce friction by minimizing the force transmitted through the belt.

To install the timing belt I fixed one crankshaft and moved the second until the belt was taut and firmly seated in the pulley grooves. When tension felt right, the second crankshaft was locked into place. At this point, the pulleys were free to turn on the shafts, making it easy to align the cranks. When crank orientation was right, the hubs were locked and the synchronizer was ready to run.

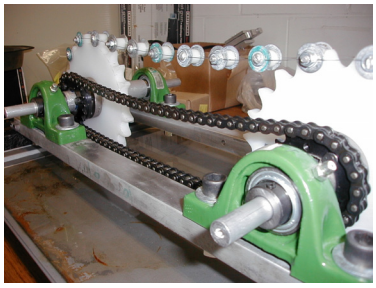

(a) Roller chain drive.

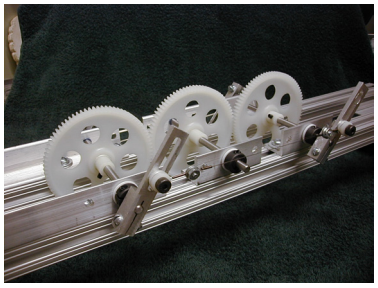

(b) Plastic spur gears.

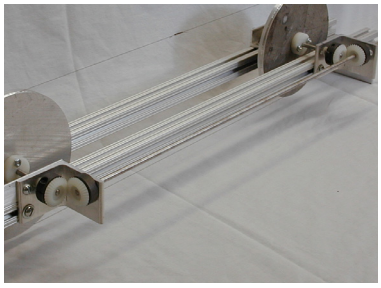

(c) Right-angle drive.

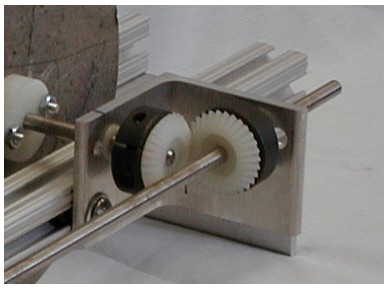

(d) Plastic miter gears.

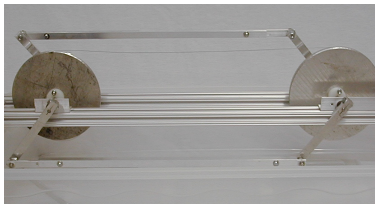

(e) Offset linkages.

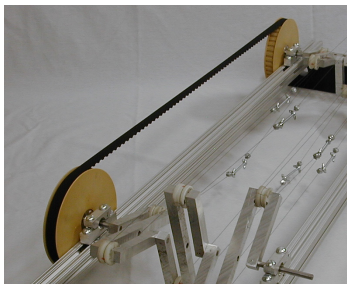

(f) Timing belt.

Figure 5.3: Synchronizer concepts (some synchronizers are shown connected to equipment, unrelated to the proposed design).

5.2.4 Bearings

Bearings carry the shaft loads. Because only a small percentage of the force generated in the wire during heating is output as power, the rest passes through the bearings. Accordingly, low bearing friction is important to efficiency.

The first engine concept, studied with this project, used large tractor-style bearings with a 0.5 in bore. Figure 5.4 (a) is a photo of one such bearing. A greased aluminum shaft passed through the bearing's hub, but the setscrews were never tightened. When the machine was hand turned the shaft rotated without turning the bearings. During development of subsequent engine concepts, these substantial bearings were abandoned in favor of smaller, lower friction versions.

Two varieties of small plastic bushings, shown in Figures 5.4 (b) and (c), were used throughout the development process. Both types of bushings performed well, were easy to mount and were easy to separate from their supported shafts. It was not until building the final prototype that I opted to upgrade the bushings to low friction roller bearings, shown mounted in Figure 5.4 (d). The bearings turned out to have far less friction than the bushings; but, as was the reason for not using them until that point, they require permanent mounting. Shafts had to be press-fit into the bearings, eliminating the possibility of modifying the setup after installation. Fortunately, the final prototype worked and the bearings have remained intact.

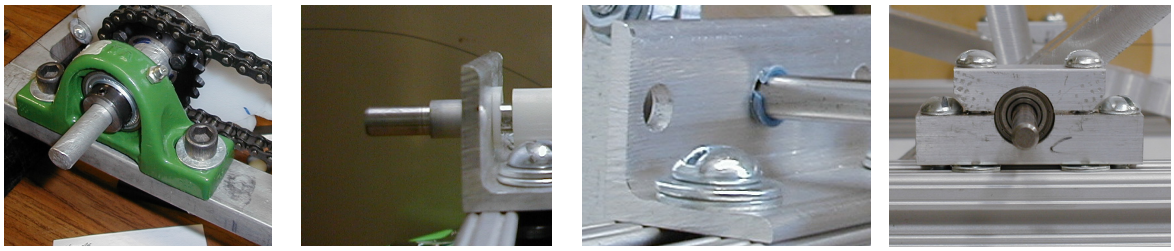

(a) Large ball bearing. (b) Nylon bushing. (c) Panel mount bushing. (d) Roller bearing.

Figure 5.4: Bearings choices.

5.2.5 Frame

Although the frame is the backbone of the engine, it is discussed last due to its relative simplicity. The prototype frame consists of two slotted aluminum rails. Adjustable legs and perforated cross-members, for easy width adjustment, are added features. Because of the machine's prototype nature, easy adjustment was a top priority. The rails provided ample mounting locations and helped keep all components aligned and secure.

5.3 Total Package

The finished prototype is shown in Figures 5.5 (a), (b) and (c). A list of the major parts is included as Table 5.1. Only components that would be required to build this final version are included.

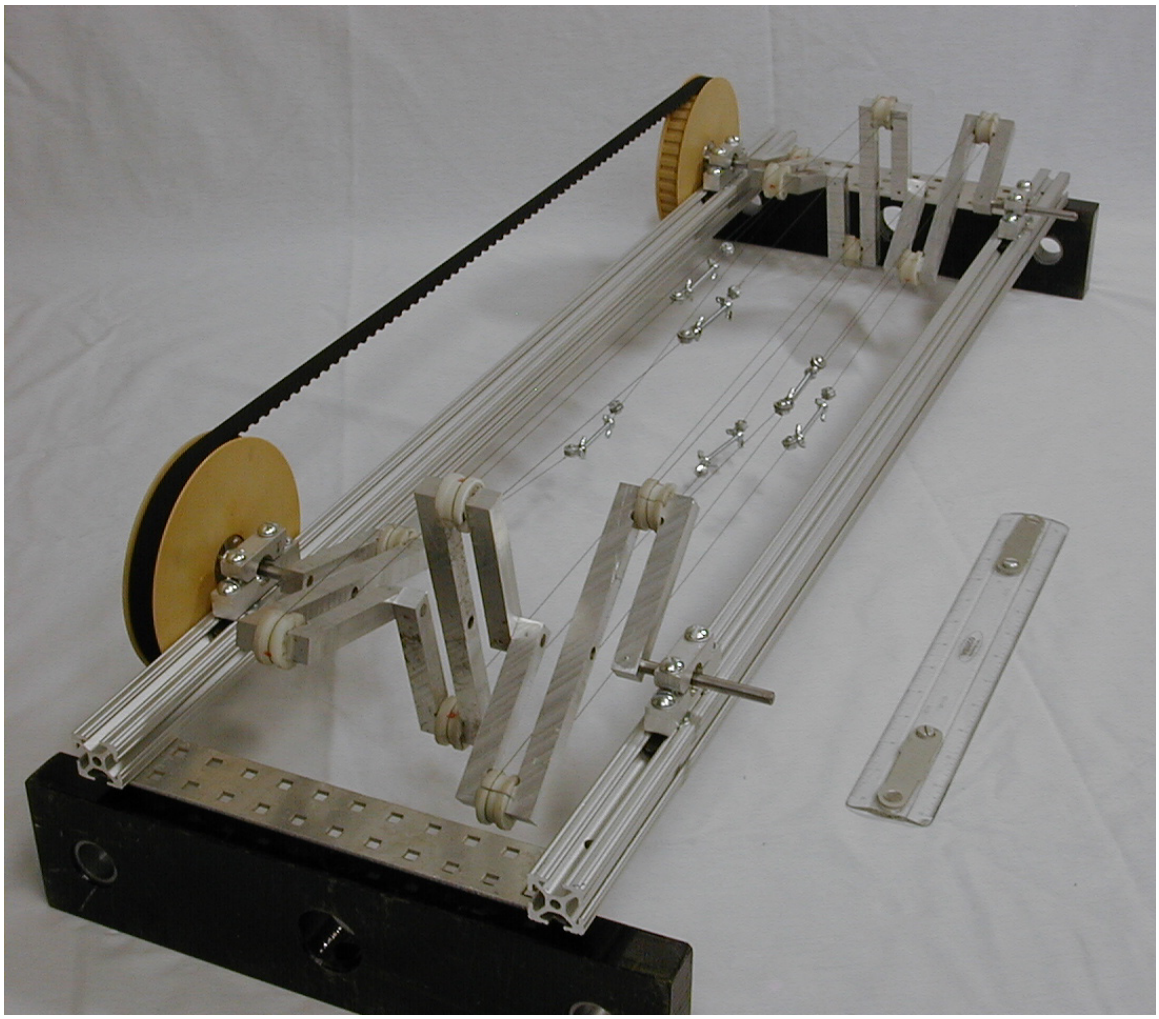

(a) Large isometric view.

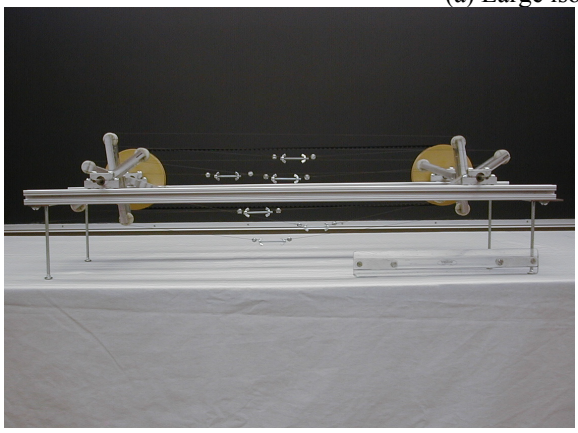

(b) Side view.

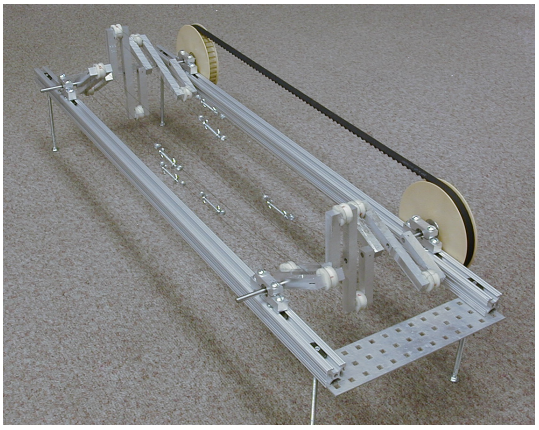

(c) Isometric view with adjustable legs.

Figure 5.5: The final working prototype of the SMA heat engine.

Table 5.1: Parts and material list for final working prototype.

Description	Vendor	Part Number	Quantity	Unit Cost
Wire, 0.015 in diameter Flexinol ™ actuator wire, 70 °C	Dynalloy		8.5	7.5 / meter
Crank stock, 0.5 in thick aluminum plate, 12 in x 12 in (found in a scrap yard at 0.50 / lb - price shown is if purchased from McMaster-Carr)	McMaster-Carr	9246K33	1	42.03
Sliders stock, white nylon 6/6 1.25 in diameter	McMaster-Carr	8538 K251	1	4.47 / ft
Plain steel standard duty coiled spring pins, 1/16 in diameter, 1 in length	McMaster-Carr	91598 A114	1	4.07 / pkg
12L14 steel shaft, 0.25 in diameter, 24 in length	McMaster-Carr	1327 K68	1	7.88 each
L-series timing belt, 0.5 in wide, 0.375 in pitch, 66 in pitch length, nylon covered, fiberglass reinforced, neoprene	SDP/SI	A 6R 4-176050	1	14.26 each
L-series timing pulleys, double flange, 0.5 in wide, 0.375 in pitch, 0.5 in bore, 4.775 in pitch diameter	SDP/SI	A 6Z 4-40DF05016	2	20.69 each
Shaftloc sleeve hubs	SDP/SI	A 7Z39-0816	2	23.37 each
Steel bearing, ABEC-1, double shielded for 0.25 in shaft	McMaster-Carr	60355 K73	4	3.96 each
Bearing mounting stock, 0.5 in wide, 1 in tall, 16 in length	80/20 Inc.	8316	1	2.72 each
Frame, 1x1 in T-slotted extrusion	80/20 Inc.	1010	72	0.21 / in
10 S economy T-nut 1/4-20 thread	80/20 Inc.	3382	16	0.20 each
Perforated aluminum cross-pieces, 2 in x 10 in, (found in a scrap yard at 0.50 / lb - price shown is if purchased from McMaster-Carr)	McMaster-Carr	9041K11	1	6.22 each
#6 bolt, 1/4 in length	Hardware Store		12	≈ 0.05 each
#6 nuts	Hardware Store		12	≈ 0.05 each
#6 washers	Hardware Store		24	≈ 0.05 each
#8 bolt, 2 in length	Hardware Store		6	≈ 0.10 each
#8 wing nut	Hardware Store		12	≈ 0.20 each
1/4-20 bolt, 3/4 in length	Hardware Store		8	≈ 0.10 each
1/4-20 bolt, 1.5 in length	Hardware Store		8	≈ 0.20 each
1/4-20 bolt, 1/2 in length	Hardware Store		4	≈ 0.10 each
≈ represents approximate cost			**Total**	**275.88**

5.4 Heating

To run, the engine needs a source that can transfer heat at or above the temperatures required for martensite to austenite phase transformation. Although, A_f, is not known, the unstressed A_s temperature is near 70 °C. If A_f is 10 °C higher, and stress shifts the transformation temperatures upward, I expected to need a heat source capable of sustaining at least 85 °C. A heat gun, which resembles a consumer hair dryer but produces more heat and less air, works for heating small section of the engine at a time. The heat gun was not practical for uniformly heating half of the engine at a time, so a hot water bath was assembled.

The first heating system was a clear plastic box measuring 13 cm deep by 30 cm wide by 81 cm long. A heating element, designed for use in residential hot water heaters, was mounted in the container. With the engine frame resting on the edges of the box, half of the cranks could dip into the water while the other half were in open air. Even after a several hours of operation, the 1,000-W heating element could not force the water temperature above the low 70's °C. The first test box did not have sufficient insulation or heating power. Figures 5.6 (a) and (b) show the setup and the heating element respectively.

To test the final prototype, a water box was fabricated from sheet steel. It was framed with 2x4 lumber, and sealed with silicone caulk. Measuring approximately 13-cm by 36-cm by 91-cm, it held 41 liters of water

and could be placed over two stovetop burners simultaneously. At full burner power, the water temperature barely reached 85 °C, but was high enough to run the engine.

Cooling is the other half of the process and affects engine speed. The slower the wire cools the longer it takes to deform. While room temperature air, around 25 °C, is cool enough, steam rising from the water surface makes the temperature just above the tank substantially higher. Since the wire never gets strained to its limit, it does not have to cool all the way to the M_f temperature. For example, if the strain limit were 8% and the maximum imposed strain only 4%, then the lowest required temperature would be halfway between M_s and M_f. Even so, a low-velocity house fan was positioned to send air across the water surface and improve convective heat transfer. Figure 5.6 (c) shows the prototype heating apparatus.

(a) Plastic box.

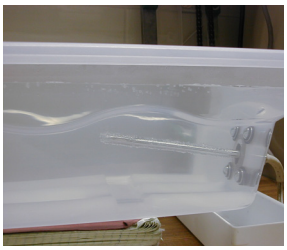

(b) Heating element.

(c) Steel box on stove with fan.

Figure 5.6: Hot water baths.

Chapter 6: Experimental Results

6.1 Testing

This chapter describes experimental validation of the proposed engine design.

6.1.1 Heat Gun Testing

It takes time to set up the test tank and heat the water, so for the early trials it was more convenient to use a heat gun. By heating successive wires, independently, the engine could be coaxed through several complete revolutions. The gun's heating zone is small, so getting an entire length of wire to reach transformation temperature at the same time was a struggle. For this reason, the engine rotated very slowly when heated with the heat gun; two revolutions took 3-5 minutes. Figure 6.1 (a) is the real-time video of the engine as powered by a heat gun. Figure 6.1 (b) shows a second trial, but with the video playback speed increased by a factor of 10. Note that the two takes show two different thermometers, °C in (a) and °F in (b).

.mpg (66.7 MB)

(a) Real-time video.

.mgp (8.59 MB)

(b) Accelerated video.

Figure 6.1: Video clips of the prototype being powered by a heat gun.

6.1.2 Water Bath Testing

Heat gun demonstrations were encouraging but unimpressive. To really validate the engine, it had to be tested in the hot water bath. When the water was hot enough, the engine was flipped upside-down, compared to the photographs of Chapter 5, and placed into the tank. With the adjustable legs also reversed, the engine could be precisely positioned such that the water level covered up to just below the crankshaft bearings. After a few runs with free convection cooling (still air), a fan was used to test forced convection cooling. Figures 6.2 (a) and (b) show setup and operation without the fan, and Figures 6.2 (c) and (d) show the same but with the forced-air cooling. Table 6.1 summarizes engine speed for both cases.

.mpg (6.78 MB)

(a) Without fan and with setup.

.mpg (4.27 MB)

(b) Without fan and without setup.

.mpg (7.86 MB)

(c) With fan and setup.

.mpg (1.59 MB)

(d) With fan and without setup.

Figure 6.2: Video clips of the engine in a hot water bath.

Table 6.1: Prototype engine speed when cooled by free and forced convection.

Conditions: water temperature at 85 °C, air temperature at 26 °C				
Free Convection	**Revolutions**	**Elapsed Time (s)**	**Average Cycle Time (s/rev)**	**Average Shaft Speed (rpm)**
Trial 1	5	25	5	12
Trial 2	4	20	5	12
Forced Convection				
Trial 3	4	9	2.25	26.7
Trial 4	4	10	2.5	24

6.2 Observations

Even with limited objective results, testing helps to highlight qualitative issues. Observations regarding the prototype's demonstration are discussed in this section.

6.2.1 Startup

Though it may be difficult to see in the videos, engine rotation starts abruptly when first placed into the hot water bath. After the first half-revolution, rotation steadies and proceeds in a controlled manner. Startup is sudden because, when the hot wires hit the water they contract almost immediately. The cold wires are already cold and ductile, so they do not provide significant resistance to the movement. When half of the first rotation is complete, wires located on the cold side of the engine have recently emerged from the hot water. Now, as these wires start hot then cool, their stress levels start high and drop with temperature. Cooling is slower than heating so rotation speed is governed by cooling time, as opposed to heating time, as it was at first. Data in Table 6.1 includes the first half-rotation, so steady-state speeds are expected to be slightly slower than the values listed.

6.2.2 Bolt Movement

If one pays close attention to the video clips, they will note that the wire tensioning bolts migrate from one end of the engine to the other. What is not shown in the video is that after about five rotations the bolts bind-up in the cranks.

The phenomenon is due the use of fixed nylon sliders instead of rolling elements. Friction between the wire and slider is too great to allow one to slip past the other, as intended. Instead, friction forces the wire to roll over the slider. With each crank revolution, the wire rolls a distance equal to the circumference of the slider. When the bolts get too close to the cranks, they bind, making the engine's effective period of operation only about five complete revolutions. Rolling elements would themselves, revolve about the crank axles, such that the wire loops could remain stationary.

To visualize the problem, consider Figure 6.3, a slightly angled side view of one crankshaft, surrounded by close-ups of each slider. Note from the figure, that each slider is composed of two halves and that the joint shows the relative angle of rotation between slider positions.

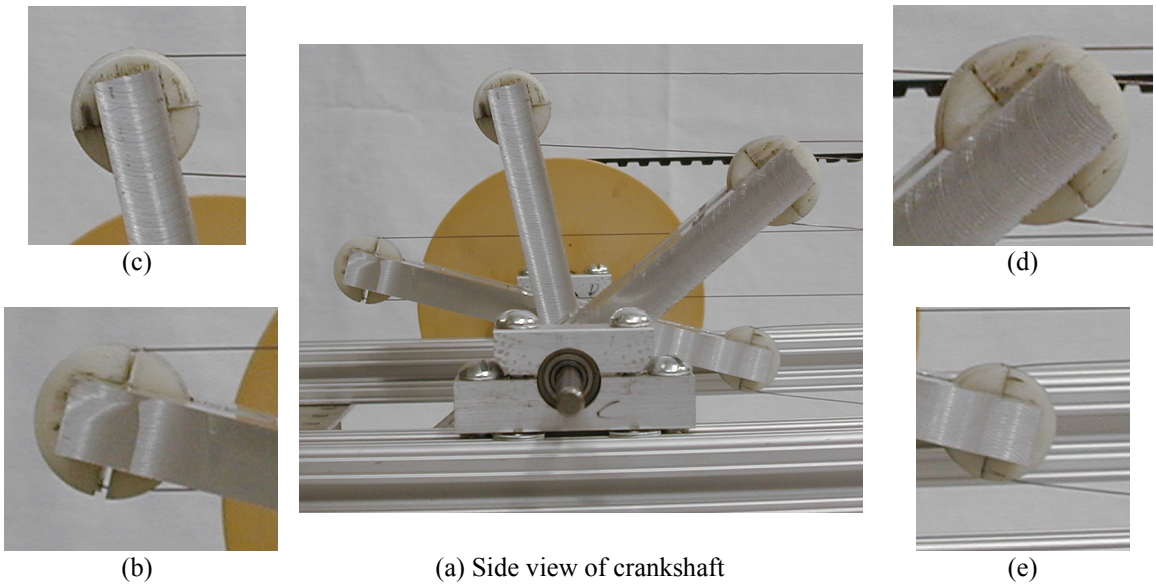

Figure 6.3: Explanation of bolt migration.

Imagine that each of the enlarged slider pictures represents the same part but at different points along its rotation. Starting with Figure 6.3 (b) and progressing clockwise to (e), the slider has rotated 180° relative to the viewer's fixed frame. Since friction prevents sliding, any wire in contact with the slider is carried through the same 180° rotation. Being a loop, if one wire segment moves, so do the rest; causing the loop as a whole, to circulate around the sliders.

Solving this problem will require a lower-friction sliding joint, replacing the sliders with rollers or eliminating the tensioning bolts in favor of continuous loops of wire. Again, as originally, joining wire into seamless loops is challenging. However, if it were possible to manufacture such loops, the wire precession may actually be beneficial to wire life in that the continuous rotation would uniformly distribute any wear or fatigue. Once this issue is resolved, the engine should run for extended periods, without intervention.

6.2.3 Irregular Rotation

Engine rotation is sporadic, especially during the free convection tests. The engine completes its rotations, but some portions of the cycle are faster than other portions. This is especially noticeable when performing the heat gun tests. Certain wires seem to perform better than others, perhaps due to variations in tension or pre-strain. Although effort was made to install the wires uniformly, tension adjustments are based on feel. The development of more mechanized means for cutting, fastening and installing wire segments would be an improvement.

6.2.4 Heating Problems

The testing process reinforced the realization that an open-topped water bath is not a great way to power a heat engine. The main issue is with getting the water to a high enough temperature. A related problem is keeping the cold side cool in the presence of steam rising from below. The fan does a good job, but represents another unrealistic advantage for the engine. Granted, using wire with lower transformation temperatures would help. However, if it is ever to be practical, the machine needs to run under less contrived conditions.

Chapter 7: Summary, Applications and Conclusion

7.1 Closing

Research often raises more questions than it answers and this project is no exception. Answering the question, "Can the design work?" has been the focus of this effort. Questions such as, "How fast will it go?" and, "What's its efficiency?" were subordinate concerns. Yes, the design can work and it has been validated with a working prototype. Limited data and model-based predictions have been provided for engine speed. Efficiency is left to subsequent research.

This chapter begins by reviewing important attributes of the proposed design. Possible uses for the machine are mentioned followed by a listing of unanswered questions and other opportunities for improvement. A concluding statement summarizes the results and contributions of this work.

7.2 Pros and Cons

The proposed engine design has several advantages over previous SMA and conventional heat engines:

- *Solid-State* - The engine is ultimately powered by the phase transformation between high-temperature austenite and low-temperature martensite. This diffusionless, solid-solid transformation happens internal to the wire [28][31]. Unlike in more traditional heat engines, here, the working medium is the actuator. Without needing to pump fluid through pipe or other auxiliary equipment, a solid-state engine can avoid the mess and losses inherent in conventional heat engine designs.
- *Simplicity* - Straight wires are the simplest actuators available. The few additional parts are common and relatively easy to manufacture, especially in contrast to the tight tolerances held between pistons and cylinders, or the complex curvature of a turbine blade.
- *Reliable and Low Maintenance* - Since there are not many parts, there are not many ways for the engine to fail. If the wire is set up properly is should operate free of intervention for millions of cycles. When failures do occur, replacing parts should be straight forward.
- *Scalable* - Adding more cranks, adding more wires per crank, increasing the center distance, increasing the wire diameter and increasing the temperature of the heat source, are all options for raising the engine's power output. Increasing power production will raise the shaft speed for a given load, as will more effective cooling on the cold side of the engine. These are immediate tangible improvements, separate from benefits that could be realized with advances in material capability, such as larger recoverable strains, higher forces, etc.
- *Flexible Heating Requirements* - For the temperatures of the heat source and sink, higher and lower are better, respectively. However, there are no constraints on how these temperatures can be achieved. For example, the prototype sat in a tank of water heated on an electric stove. The tank of water could have been heated over a campfire, propane burner, or volcanic vent. Any heat source, of sufficient temperature, can be used to power the engine.

Potential shortcomings of the proposed design may include:

- *Low Thermal Efficiency* - SMA material produces a small amount of mechanical work for the thermal input it requires. Accordingly, SMA based engines are not viable alternatives to bulk, mainstream power production. Instead, they could be applicable to waste heat recovery and niche applications.
- *Low Power Output* - Traditionally, SMA engines have not been able to produce much power. The highest output was 665 W, from a pulley type engine that used 252 Nitinol springs arranged in parallel loops [23]. Note, because the 665 W engine used springs, instead of the more efficient straight wires, a larger engine, modeled after the prototype, should be capable of higher power outputs.
- *Expense* - Nickel-Titanium wire is relatively expensive. In the current energy market, and in prototype quantities, it may be difficult to recoup the cost of building an engine from the cost of the energy it saves. In time, especially with widespread use, the ratio of engine cost to energy cost could become more favorable.

- *Difficult to Heat* - Temperatures required to operate the prototype are more extreme than those commonly available from low-grade sources. Here again, with widespread use it should be possible to obtain SMA material with transformation temperatures more applicable to a particular application.

7.3 Potential Applications

This section includes speculation on possible uses for SMA heat engines. These ideas are only rough concepts, which have not been studied in detail or evaluated for practicality.

7.3.1 Distributed Energy Generation

There is a need for clean, sustainable alternatives to fossil fuel. Not necessarily for conversion to electricity, but instead for direct use as shaft power. Pumping from wells or driving irrigation systems might be feasible, especially in developing areas with ample sunlight. The solar energy could be stored, perhaps by heating a covered tank of water or oil, maybe in a greenhouse structure. When the storage medium reaches an adequate temperature the engine could run, transferring heat from storage back the cooler air. If the air were hotter than the storage medium, the engine would run in reverse. Maybe the heat would have to be stored until nightfall, when the air temperature drops to a lower level. The temperature difference required to cycle the wire can be as low as 10 °C with current SMA technology. Powering an SMA engine with solar power is discussed in reference [22].

Photovoltaic modules, in current production, have efficiencies on the order of 8% [32]. They are also expensive. If a photovoltaic solar cell were to power an electric motor with an electrical to mechanical conversion efficiency of 80%, the net efficiency from sunlight to mechanical work would be about 6.4%. SMA engines, though not proven, should be able to match that level and deliver the shaft power in a single step and at a lower cost. That is, once the engine's thermal reservoirs are set up. The two technologies may be perfect complements to one another. Photovoltaics handle electrical needs while SMA's do mechanical work.

7.3.2 Thermal Recycling in Industry

Waste heat is common in industrial operations. Passing heated coolant through a bank of SMA engines could salvage mechanical energy while transferring heat from the coolant to another medium, air or water. If the engines were arranged in a serial manner, the wire in latter engines could be selected to work at lower temperatures, making them capable of extracting energy even as the coolant temperature falls.

While the thermal efficiency is low, meaning that for the thermal energy it moves between hot and cold reservoirs the engine does not produce much work; it does move the heat. The engine is a self-propelled heat exchanger - it moves heat, rotates and the rotation aids further convective heat transfer.

7.3.3 Novelties

Any application requiring a simple, durable source of mechanical power is a potential application for an SMA heat engine.

Fans are used in furnaces and heaters to move hot air near a flame or heating element, out into a cooler room. By straddling a boundary separating these two thermal regions, an SMA heat engine may be able to drive the fan without using electricity.

The prototype engine works by dipping alternate sets of cranks and wires into a tank of hot water. Perhaps this motion could be used to stir the contents of a heated chemical tank or to aerate a cold pond. Wires used to power the prototype are extremely corrosion resistant and the engine is simple enough that it may be ideally suited for service in harsh environments.

Again, the sweeping motion of the wires may be useful for sweeping debris out of a swimming pool or irrigation channel. Maybe the machine could scare birds away from a vegetable garden.

7.4 Loose Ends and Opportunities for Improvement

Questions that remain at the conclusion of this study, opportunities for improving the design and areas in need of further research are listed as follows:

- *Efficiency* - What is the engine's thermal efficiency?
- *Friction* - How important is friction? Equations for bearing load were derived, but the effects of friction were never added to the model.
- *Fatigue* - Does the wire fatigue?
- *Service Life* - Does wire performance vary with age or the amount of time in service?
- *Bolt Precession* - The most necessary improvement is to fix the bolt precession problem, mentioned in Chapter 6. Replacing the sliders with rolling elements should let the engine run for extended periods.
- *Wire Tensioning* - There is a need for more convenient means of adjusting wire tension and ensuring that it is consistent across all the loops. Alternatively, if there were a better system for forming loops of consistent dimension, the adjustment would be less significant.
- *Continuously Taut Wires* - Should the wires be taut for the entire cycle? Near the 180° points, the wire does not exert much force; would making the wire loose at those points help to move the engine smoothly through the limit positions?
- *More Effective Heating* - The prototype used a tank of water at 85 °C for its power source. Engine wires move up and down, across the engine's center plane, between the hot water and the cooler air. The boundary between hot and cold thermal regions cannot be insulated because the wires need to move through it. Consequently, heat escapes from the water surface and raises the air temperature where the wires should be cooling. This makes the wires cool more slowly, reduces speed and lowers overall performance. A more suitable means of applying heat would better the engine's chances of filling a practical application.
- *Heating/Cooling Balance* - Should exactly half of the engine be heated while the other half is cooled? Or, since cooling is the rate determining process, is there some optimum percentage of the cycle that should be devoted to cooling, with the balance used for heating?
- *Use SMA Ribbon* - Perhaps loops of SMA ribbon could be used instead of wire. An easy way to increase power output is to add more wire between each pair of cranks. The wires have a propensity for tangling. A single loop of ribbon could offer the same performance benefits as several loops of wire, but in a more convenient and elegant package.
- *Wire Specification* - Wire behavior is the significant factor in engine performance. Transformation temperatures should be matched to the application, as opposed to finding an application that works with the transformation temperatures. Smaller hysteresis widths would also make an engine applicable in more situations. For a particular application, it is likely that that there are more suitable material property combinations than those used for the prototype.
- *Stretching the Wire* - Could the engine be improved by working against gravity or a spring, where the potential energy is returned? Is there a better way to stretch cold wires than antagonistically, with the hot wires?
- *Power Density* - Do SMA engines have a higher power density than a solar cell? Can more power be produced in the same footprint with SMA's than with photovoltaics?
- *Thorough Study of Applicability* - What are the applications for this machine? Some conjecture is given in the following section, but without supporting material, it is unconvincing.
- *Economic Study* - For an engine designed to a specific application, what is the final cost per Watt of power output? Is this technology economically viable? Nickel-Titanium alloys are four times more expensive than copper-based alloys [6]. Could copper alloys be used in heat engine applications?

7.5 Conclusion

A novel design has been proposed for creating a heat engine from shape memory alloy contractile wire. Following a review of alloy behavior and the prior art of SMA engines, it was suggested that this design advances that art. Subsequent analysis and creation of a working prototype helped to substantiate the claim, though additional experimentation will be needed to make a conclusive determination.

Due to geometric constraints, crank engines have traditionally been limited to using coil springs as their force generating elements. By synchronizing parallel crankshafts to rotate in the same direction, instead of

opposite directions as has been done in the past, the proposed design eases these restrictions. Consequently, straight wire, which stretches and contracts axially, can be substituted for the less efficient, torsion-based, coil springs. The predicted result is a simpler and better performing heat engine.

An analytical model, partially based on experimental data, has been developed and used to predict output characteristics of the proposed design. The model predicts that the maximum output power for the prototype, under test conditions, should be 0.75 W. To increase power output, any of the following changes could be made to the prototype configuration:

- Increase the number of evenly spaced cranks (also makes operation more uniform)
- Increase the number of wires between each pair of cranks
- Increase the center distance between crankshafts
- Increase the strain range
- Increase the maximum strain (reduces wire life)
- Increase the wire diameter (limited by heat transfer)
- Increase the temperature of the hot source
- Decrease the temperature of the cold source
- Increase the heat transfer rate for heating, cooling or both

Although the model does not rigorously account for all relevant phenomenon, is should be a valuable tool for guiding future research in this area.

Appendix 1

Notation

Table A1-1: Text, graphics and computer code notation.

Quantity	Text / Equations	Graphics	Code	Units (metric)
unstressed martensite finish temperature	M_{fo}	Mfo	Mfi	°C
unstressed martensite start temperature	M_{so}	Mso	Msi	°C
unstressed austenite start temperature	A_{so}	Aso	Asi	°C
unstressed austenite finish temperature	A_{fo}	Afo	Afi	°C
martensite finish temperature	M_f	Mf	Mf	°C
martensite start temperature	M_s	Ms	Ms	°C
austenite start temperature	A_s	As	As	°C
austenite finish temperature	A_f	Af	Af	°C
temperature above which, martensite cannot form	M_d	-	-	°C
martensite peak temperature	M_p	-	-	°C
austenite peak temperatures	A_p	-	-	°C
transformation hysteresis	-	T_1	-	°C
Young's modulus (of elasticity), martensite	Y_M	-	YM	Pa
Young's modulus (of elasticity), austenite	Y_A	-	YA	Pa
stress influence coefficient for martensite	C_M	CM	CM	Pa/°C
stress influence coefficient for austenite	C_A	CA	CA	Pa/°C
thermoelastic tensor	Θ	-	H	Pa/°C
strain	ε	s	s	(%)
martensitic strain limit (maximum recoverable strain)	ε_L	εL	sL	(%)
strain range	ε	-	s_range	(%)
maximum applied strain	ε_{max}	-	s_max	(%)
minimum applied strain	ε_{min}	-	s_min	(%)
stress	σ	σ	S	Pa
stress at start of stress-induced martensite formation	σ_s^{cr}	σcrs	S_crs	Pa
stress at finish of stress-induced martensite formation	σ_f^{cr}	σcrf	S_crf	Pa
stress in wire on hot side	σ_{wh}	-	-	Pa
stress in wire on cold side	σ_{wc}	-	-	Pa
emissivity	e	-	emis	
convection coefficient	h	h	h	$W/m^2/°K$
convection coefficient for hot side	h_h	-	hh	$W/m^2/°K$
convection coefficient for cold side	h_c	-	hc	$W/m^2/°K$
Stefan-Boltzmann constant	SB	-	sb	$W/m^2/°K^4$
specific heat	c	-	c	$J/kg/m^3$
mass density	ρ	-	rho	kg/m^3
pi	π	-	pi	
time constant for cooling	J_c	-	Jc	s
temperature	T	T	T	°C (°K)
free stream temperature	T_∞	-	T_inf	°C (°K)
heating free stream temperature	$T_{h\infty}$	-	Th_inf	°C (°K)
cooling free stream temperature	$T_{c\infty}$	-	Tc_inf	°C (°K)
temperature of surroundings	T_{sur}	-	T_sur	°C (°K)
heating temperature of surroundings	T_{hsur}	-	Th_sur	°C (°K)
cooling temperature of the surroundings	T_{csur}	-	Tc_sur	°C (°K)
change in temperature	dT	-	dT	°C (°K)
cooling target temperature	T_c	-	Tc	°C (°K)
change in time	dt	-	dt	s
time to reach cooling target temperature	t_c	-	tc	s
time	t	-	t	s
volume fraction of martensite	fM	fM	fM	
volume fraction of stress-induced martensite	fM_S	fM_S	fM_S	

volume fraction of temperature-induced martensite	fM_T	fM_T	fM_T	
initial fraction of martensite	fM_o	-	fMo	
initial fraction of stress-induced martensite	fM_{So}	-	fMo_S	
initial fraction of temperature-induced martensite	fM_{To}	-	fMo_T	
SMA spring	S1	S1	-	
SMA spring	S2	S2	-	
SMA spring	S3	S3	-	
SMA spring	S4	S4	-	
longer crank, crankshaft with longer cranks	A	A	A	
shorter crank, crankshaft with shorter cranks	B	B	B	
wire diameter	d	-	d	m
crank radius	r	r	r	m
synchronizer radius	r_s	rs	rs	m
radius of crank A	r_A	rA	rA	m
radius of crank B	r_B	rB	rB	m
wire length	r_w	rw	rw	m
length of stretched wire	r_{ws}	rws	rws	m
length of retracted wire	r_{wr}	rwr	rwr	m
center distance	r_c	rc	rc	m
perpendicular distance	r_p	rp	rp	m
perpendicular distance for crank A	r_{pA}	rpA	rpA	m
perpendicular distance for crank B	r_{pB}	rpB	rpB	m
angle	θ	θ	a	degrees
angle of wire	θ_w	θw	aw	degrees
angle of wire on hot side	θ_{wh}	-	-	degrees
angle of wire on cold side	θ_{wc}	-	-	degrees
angle of A	θ_A	θA	aA	degrees
angle of B	θ_B	θB	aB	degrees
angle of ground	θ_g	-	-	degrees
weight of crankshaft A	$weight_A$	-	-	N
weight of crankshaft B	$weight_B$	-	-	N
force in synchronizer	F_s	Fs	-	N
force in side 1 of synchronizer	F_{s1}	Fs1	-	N
force in side 1 of synchronizer	F_{s2}	Fs2	-	N
force in wire	F_w	Fw	-	N
force in cold wire	F_{wc}	Fwc	-	N
force in hot wire	F_{wh}	Fwh	-	N
force in x direction at crankshaft A	F_{Ax}	FAx	-	N
force in y direction at crankshaft A	F_{Ay}	FAy	-	N
force in x direction at crankshaft A	F_{Bx}	FBx	-	N
force in y direction at crankshaft A	F_{By}	FBy	-	N
moment about crankshaft A	M_A	-	-	N-m
moment about crankshaft B	M_B	-	-	N-m
stalling torque	M_{stall}	Mstall	Mstall	N-m
net stalling torque	M_{stall}^{net}	-	-	N-m
load torque	M_{load}	-	Mload	N-m
power	P	-	power	W
shaft velocity	ω	-	-	rpm
shaft speed	N	-	rpm	rpm
number of cranks	n_c	nc	nc	
number of wires per crank	n_w	nw	nw	

Appendix 2

Material Property Data

Table A2-1: Example transformation temperatures for Ni-Ti wires (°C) [2h].

Examples	M_f	M_p	M_s	A_s	A_p	A_f	Hysteresis (A_p-M_p)	Overall Temperature Span (A_f-M_f)
1	-53	-40	-33	-24	-14	-5	26	48
2	-45	-30	-24	-15	-3	+7	27	53
3	-3	+3	+6	+23	+30	+35	27	38
4	24	31	36	54	66	71	35	45
5	59	68	79	100	114	121	46	62

Table A2-2: Property comparison between the common shape memory alloys [6].

Property	Ni-Ti	Cu-Zn-Al	Cu-Al-Ni
Maximum A_s Temperature (°C)	100	120	200
Maximum One-Way Strain (%)	8	6	5
Hysteresis (°C)	12-50	10-25	15-20
High Temperature Yield Strength (MPa)	415	350	400
Low Temperature Yield Strength (MPa)	70	80	130
Ultimate Tensile Strength (MPa)	700	600	500-800

Appendix 3

Patent Search Results

Click here for the linked spreadsheet file represented in Table A3-1.

Table A3-1: Patents relating to shape memory alloy heat engines.

Patent Number	Title	Date	Inventor(s)	Type	Comments
6226992	Heat converter engine using a shape memory alloy actuator	2001-05-08	Kutlucinar, Saul	crank	SMA heat engine - rollers on a track form the offset crank arrangement
6192683	Device for converting thermal energy into electrical energy	2001-02-27	Stock	reciprocating	SMA driven reciprocating pistons pump fluid through a turbine
6151897	Shape memory alloy actuator	2000-11-28	Baumbick	na	SMA controllable micro-actuator
6121588	Thermal actuation device	2000-09-19	Cerruti	na	reciprocating rotary actuator
6084321	Conducting polymer driven rotary motor	2000-07-04	Hunter, Lafontaine, Madden	sequential	motor driven by successive expansion and contraction of a polymer ring (could be done with SMA's)
6065934	Shape memory rotary actuator	2000-05-23	Jacot, Julien, Clingman	na	reciprocating rotary actuator - SMA torque tube
6052992	Heterogeneous structure for accumulating or dissipating energy, methods of using such a structure and associated devices	2000-04-25	Eroshenko	na	porous capillary matrix for storing and releasing energy
5975468	Rotary actuator using shape memory	1999-11-02	Moignier, Chenut, Jabs	na	rotary actuator with a limited angular range - uses and SMA bar
5901554	Expansion rotary engine	1999-05-11	Greschik	sequential	caterpillar and squeeze rotary engines - uses phase changes in paraffin (could be done with SMA's)
5685148	Drive apparatus	1997-11-11	Robert	na	SMA actuator drive mechanism
5631514	Microfabricated microengine for use as a mechanical drive and power source in the microdomain and fabrication process	1997-05-20	Garcia, Sniegowski	reciprocating	oscillating linear actuators coupled to gear to create rotary motion (could be done with SMA's)
5442914	Shape memory alloy heat engine	1995-08-22	Otsuka	crank	SMA-CDS (conical-disc-springs) engine, uses an offset crank
5430333	Energy generating system and method	1995-07-04	Binford	field	a loop of bellows under water - SMA compresses bellows in response to increasing temperature at the surface
5396769	Rotary actuator	1995-03-14	Brudnicki	na	SMA coils form a rotary actuator with limited angular range
5306979	Multiplexing incremental linear actuator system	1994-04-26	Schwarz, Jr.	sequential	SMA linear inch-worm style motor
5279123	Apparatus for recovery and use of waste thermal energy	1994-01-18	Wechsler, Van Gerpen	crank	offset crank SMA engine
5127228	Shape memory bi-directional rotary actuator	1992-07-07	Swenson	na	rotary actuator with a limited angular range - uses a SMA torque tube
5031711	Conveyance device	1991-07-16	Tanaka, Saito	pulley	simple pulley engine using SMA belt
5020325	Heat motor	1991-06-04	Henault	na	electrically heated wax actuator
5003779	Geothermal energy conversion system	1991-04-02	Goldstein	sequential	engine driven by a SMA gear, sequentially heated
4996842	Heat engine with corrugated shape memory drive belt	1991-03-05	Goldstein	pulley	corrugated SMA belt around pulleys
4965545	Shape memory alloy rotary actuator	1990-10-23	Johnson	pulley	SMA chain seated on pulleys to form a rotary actuator with limited angular range
4955196	Internal energy engine (IEE)	1990-09-11	Lin, Wang	reciprocating	SMA actuator - uses hollow SMA coiled tube
4938026	Heat engine based on shape memory alloys	1990-07-03	Goldstein	sequential	heat engine driven by a tubular SMA gear, sequentially heated
4922718	Thermal energy scavenger	1990-05-08	Hochstein, Pringle	reciprocating	thermal energy extractor using an array of SMA's in a reciprocation manner
4800722	Method and equipment for converting thermal energy to mechanical energy	1989-01-31	Arvola, Kajamaa	crank	SMA heat engine composed of offset cranks and method for thermally cycling the elements
4798051	Rotary actuator with tailored torque output	1989-01-17	Foote	na	rotary actuator composed of SMA torque tube heated by burning a chemical grain
4785627	Drive device	1988-11-22	Al-Jaroudi	pulley	simple pulley engine using SMA belt - for driving a fan or generator
4761955	Rotary actuator utilizing a shape memory alloy	1988-08-09	Bloch	na	rotary actuator - SMA wire wrapped multiple times around a spring biased spool
4759187	Wire engine	1988-07-26	O'Hare	reciprocating	reciprocating heat engine composed of an array of SMA wire - opposing pumps heat and cool the array
4756158	Method and equipment for converting thermal energy to mechanical energy	1988-07-12	Arvola, Kajamaa	crank	SMA heat engine composed of offset cranks and method for thermally cycling the elements
4691518	Vertically oscillating heat engine	1987-09-08	Banks	crank	4-bar linkage and flywheel move SMA wire between hot and cold baths
4691517	Laterally oscillating nitinol engine	1987-09-08	Banks	crank	4-bar linkage and flywheel move SMA wire between hot and cold baths
4691516	Thermally-activated device for creating considerable power	1987-09-08	Fornasari	na	simple wax based linear actuator
4683721	Twin-crank type heat engine	1987-08-04	Shin, Kim, Chung, Jee	crank	twin crank based SMA heat engine
4646523	Wire engine for water pumps	1987-03-03	O'Hare	reciprocating	reciprocating SMA wire based heat engine, solar heating apparatus
4598550	Radiant heat engine	1986-07-08	Abbott	crank	SMA wire drives an eccentric disk, the wires are alternately shaded and heated to produce rotation
4563876	Linear output nitinol engine	1986-01-14	Banks	reciprocating	Complex reciprocating pulley and linkage based SMA heat engine
4503676	Apparatus for directly converting thermal to rotational energy	1985-03-12	Rutledge	swash	long elastic shaft spirally arranged in a plane to form a heat engine
4490976	Two-way shape memory alloy heat engine	1985-01-01	Johnson	crank	eccentric disc connected to SMA wires forming a heat engine
4472939	Energy conversion system	1984-09-25	Wang	pulley	planetary pulley SMA engine, wires operate in the bending mode
4472113	Pumping by martensitic transformation utilization	1984-09-18	Rogen	na	plunger operated by a SMA spring
4450686	Single wire nitinol engine	1984-05-29	Banks	crank	offset crank and flywheel move SMA wire between hot and cold baths

Table A3-1 continues on the following page

Table A3-1, continued from the previous page.

4435229	Method of preparing a two-way shape memory alloy	1984-03-06	Johnson	na	method of preparing a 2-way SMA
4434618	Engine construction	1984-03-06	Dillon	crank	piston cylinder crank engine using SMA springs to drive pistons
4423596	Thermal engine	1984-01-03	Karnes, Trupin	reciprocating	SMA strip separates fluids in a chamber, chamber tilts to heat and cool the strip, reciprocating output
4407124	Memory power engine	1983-10-04	Pelley	crank	SMA elements act on an eccentric crankshaft
4397151	Heat engine	1983-08-09	Houlton	pulley	rack-and-pinion type reciprocating linear SMA engine, wires operate in bending mode
4393654	Shape memory element engine	1983-07-19	Pelley	crank	hollow SMA springs turn a crankshaft
4388805	Power plants deriving their energy from expansion and contraction	1983-06-21	Rideout, Jr.	reciprocating	thermal expansion and contraction drives a rack and pinion to create reciprocating output
4343154	Motive device for converting a variation in temperature into mechanical energy	1982-08-10	Jarret, Jarret	reciprocating	elastomer based piston cylinder engine
4341072	Method and apparatus for converting small temperature differentials into usable energy	1982-07-27	Clyne	reciprocating	piston cylinder arrangements are driven by an expansion medium, includes a system diagram
4325217	Solid state engine with alternating motion	1982-04-20	Golestaneh	reciprocating	SMA driven piston cylinder engine, includes valving system for heating and cooling the SMA elements
4307571	Device driven by heat energy	1981-12-29	Jackson	field	weighted SMA arms elongate in the sun and shrink in the shade, gravity rotates the unbalanced assembly
4306415	Thermal energy scavenger (flow control)	1981-12-22	Hochstein, Pringle, Milton, Jr.	reciprocating	thermal energy extractor using SMA wires to drive hydraulic pistons
4305250	Solid state heat engine	1981-12-15	Cory	pulley	heat engine using multiple pulleys and liquid baths to heat and cool a SMA belt
4302939	Solid state engine using nitinol memory alloy	1981-12-01	Golestaneh	sequential	SMA wire loops are attached to a floating ring and are successively dipped into high temperature bath
4302938	Nitinol engine for low grade heat	1981-12-01	Li	pulley	SMA belt threaded through complex roller assembly, discusses cycle and some calculations
4281513	Field effect memory alloy heat engine	1981-08-04	Johnson, Kirkpatrick	field	Ferris-wheel style, gravity driven SMA engine
4275561	Energy conversion system	1981-06-30	Wang	pulley	SMA belt and pulley based heat engine, non-synchronized with multiple belts in parallel
4257231	Heat engine	1981-03-24	Banks	reciprocating	complex mechanism converts reciprocating motion of SMA bands into rotary output
4246754	Solid state thermal engine	1981-01-27	Wayman	pulley	synchronized SMA belt driven heat engine, belt and gear synchronized embodiments shown
4236377	Heat expansion machine	1980-12-02	Weinert	field	gravity driven engine based on imbalances caused by SMA displaced rotor arms
4235075	Method and apparatus for converting relatively low temperature heat energy into useful work	1980-11-25	Erb	reciprocating	volume changes associated with melting and solidification of wax are used drive a piston and produce work
4231223	Thermal energy scavenger (rotating wire modules)	1980-11-04	Pringle, Hochstein, Milton, Jr.	reciprocating	thermal energy extractor using SMA wires to drive hydraulic pistons
4222239	Heat engine	1980-09-16	Negishi	reciprocating	reciprocating wax based heat engine
4197709	Thermal energy scavenger (stress limiter)	1980-04-15	Hochstein	reciprocating	thermal energy extractor using SMA wires to drive hydraulic pistons
4197708	Thermal energy scavenger (alternating stress limiters)	1980-04-15	Milton, Jr., Hochstein, Pringle	reciprocating	thermal energy extractor using SMA wires to drive hydraulic pistons
4186558	Thermal conversion engine	1980-02-05	Kuo	reciprocating	reciprocating heat engine based on the freezing and thawing of water
4175390	Solid stress motor	1979-11-27	Koslow	swash	heat engine in which a bowed elastic member is partially heated to induce rotation
4150544	Engine	1979-04-24	Pachter	pulley	synchronized SMA belt driven heat engine
4117680	Continuous loop shape memory effect heat engine	1978-10-03	Smith	pulley	heat engine consisting of a SMA belt riding on planetary rollers
4087971	Devices and methods for converting heat energy to mechanical energy	1978-05-09	Hart	crank	twisted SMA ribbon exert force on a cam to produce rotation, many heat engine concepts
4086769	Compound memory engine	1978-05-02	Smith	crank	crankshaft driven by SMA springs
4075847	Direct conversion of solar energy to mechanical energy	1978-02-28	Ray	field	cylinder made of polymer strips, deforms in heat to cause gravity driven rotation
4075846	Thermal engine with entrapped working medium	1978-02-28	Li	pulley	heat engine with continuous SMA belts wrapped around multiple rollers of different sizes
4055956	High torque solar motor	1977-11-01	Matovich, Jr.	swash	vanes expand and contract in response to solar energy, an overrunning clutch mechanisms extracts work
4055955	Memory alloy heat engine and method of operation	1977-11-01	Johnson	pulley	heat engine composed of SMA wire belts wrapped around pulleys, synchronized with bevel gears
4041706	Linear force generator and heat engine embodying same	1977-08-16	White	crank	arrays of SMA wires drive a crank
4037411	Thermal energy converting assembly	1977-07-26	Hochstein	crank	cam and follower engine in which deformed SMA wires follow an eccentric inside surface of a circle
4030298	Thermal motor	1977-06-21	Sandoval	pulley	unsynchronized SMA belt driven engine, shows non-slip, sprocket-like elements
4027479	Variable density heat engine	1977-06-07	Cory	field	weighted SMA belt, gravity driven
4010612	Thermal motor	1977-03-08	Sandoval	pulley	unsynchronized SMA belt and pulley heat engine, works by bending, uses sprockets to eliminate slip
4006594	Solar power plant	1977-02-08	Horton	swash	solar energy drives the engine which uses out of plane disks with SMA materials attached between
3987630	Mechanical thermal motor	1976-10-26	Hein, Myers	reciprocating	reciprocating thermal motor
3986354	Method and apparatus for recovering low-temperature industrial and solar waste heat energy previously dissipated to ambient	1976-10-19	Erb	reciprocating	heat engine driven by expansion of some medium in a cylindrical walled structure
3937019	Thermal engine	1976-02-10	Renner	crank	crankshaft driven by SMA material, also shows a swash plate output
3913326	Energy conversion system	1975-10-21	Banks	crank	SMA spoke based rotary heat engine

Click here for the linked spreadsheet file represented in Table A3-1.

Appendix 4

Material Property Search Results

Table A4-1: Collection of SMA material properties from various sources.

Source	[15]	[33]	[3]	[28]	[10]	[34]	[2g]	[12]	[31]
Property									
transformation temperatures (°C)									
M_f		42	9	21	9	42		1	49
M_s		77	18.4	32	18.4	52		11	59
A_s	70	81	34.5	38	34.5	68		40	72
A_f		106	49	49	49	78		45	82
transformation constants									
CM (MPa/°C)		14.2	8		10.3				
CA (MPa/°C)		14.2	13.8		10.3				
σ_s^{cr} (MPa)		62	100						
σ_f^{cr} (MPa)		160	170						
moduli (GPa)									
Y_A		49.5	67		67		83	52.8	
Y_M		23.2	26.3		26.3	28	28	17.5	
thermoelastic coefficient, Θ, (MPa/°C)		0.44	0.55		0.55				
maximum recoverable strain, ε_L (%)		6.3	6.7		6.7	8	8		
mass density, ρ, (kg/m^3)				6500		6450	6450		
specific heat, c_p, (J/kg/°K)				250		322			
latent heat of transformation, Δh, (kJ/kg)				30			24.2		
convection coefficient, h, ($W/m^2/°K$)									140
maximum recovery stress (MPa)	172					600			
recommended recovery stress (MPa)	115					190			
recommended deformation stress (MPa)						35			

MATLAB Codes

Table A4-2: Description of included codes.

Filename	**Description**
Main_Analysis.m	Compilation of analysis topics into a single routine
Crank_Study.m	Produces plots relating kinematic and geometric quantities - no SMA info.
Brinson2D.m	Shows a path in stress-temperature space, including boundaries and strain
Brinson3D.m	Shows a 3D plot of strain as a function of temperature at constant stresses
Output_Plots.m	Creates trend plots for the implication section of Chapter 4
StrainVstressCtemp.m	Finds strain by varying stress at constant temperature
StressVtempCstrain.m	Finds stress by varying temperature at constant strain
Wire_Temperature.m	Compares theoretical and empirical heat transfer models

fun_crank_geometry.m	Function for relating position to strain and calculating perpendicular distances
fun_fm	Function for determining the constituent fractions of martensite
fun_int.m	Function determining the equation of a line given two points
fun_line.m	Function determining the interceptions between a path and boundary lines
fun_strainVstressCtemp.m	Function providing strain values by varying stress at a constant temperature
fun_stressVtempCstrain.m	Function providing stress values by varying temperature at a constant strain
fun_wire_temp	Uses the theoretical expression to find wire temperature as a function of time

Reference List

Table R1-1: List of cited references.

Ref.	Source
[1]	Banks, R., "Getting Warmer: The Nitinol Engine," #12, R&D Innovator Vol. 1, No. 4, November 1992, *http://www.winstonbrill.com/bril001/html/article_index/articles/1-50/article12_body.html*, accessed 1-12-2002.
[2]	Hodgson, D. E., Wu, M. H. and Biermann, R. J., "Shape Memory Alloys," *http://www.sma-inc.com/SMAPaper.html*, pp. 1-9, accessed 7-19-2001.
[2b]	"Glossary of NiTi Terminology," *http://www.sma-inc.com*, accessed, accessed 7-19-2001.
[2c]	"#2 Introduction to Shape Memory and Superelasticity," *http://www.sma-inc.com/SMAandSE.html*, accessed 7-19-2001.
[2d]	"#13 Specifying NiTi Materials," *http://www.sma-inc.com/SpecifyingNiTi.html*, accessed 7-19-2001.
[2e]	"#11 Measuring Transformation Temperatures in NiTi Alloys," *http://www.sma-inc.com/ttrmeas.html*, accessed 7-19-2001.
[2f]	"#14 Joining NiTi Materials," *http://www.sma-inc.com/joining.html*, accessed 7-19-2001.
[2g]	"#3 Selected Properties of NiTi," *http://www.sma-inc.com/NiTiProperties.html*, accessed 7-19-2001.
[2h]	"#12 Transformation Temperature Hysteresis in NiTi Alloys," *http://www.sma-inc.com/hysteresis.html*, accessed 7-19-2001.
[3]	Brinson, L. C., "One-Dimensional Constitutive Behavior of Shape Memory Alloys: Thermomechanical Derivation with Non-Constant Material Functions and Redefined Martensite Internal Variable," *Journal of Intelligent Material Systems and Structures*, Vol. 4, pp. 229-242, April 1993.
[4]	"White Oak Fact Sheet - Prepared by the US Navy," *http://www.nteu282.org/whiteoak/000523fs.html*, accessed 9-11-2002.
[5]	Leo, D., "M7S442001," *Class Notes ME5984: Smart Structures*, Virginia Tech, 2001.
[6]	Raychem Corp., Actuator Design Using Shape Memory Alloy Actuators.
[7]	"The History of Nitinol," *http://www.imagesco.com/articles/nitinol/02.html*, accessed 6-1-2002.
[8]	Brown, C., "Mini Motor Formed by Shape-Memory Alloy," *http://www.edtn.com/story/tech/OEG20010905S0081*, accessed 1-14-2002.
[9]	Marks, P., "Shirt Rolls Up Its Own Sleeves," NewScientist.com, July 2001, *http://www.newscientist.com/news/news.jsp?id=ns99991073*, accessed 1-12-2002.
[10]	Zhang, X. D., Rogers, C. A. and Liang, C., "Modeling of the Two-Way Shape Memory Effect," *Journal of Intelligent Material Systems and Structures*, Vol. 8, pp. 353-362, April 1997.
[11]	Johnson, A. D., "Nitinol Heat Engines," *Intersociety Energy Conversion Engineering Conference – conference record*, pp. 530-534, 1975.
[12]	Lu, Z. K. and Weng, G. J., "A Micromechanical Theory for the Thermally Induced Phase Transformation in Shape Memory Alloys," *Smart Materials and Structures*, Vol. 9, pp. 582-591, 2000.
[13]	Callister, W. D. Jr., "Materials Science and Engineering An Introduction -- 4th ed.," John Wiley & Sons, New York, pp. 38, 119, copyright 1997.
[14]	Liang, C. and Rogers, C. A., "Design of Shape Memory Alloy Actuators," *Journal of Intelligent Material Systems and Structures*, Vol. 8, pp. 303-313, April 1997.
[15]	http://www.dynalloy.com, accessed 9-11-2002.
[16]	Peng, X., Yang, Y. and Huang, S., "A Two-Phase Mixture Model for SMAs and Application to the Analysis for Pseudoelasticity of a SMA Polycrystal," *Smart Materials and Structures*, Vol. 9, pp. 604-612, 2000.
[17]	Zhu, J. J., Liang, N. G., Liew, K. M. and Huang, W. M., "Energy Conversion in Shape Memory Alloy Heat Engine Part I: Theory," *Journal of Intelligent Material Systems and Structures*, Vol.

12, pp. 127-132, February 2001.
[18] Tobushi, H., Kimura, K., Iwanaga, H. and Cahoon, J. R., "Basic Research on Shape Memory Alloy Heat Engine (Output Power Characteristics and Problems in Development)," *JSME International Journal Series*, Series 1, Vol. 33, No. 2, pp. 263-267, 1990.
[19] Tanaka, M., "Shape Memory Alloy Engine," *27th Intersociety Energy Conversion Conference*, Vol. 3, pp. 3.87-3.91, 1992.
[20] Zhu, J. J., Liang, N. G., Liew, K. M. and Huang, W. M., "Energy Conversion in Shape Memory Alloy Heat Engine Part II: Simulation," *Journal of Intelligent Material Systems and Structures*, Vol. 12, pp. 133-140, February 2001.
[21] Iwanga, H., Tobushi, H. and Ito, H. "Basic Research on Output Power Characteristics of a Shape Memory Alloy Heat Engine," *JSME International Journal*, Series I, Vol. 31, pp. 634-637, 1988.
[22] Tobushi, H. and Cahoon, J. R., "Mechanical Analysis of a Solar-Powered Solid State Engine," *Transactions of the Canadian Society for Mechanical Engineering*, Vol. 9, No. 3, pp. 137-141, 1985.
[23] Tanaka, H., Kohda, M. and Okuda, T., "A Study Of The High-Power Nitinol Heat Engine," *20th Intersociety Energy Conversion*, Vol. 2, pp. 2.729-2.734, 1985.
[24] Mabie, H. H. and Reinholtz, C. F., "Mechanisms and Dynamics of Machinery -- 4th edition," John Wiley & Sons, New York, copyright 1987, pp. 1.
[25] Incropera, F. P. and Dewitt, D. P., "Fundamentals of Heat and Mass Transfer -- 4th ed.," John Wiley & Sons, New York, copyright 1996, pp. 8-18.
[26] Liang, C. and Rogers, C. A., "One-Dimensional Thermomechanical Constitutive Relations for Shape Memory Materials," *Journal of Intelligent Material Systems and Structures*, Vol. 1, pp. 207-234, April 1990.
[27] Cady, E. C., McNichols, J. L. and Cory, J. S., "Nitinol Heat Engine Thermodynamic Cycle Analysis," *20th Intersociety Energy Conversion*, Vol. 2, pp. 2.735-2.741, 1985.
[28] Thrasher, M. A., Shahin, A. R., Meckl, P. H. and Jones, J. D., "Efficiency Analysis of Shape Memory Alloy Actuators," *Smart Materials and Structures*, Vol. 3, pp. 226-234, 1994.
[29] Gorbet, R., "The SMAList," *http://kingcong.uwaterloo.ca/~rbgorbet/smalist/suppliers.html*, accessed 2001-09-24.
[30] "World of Timing Belts - Catalog D260-1," Stock Drive Products Sterling Instruments, copyright 1998.
[31] Amalraj, J. J., Bhattacharyya, A. and Faulkner, M. G., "Finite-element Modeling of Phase Transformation in Shape Memory Alloy Wires with Variable Material Properties," *Smart Materials and Structures*, Vol. 9, pp. 622-631, 2000.
[32] Wolcott, B., "Solar Gains," *Mechanical Engineering*, Vol. 123, No. 10, pp. 66-69, October 2001.
[33] Wang, G. and Shahinpoor, M., "Design, Prototyping and Computer Simulations of a Novel Large Bending Actuator made with a Shape Memory Alloy Contractile Wire," *Smart Materials and Structures*, Vol. 6, pp. 214-221, 1997.
[34] "Flexinol Material Properties," *http://www.frasco.demon.co.uk/boris/flexinol.htm*, accessed 9-13-2001.
[35] Wakjira, J. F., "The VT1 Shape Memory Alloy Heat Engine Design," Master's thesis, Department of Mechanical Engineering, Virginia Polytechnic Institute and State University, Blacksburg, VA, 2001.

Vita

Ean Harrison Schiller was born on April 3, 1978 in Dyke VA. He completed a B.S. degree in Mechanical Engineering from Virginia Tech in 2000. In 2002, he will receive a M.S. degree in Mechanical Engineering upon the acceptance of this document.